University of Nevada, Reno

Studies of nonstructural components in tall mass timber buildings with cross-laminated timber rocking walls

A dissertation submitted in partial fulfillment of the

requirements for the degree of Doctor of Philosophy

in Civil and Environmental Engineering

by

Hamed Hasani

Dr. Keri L. Ryan/Dissertation Advisor

August 2021

THE GRADUATE SCHOOL

We recommend that the dissertation
prepared under our supervision by

Hamed Hasani

entitled

Studies of nonstructural components in tall mass timber buildings with cross-laminated timber rocking walls

be accepted in partial fulfillment of the
requirements for the degree of

Doctor of Philosophy

Keri L Ryan
Advisor

Ramin Motamed
Committee Member

Gokhan Pekcan
Committee Member

Hamed Ebrahimian
Committee Member

Michael H Gardner
Graduate School Representative

David W. Zeh, Ph.D., Dean
Graduate School

August, 2021

Abstract

In recent years, the performance-based design methodology is helping to meet objectives for resiliency against natural hazards. Post-tensioned cross-laminated timber (CLT) rocking walls are being developed as a seismic resilient lateral load resisting system for mass timber building construction. However, achieving whole building resiliency heavily depends on the resiliency of nonstructural systems, as they comprise the majority of construction costs and are sensitive to low shaking intensities. Nonstructural components can be drift-sensitive, acceleration-sensitive, or sensitive to both drift and acceleration. The mass timber building integrated with the post-tensioned rocking wall system has some features that can affect all nonstructural components. These buildings are flexible and incur significant inter-story drift without much damage to the structural system. Moreover, a rocking wall can induce impact-related high-frequency acceleration spikes. The current study addresses these concerns by evaluating the dynamic response of mass timber buildings integrated with a post-tensioned rocking wall, proposing and investigating low-damage details of partition walls, and evaluating the structural/non-structural interaction effects of including the stiffness and strength of partition walls response in the simulation of the dynamic response of these types of buildings.

Initially, a two-story mass timber building tested at the NHERI@UCSD large high-performance outdoor shake table was studied. Data from this experiment showed that although the high-frequency spikes occurred in post-tensioned CLT rocking walls, they were attenuated in the diaphragm. Moreover, it was shown that modeling assumptions such

as flexible diaphragm and wall to diaphragm connection could affect the numerical simulation of accelerations in the rocking walls and floor diaphragms of the mass timber building.

Subsequently, a few details aimed to reduce the seismic damage to the partition walls were developed and investigated in a series of experiments performed at the NHERI@Lehigh equipment facility. These experiments showed that bidirectional loading had an insignificant influence on the in-plane resistance of the partition walls, and the overall resistance of the partition walls was trivial compared to the entire sub-assembly. In experiment Phase 1, telescoping detailing (nested or double slip track) was shown to eliminate the damage to the framing at the wall ends compared to traditional slip-track detailing. In Phase 2, including a gap through the corner could eliminate all but cosmetic damage up to more than 2% drift, while including distributed gaps (expansion joints) throughout the wall delayed the onset of damage at the wall intersection to about 1% drift.

Finally, structure/nonstructure interaction effects were evaluated in two 5 and 12 story mass-timber buildings integrated with post-tensioned cross-laminated timber rocking walls. Two-dimensional models of representative coupled rocking wall units were developed in OpenSees, and concentrated spring models representing different partition walls with different densities were integrated into these models. Different analyses were performed on the bare rocking wall structure, and the structure integrated with partition walls. Partition walls with classic fixed connection detailing were found to reduce story drift and story shear forces, which can benefit the design of the structure. Partition walls detailed to slip, however, offer little resistance and do not affect the structural response.

To my family

For their love, encouragement, and constant support

Acknowledgment

This research is based upon work funded by National Science Foundation (NSF) under grant numbers CMMI-1635363, 1635227, and 1635227: Collaborative Research: A Resilience-based Seismic Design Methodology for Tall Wood Buildings. Any opinions, findings, conclusions, or recommendations expressed in this document are those of the investigator and do not necessarily reflect the views of the National Science Foundation.

I would like first to acknowledge my advisor, Dr. Keri L Ryan, for her advice, comments, thoughts, criticism, and for helping me in my academic progress. I am also grateful to my other committee members, Dr. Gokhan Pekcan, Dr. Ramin Motamed, Dr. Hamed Ebrahimian, and Dr. Michael H. Gardner.

I would like to thanks the entire NHERI Tall Wood Project research team, including, but not limited to: Dr. Shiling Pei at Colorado School of Mines, Dr. Jeffrey Berman, Dr. John W. van de Lindt at Colorado State University, Dr. J. Danel Dolan at Washington State University, Dr. James Ricles and Dr. Richard Sause at Lehigh University. Additional thanks to the industry partners of the project, including Eastern Exterior Wall Systems Inc, Duggan and Marcon Inc, Simpson Strong-Tie, TallWood Design Institute, Katerra, Forest Products Laboratory, Softwood Lumber Board, DR Johnson Lumber, and the City of Springfield, Oregon.

The experiments in this research could not be completed without the efforts of Lehigh University collaborators and laboratory personnel and NHERI at UCSD site management and staff.

Most importantly, I would like to thank my family for all they have done for me in my entire life. My father, who devoted his life to my success, his memory will be with me always; my mom for her unconditional love and support and my brother and sister for being my closest friend. Their emotional and spiritual supports helped me considerably during the past several years.

Table of Contents

List of Tables

List of Figures

1 Introduction

1.1 Introduction

Mass timber construction has received considerable attention from the growing number of structural engineers and public officials because of several advantages over conventional building materials such as steel, concrete, and light-framed timber. Some of these advantages are design flexibility, thermal performance, energy efficiency, cost-effectiveness, reduced waste, positive environmental effect, fast installation, fire protection, seismic performance, and acoustic performance. Specifically, cross-laminated timber (CLT) panels, one of the most utilized engineered wood products, provide dimensional stability in humidity and temperature change, strength, and rigidity for construction in both directions. In contrast, traditional wood provides the highest strength only in the direction parallel to the grain.

Nowadays, the performance-based design methodology is used by different design codes (ASCE 2007; FEMA 2000), which targets overall building performance rather than strength alone. The performance in this methodology varying from collapse prevention to immediate occupancy (resilience against natural hazards). The most recent effort, led by the Federal Emergency Management Agency (FEMA), has initiated Phase 2 of the performance-based design by incorporating the design's resilience. For the past ten years, this effort has culminated in the FEMA P-58 (FEMA 2012) guidelines for performance-based design methodology.

One developing approach that can offer seismic resilience for mass timber buildings is utilizing post-tensioned CLT rocking walls as the lateral load resisting system. This system is not fixed at the base, and energy dissipation without any damage to the wall depends on the gap opening between the wall and foundation and other devices, such as U-shaped flexural panels (UFP) and other types of steel energy dissipators. The post-tensioning bars are also used as a recentering force. This approach, adapted from concrete rocking walls, began in New Zealand (Palermo et al. 2006).

Whole building resilience requires the resilience of the structural elements and the resilience of nonstructural systems. The damage from nonstructural elements has dominated economic losses compared to the structural elements in the recent earthquakes (Taghavi and Miranda 2003). Nonstructural components can be divided into three categories based on their sensitivity to the response parameter. The first one is the drift-sensitive components that span between floors, including partition walls, windows, electrical systems within partitions, and stairs. The second category pertains to the acceleration-sensitive elements, for instance, suspended ceilings, ducts, boilers, and chillers. The third category includes components sensitive to drifts and accelerations, such as fire sprinklers, cold and hot water pipes, gas pipes, and elevators.

The rocking wall systems have specific response features, such as large inter-story drift, high-frequency acceleration, and higher mode effects due to wall rocking and vertical displacement incompatibility between the wall and the floor diaphragms. Thus, the seismic demands in these buildings can affect all types of nonstructural components. Therefore,

quantifying and improving the response of nonstructural elements in these structures is critical to the overall resilience of mass timber buildings.

1.2 Literature review

Previous experiments have shown that CLT rocking walls can function as resilient lateral load resistant systems for buildings in high seismic areas (Buchanan et al. 2008; Ganey 2015). However, high-frequency acceleration spikes were observed during various shake table tests of confined masonry and the concrete rocking walls (Belleri et al. 2014; Toranzo-Dianderas 2002). These acceleration spikes were also studied and validated in different numerical studies (Belleri et al. 2014; Qureshi and Warnitchai 2016). In addition, acceleration-sensitive nonstructural components, such as the suspended ceiling (Aragaw and Calvi 2018), have vibration periods as low as 0.01 seconds. Thus, the component vibration periods can be tuned with the high-frequency acceleration spikes of the post-tensioned rocking wall system.

The rocking wall system also leads to larger inter-story drifts than the traditional shear walls (Zhou et al. 2012). For example, in the experimental test conducted by Pei et al. (2019), drift ratios of 1.59% to 2.40% were observed for design basis earthquakes in a two-story mass-timber building. Another particular behavior of the rocking wall system is the vertical displacement incompatibility between the wall and floor diaphragm. When the rocking wall moves laterally, it uplifts as it rocks. This uplift causes a vertical displacement incompatibility between the wall and the collector beam or floor diaphragm. Moroder (2016) studied a few types of connections between the collector beam and the wall. A pin-

slotted connection was used to reduce the displacement incompatibility, but this joint did not work correctly due to the friction. In tests conducted as a part of the NHERI Tall Wood Project at NHERI@Lehigh and NHERI@UCSD, a pin-slotted connection with modified details such as an epoxy filler for reduction of the friction was used. Moreover, the pin-slotted connection has the potential to alleviate the effect of acceleration spikes.

Drywall partition walls are among the most common drift-sensitive components in building construction, and the overall building resilience relies highly on these components. Partition walls are susceptible to damage at inter-story drift ratios as low as 0.2%. The steel-framed partition walls are more common than wood-frame partition walls due to behaving more ductile (Tasligedik et al. 2012). Three types of experiments have been conducted on drywall-partition walls: local connection tests (Fiorino et al. 2017; Rahmanishamsi et al. 2016b; a; Swensen et al. 2015), component tests (Araya-Letelier et al. 2019; Fiorino et al. 2018; Freeman 1971, 1974, 1976; John A. Blume and Associates 1966, 1968; Lee et al. 2007; Magliulo et al. 2014; Memari et al. 2008; Pali et al. 2018; Peck et al. 2012; Petrone et al. 2015; Restrepo and Bersofsky 2011; Restrepo and Lang 2011; Retamales et al. 2013; Rihal 1982; Tasligedik et al. 2012, 2013), and system-level tests (Fiorino et al. 2019; Jenkins et al. 2016; Matsuoka et al. 2008; McCormick et al. 2008; Retamales et al. 2011; Soroushian et al. 2012; Wang et al. 2015). These experiments had different goals, including determination of the effect of construction details on the seismic behavior of partition walls, the definition of damage states and fragility curves, estimation of repair cost, determination of the effect of the loading protocol, and determination of the contribution of nonstructural components in structural response (Hasani and Ryan 2021).

The most crucial detail that affects the partition wall seismic response is the connection details of the walls to surrounding elements (Pali et al. 2018). There are two main approaches for connecting the partition walls to the structural system: fixed connection and the slip-track connection. The latter allows relative slip between the partition wall and the diaphragm but induces damage at the wall intersection (Davies et al. 2011). Therefore, refining the detail at the corner and intersecting walls is essential for making the slip-track approach effective. A few experiments have been conducted for reducing damage due to drift at the wall intersection (Araya-Letelier et al. 2019; Retamales et al. 2013). Retamelas et al. (2013) tested two details: the corner gap detail and the double slip-track detail, and Araya-Letelier (2019) evaluated a new detail named sliding/frictional detail.

While their overall resilience is of concern, the nonstructural components can also affect the dynamic behavior of the mass-timber building integrated with cross-laminated timber rocking wall significantly. A few researchers studied the effect of partition walls on the static and dynamic characteristics of other types of buildings. The partition walls significantly contributed to the stiffness and strength of a moment frame when they were built as infill walls (Lee et al. 2007 and Tasligedik et al. 2012). In prior studies, including the stiffness of partition walls was shown to decrease the fundamental period of a steel-framed building up to 14% (Wood and Hutchinson 2012), and the fundamental period of a 10-story reinforced concrete building by 10% (Tasligedik et al. 2013). Therefore, because of the flexibility of mass-timber buildings with post-tensioned CLT rocking walls, it is expected that the partition walls may affect the behavior of timber buildings with a CLT rocking wall system significantly.

1.3 Scope of investigation

The primary objectives of this research are 1) to investigate the influence of impact-related acceleration spikes on acceleration-sensitive nonstructural components in buildings with CLT rocking walls, 2) to evaluate partition walls with innovative details aimed at reducing drift-induced damage, and 3) to assess the contribution of different types of partition walls to the overall structural strength, stiffness and dynamic response of buildings with CLT rocking walls.

A mix of experimental and computational efforts was undertaken to meet the above objectives, as mentioned above. First, the results of an experimental investigation conducted at NHREI@UCSD on a two-story mass timber building with the CLT post-tensioned rocking wall were evaluated with a focus on how the accelerations transmit through the building. It is shown that these horizontal acceleration spikes observed in the wall accelerations attenuated significantly in the accelerations recorded in the floor diaphragms. A 2D model of the rocking wall developed by the University of Washington was extended by the author to accurately include the effects of the flexible diaphragm and thus represent both the acceleration of the rocking wall and diaphragm. This model, developed in OpenSees (Mazzoni et al. 2007), was validated by the experimental data from the aforementioned two-story shake table test.

Second, experiments were conducted to gather data and observe the seismic response of the drywall partition walls and evaluate innovative details under systematic bidirectional loading. Two C-shaped walls were assessed. First, the corner gap detail incorporated a full

gap through the wall intersecting wall. Second, the distributed gap detail includes more frequent expansion joints through the length of the wall. The author designed the walls, developed the shop drawings, developed the instrumentation plan, and developed a bidirectional cyclic drift loading protocol for this test. These walls were integrated with a timber rocking wall building, which allowed the author to explore the effect of timber rocking walls on the partition walls. At the NHERI@Lehigh facility, the author was on-site for six weeks to supervise the wall construction, testing, and inspection.

Last, the partition wall effect on mass-timber buildings with post-tensioned CLT rocking walls was studied to determine the importance of the inclusion of these components in the overall building resistance during the design. Two-dimensional models of 5 and 12 story buildings, designed by Wilson (2018), were modeled in OpenSees (Mazzoni et al. 2007). Different partition wall models with widely varying stiffness and strength were integrated into these models, and the dynamic behavior of combined models was evaluated to determine the effect of different partition walls on the overall system response.

1.4 Document outline

- Chapter 1 includes a general introduction of the dissertation, a brief literature review, and the methodology used to achieve the research objectives.
- Chapter 2 focuses on the pre-test seismic evaluation of drywall partition walls integrated with a timber rocking wall, including a literature review of previous tests on drywall partition walls. Chapter 2 represents a conference paper published in the 11th National Conference on Earthquake Engineering (11NCEE) proceedings

(Hasani, H., Ryan, K. L., Amer, A., Ricles, J. M., and Sause, R. (2018). Pre-test seismic evaluation of drywall partition walls integrated with timber rocking wall. Proceedings of the *11th National Conference in Earthquake Engineering,* Earthquake Engineering Research Institute, Los Angeles, CA.)

- Chapter 3 evaluates the results of an experimental investigation conducted on NHERI@UCSD on a two-story timber building with the CLT rocking wall regarding how the accelerations transmit through different building components. Moreover, a modeling approach was developed for capturing the acceleration of the CLT rocking wall and floor system, validated by the experimental data. This study demonstrates that the acceleration spikes alleviate significantly from wall to floor diaphragm due to the flexibility of the diaphragm and wall-to-floor connection. This study also showed that the acceleration-sensitive components are not of particular concern. This conclusion led the author to pivot his attention to the drift-sensitive nonstructural walls for the rest of the dissertation. Chapter 3 represents a journal paper submitted to the journal of Earthquake Engineering and Structural Dynamics (Hasani, H., Ryan, K., Wichman S., Berman, J. (2021). (Submitted) Dynamic behavior of mass timber building with cross-laminated timber rocking wall, *Earthquake Engineering and Structural Dynamics*)
- Chapter 4 discusses the experimental results of two sets of partition walls with innovative details to reduce drift-induced damage in a mass timber subassembly with a post-tensioned CLT rocking wall. This chapter represents a paper is published in the Journal of Earthquake Engineering (Hasani, H., Ryan, K. L.

(2021). Experimental cyclic test of reduced damage detailed drywall partition walls integrated with a timber rocking wall. *Journal of Earthquake Engineering*. DOI: 10.1080/13632469.2020.1859005).

- Chapter 5 presents the results of a parametric study on the effect of different partition walls on the seismic demand of mass timber buildings with post-tensioned CLT rocking walls. This chapter represents a journal paper submitted to the journal of Engineering Structures (Hasani, H., Ryan, K. L. (2021). (Submitted) Effect of partition walls on the seismic response of mass-timber buildings with a post-tensioned rocking wall system. *Engineering Structures*).

1.5 References

Aragaw, L. F., and Calvi, P. M. (2018). Earthquake-induced floor accelerations in base-rocking wall buildings. Journal of Earthquake Engineering, 25(5), 941-969.

Araya-Letelier, G., Miranda, E., and Deierlein, G. (2019). Development and testing of a friction/ sliding connection to improve the seismic performance of gypsum partition walls. Earthquake Spectra, 35(2), 653–677. https://doi.org/10.1193/123117EQS270M

ASCE. (2007). American Society of Civil Engineers: ASCE/SEI 41-06: Seismic rehabilitation of existing buildings. Reston, Virginia: American Society of Civil Engineers.

Belleri, A., Torquati, M., and Riva, P. (2013). Finite element modeling of 'rocking walls. 4th International Conference on Computational Methods in Structural Dynamics and

Earthquake Engineering (COMPDYN 2013). DOI: 10.7712/120113.4706.C1213.

Buchanan, A., Deam, B., Fragiacomo, M., Pampanin, S., and Palermo, A. (2008). Multi-story prestressed timber buildings in New Zealand. Structural Engineering International: Journal of the International Association for Bridge and Structural Engineering (IABSE), 18(2), 166–173. https://doi.org/10.2749/101686608784218635

Davies, R. D., Retamales, R., Mosqueda, G., and Filiatrault, A. (2011). Experimental seismic evaluation, model parameterization, and effect of cold-formed steel-framed gypsum partition walls on the seismic performance of an essential facility-MCEER-11-0005.

FEMA. (2000). Prestandard and commentary for the seismic rehabilitation of buildings (FEMA 356). Washington, DC: Federal Emergency Management Agency.

FEMA (Fema Emergency Management Agency). (2012). Seismic performance assessment of buildings. Volume 1- Methodology. FEMA P-58-1, 1, 278.

Fiorino, L., Bucciero, B., and Landolfo, R. (2019). Evaluation of seismic dynamic behavior of drywall partitions, façades, and ceilings through shake table testing. Engineering Structures, 180(November 2018), 103–123. https://doi.org/10.1016/j.engstruct.2018.11.028

Fiorino, L., Macillo, V., and Landolfo, R. (2017). Experimental characterization of quick mechanical connecting systems for cold-formed steel structures. Advances in

Structural Engineering, 20(7), 1098–1110. https://doi.org/10.1177/1369433216671318

Fiorino, L., Pali, T., and Landolfo, R. (2018). Out-of-plane seismic design by testing of nonstructural lightweight steel drywall partition walls. Thin-Walled Structures, 130, 213–230. https://doi.org/10.1016/j.tws.2018.03.032

Freeman, S. A. (1971). Third progress report on racking tests of wall panels-Report JAB-99-54. San Francisco, California, United States. https://doi.org/10.2172/4663288. Retrieved from https://www.osti.gov/scitech/biblio/4663288.

Freeman, S. A. (1974). Fourth progress report on racking tests of wall panels-Report JAB-99-55. San Francisco, California, United States. Retrieved from https://inis.iaea.org/search/search.aspx?orig_q=RN:6171650

Freeman, S. A. (1976). Racking tests of high-rise building partitions. Journal of the Structural Division, Proceedings of the American Society of Structural Engineers, 103(8), 1673–1685.

Ganey, R. S. (2015). Seismic design and testing of rocking cross-laminated timber walls. The University of Washington (Doctoral dissertation).

Hasani, H., and Ryan, K. L. (2021). Experimental cyclic test of reduced damage detailed drywall partition walls integrated with a timber rocking wall. Journal of Earthquake Engineering. DOI: 10.1080/13632469.2020.1859005

Jenkins, C., Soroushian, S., Rahmanishamsi, E., and Maragakis, E. M. (2016). Experimental fragility analysis of cold-formed steel-framed partition wall systems. Thin-Walled Structures, 103, 115–127. https://doi.org/10.1016/j.tws.2016.02.015

John A. Blume and Associates. (1966). First progress report on racking tests of wall panels-Report NVO-99-15. San Francisco, California, U.S.A.

John A. Blume and Associates. (1968). Second progress report on racking tests of wall panels-Report NVO-99-35. San Francisco, California, U.S.A.

Lee, T.-H., Kato, M., Matsumiya, T., Suita, K., and Nakashima, M. (2007). Seismic performance evaluation of nonstructural components: drywall partitions. Earthquake Engineering and Structural Dynamics, 36, 367–382. https://doi.org/10.1002/eqe.638

Magliulo, G., Petrone, C., Capozzi, V., Maddaloni, G., Lopez, P., and Manfredi, G. (2014). Seismic performance evaluation of plasterboard partitions via shake table tests. Bulletin of Earthquake Engineering, 12(4), 1657–1677. https://doi.org/10.1007/s10518-013-9567-8

Matsuoka, K., Yamada, S., Shimada, Y., Akazawa, M., and Suita, Y. (2008). Nonstructural component performance in 4-story frame tested to collapse. Proceedings of the 14th World Conference on Earthquake Engineering.

McCormick, J., Matsuoka, Y., Pan, P., and Nakashima, M. (2008). Evaluation of nonstructural partition walls and suspended ceiling systems through a shake table study. Structures Congress 2008: Crossing the Borders.

https://doi.org/10.1061/41016(314)223

Memari, A. M., Kasal, B., Manbeck, H. B., and Adams, A. R. (2008). Experimental cyclic racking evaluation of light-frame wood stud and steel stud wall systems experimental cyclic racking.

Moroder, D. (2016). Floor diaphragms in multi-storey timber buildings. University of Canterbury.

Mazzoni, S., Mckenna, F., Scott, M. H., and Fenves, G. L. (2007). Open System for Earthquake Engineering Simulation (OpenSees) OpenSees Command Language Manual.

Palermo, A., Pampanin, S., Fragiacomo, M., Buchanan, A. H., and Deam, B. L. (2006). Innovative seismic solutions for multi-storey LVL timber buildings.

Pali, T., Macillo, V., Terracciano, M. T., Bucciero, B., Fiorino, L., and Landolfo, R. (2018). In-plane quasi-static cyclic tests of nonstructural lightweight steel drywall partitions for seismic performance evaluation. Earthquake Engineering and Structural Dynamics, 47(6), 1566–1588. https://doi.org/10.1002/eqe.3031

Peck, Q., Rogers; N, and Serrette, R. (2012). Cold-formed steel framed gypsum shear walls: in-plane response. Journal of Structural Engineering. https://doi.org/10.1061/(ASCE)ST.1943-541X.0000521

Pei, S., Van De Lindt, J. W., Barbosa, A. R., Berman, J. W., Mcdonnell, E., Dolan, J. D.,

Blomgren, H.-E., Zimmerman, R. B., Huang, D., and Wichman, S. (2019). Experimental seismic response of a resilient 2-story mass-timber building with post-tensioned rocking walls. Journal of Structural Engineering, 145(11), 15.

Petrone, C., Magliulo, G., Lopez, P., and Manfredi, G. (2015). Seismic fragility of plasterboard partitions via in-plane quasi-static tests. Earthquake Engineering and Structural Dynamics, 44(14), 2589–2606. https://doi.org/10.1002/eqe.2600

Qureshi, I. M., and Warnitchai, P. (2016). Computer modeling of the dynamic behavior of rocking wall structures, including the impact-related effects. Advances in Structural Engineering, 19(8), 1245–1261. https://doi.org/10.1177/1369433216642057

Rahmanishamsi, E., Soroushian, S., and Maragakis, E. "Manos." (2016a). Evaluation of the out-of-plane behavior of stud-to-track connections in nonstructural partition walls. Thin-Walled Structures, 103, 211–224. https://doi.org/10.1016/j.tws.2016.02.018

Rahmanishamsi, E., Soroushian, S., and Maragakis, M. (2016b). Cyclic shear behavior of gypsum board-to-steel stud screw connections in nonstructural walls. Earthquake Spectra, 32(1), 415–439. https://doi.org/10.1193/062714EQS091M

Restrepo, J. I., and Bersofsky, A. M. (2011). Performance characteristics of light gage steel stud partition walls. Thin-Walled Structures, 49(2), 317–324. https://doi.org/10.1016/j.tws.2010.10.001

Restrepo, J. I., and Lang, A. F. (2011). Study of loading protocols in light-gauge stud partition walls. Earthquake Spectra, 27(4), 1169–1185.

https://doi.org/10.1193/1.3651608

Retamales, R., Davies, R., Mosqueda, G., and Filiatrault, A. (2013). Experimental seismic fragility of cold-formed steel framed gypsum partition walls. Journal of Structural Engineering, 139(8), 1285–1293. https://doi.org/10.1061/(ASCE)ST.1943-541X.0000657.

Retamales, R., Mosqueda, G., Filiatrault, A., and Reinhorn, A. (2011). Testing protocol for experimental seismic qualification of distributed nonstructural systems. Earthquake Spectra, 27(3), 835–856. https://doi.org/10.1193/1.3609868

Rihal, S. S. (1982). Behavior of non-structural building partitions during earthquakes. Seventh Symposium on Earthquake Engineering, 1, 267–277. University of Roorkee

Soroushian, S., Ryan K. L., Maragakis M., Wieser J., Sasaki T., Sato E., Okazaki T., et al. (2012). NEES/E-defense tests: Seismic performance of ceiling/sprinkler piping nonstructural systems in base-isolated and fixed base building. 15th World Conference on Earthquake Engineering. (15WCEE), Lisbon, Portugal

Swensen, S., Deierlein, G. G., and Miranda, E. (2015). Behavior of screw and adhesive connections to gypsum wallboard in wood and cold-formed steel-framed wallettes. Journal of Structural Engineering, 142(4). doi: 10.1061/(ASCE)ST.1943-541X.0001307.

Taghavi, S., and Miranda, E. (2003). Response assessment of nonstructural building elements. Report PEER 2003/05, Pacific Earthquake Engineering Research Center,

University of California, Berkeley, 96.

Tasligedik, A.S., Pampanin, S., and Palermo, A. (2012). In-Plane cyclic testing of nonstructural drywalls infilled within RC frames. 15th World Conference on Earthquake Engineering (15WCEE). Lisbon, Portugal.

Tasligedik, A. S., Pampanin, S., and Palermo, A. (2013). Low damage seismic solutions for nonstructural drywall partitions. Vienna Congress on Recent Advances in Earthquake Engineering and Structural Dynamics (VEESD 2013), 11. https://doi.org/10.1007/s10518-014-9654-5

Toranzo-Dianderas, L. A. (2002). The use of rocking walls in confined masonry structures : a performance-based approach. University of Canterbury.

Wang, X., Elide Pantoli T. C., Hutchinson J. I., Restrepo R. L., Wood M. S., Hoehler P. G., Sesma F. H., and Sesma F. H.. (2015). Seismic performance of cold-formed steel wall systems in a full-scale building. Journal of Structural Engineering 141 (10): 1–11. doi: 10.1061/(ASCE)ST.1943-541X.0001245.

Wilson, A. W. (2018). Numerical modeling and seismic performance of post-tensioned cross-laminated timber rocking wall systems. Washington State University (Master Thesis).

Wood, R. L., and Hutchinson, T. C. (2012). A numerical model for capturing the in-plane seismic response of interior metal stud partition walls. Technical Report MCEES-12-0007, 2012.

2 Pre-test seismic evaluation of drywall partition walls integrated with a timber rocking wall

(This chapter is a standalone paper published in the 11NCEE conference proceedings: "Hasani, H., Ryan, K. L., Amer, A., Ricles, J. M., and Sause, R. (2018). Pre-test seismic evaluation of drywall partition walls integrated with timber rocking wall. Proceedings of the *11th National Conference in Earthquake Engineering,* Earthquake Engineering Research Institute, Los Angeles, CA.")

2.1 Abstract

Drywall partition walls (DPW) could considerably affect the seismic resilience of tall cross-laminated timber (CLT) buildings due to cost and building downtime associated with the repair. These drift-sensitive components are susceptible to damage at low shaking intensities, and thus controlling or eliminating such damage in low to moderate earthquakes is key to seismic resilience. Conversely, post-tensioned CLT rocking walls have been shown to be a resilient lateral load resistant system for tall CLT buildings in high seismic areas.

A series of tests will be performed at the NHERI Lehigh EF to compare the performance of DPWs with conventional slip-track detailing and alternative telescoping slip-track detailing (track-within-a-track deflection assembly) and to evaluate different approaches for minimizing damage at the wall intersections through the use of gaps. Moreover, a configuration is examined with a partition wall encapsulating the rocking wall for fire

protection. This paper presents a summary of pre-test studies to design the best configuration of DPW to improve the overall resiliency of the structure.

2.2 Introduction

Nonstructural components have emerged as one of the most critical elements in performance-based earthquake engineering methodology and comprise the major portion of total construction cost (Taghavi and Miranda 2003). Drywall partition walls (DPW) are among the most common nonstructural components that are used in building construction. DPW could considerably affect the seismic resilience of buildings due to cost and building downtime associated with the repair. These drift-sensitive components are susceptible to damage at low shaking intensities. In contrast, previous tests have shown the potential for post-tensioned cross-laminated timber (CLT) rocking walls as a resilient lateral load resistant system for tall buildings in high seismic areas, as they are able to develop and sustain great drift demands with little damage (Buchanan et al. 2008, Ganey 2015). Thus, special attention should be paid to DPW for improving the overall resiliency of buildings utilizing post-tensioned CLT rocking walls as a lateral system. Additionally, connections of CLT rocking walls to floor diaphragms may result in localized diaphragm deformation that will cause additional damage to DPW.

Several studies have been conducted on the seismic response of DPWs, which are framed with light gauge steel tracks and studs and covered with gypsum board. The connection of studs and drywall to the top track for both full connection and the slip-track connection is shown in Figure 2-1. Walls with slip track connection detailing have been observed to

perform better than walls with full (fixed) connections for in-plane loading. Slip track connections prevent localized visible damage to the walls upon close inspection and severe damage to the walls when return walls are not present (Mosqueda 2016). Slip track detailed walls without return walls experience detaching of boundary studs from the walls. However, slip track connected with return walls experience damage at corners and intersections with return walls, leading to damage of the return wall track connections and flanges (Davies et al. 2011).

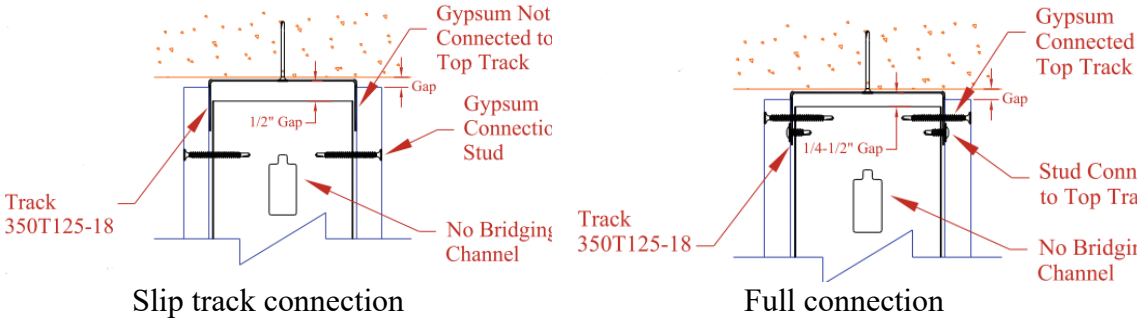

Slip track connection Full connection

Figure 2-1: Slip track and full connection detailing (Davies et al. 2011).

The most important parameter yet to be scrutinized is the behavior of slip-track connection under bidirectional loading. To the authors' knowledge, slip track connection has not been tested bi-directionally under systematic quasi-static loading, which can provide better information about damage states. Moreover, the track-within-a-track deflection assembly (referred to as telescoping hereafter) and some options for mitigating damage at the wall intersections will be tested in a series of full-scale bidirectional experiments. These experiments, which are part of the project titled "Development and Validation of Resilience-based Seismic Design Methodology for Tall Wood Buildings," will be

conducted at the NHERI Lehigh EF. The overarching objective is to investigate the seismic performance of DPW integrated with a post-tensioned CLT rocking wall.

2.3 Literature review

Researchers have conducted component-level tests that test DPWs in an isolated configuration; and system-level tests that evaluate the interaction between DPWs, the primary structural system, and other nonstructural components.

2.3.1 Component-level tests

Rihal (1982) was a pioneer in understanding the damageability of DPWs. He tested 8 ft by 8 ft DPWs, 11 with full connections, and 3 with slip-track connections. Creaking noises/popping sounds corresponding to partition distress occurred at drift ratios of 0.07%-0.26%. The first noticeable partition damage in DPWs with full connections occurred at drift ratios of 0.39%, and failure corresponded to a drift ratio of 0.52%. In walls with slip-track connections, partition distress was observed at drifts as low as 0.07%, but observable damage was not detected.

Restrepo and Bersofsky (2011) tested eight pairs of identical DPWs (all with full connections) with different variables in the quasi-static loading protocol. They grouped all damage limits into three damage states. Damage State (DS) 1 corresponded to damage requiring at most minor repairs after developing and occurred at inter-story drift ratios ranging between 0.05% and 1%. DS 2 occurred at inter-story drift ratios between 0.5% and 1.5% and would require repairs that could cause temporary business interruption. DS 3,

which referred to damage that would require a complete overhaul of partition walls, occurred at inter-story drift ratios ranging between 0.5% and 3%.

Tasligedik et al. (2012) tested steel-framed and timber-framed DPWs under quasi-static loading. To evaluate the contributions of the walls relative to structural framing, three configurations were considered: bare RC moment frame, RC moment frame infilled with steel-framed drywall, and RC moment frame infilled with timber-framed drywall. The partition wall strength was found to be significant compared to the strength of the bare structure. For the drift corresponding to significant damage (0.3% for steel-framed and 0.75% timber-framed), the steel-framed and timber-framed infill walls contributed 83% and 77% of the total lateral force, respectively. Both steel-framed and timber-framed specimens had residual force capacity beyond full yield at 1.5% drift to the end of the test (2.5% drift), but the steel-framed specimens tended to respond in a ductile manner compare to the timber-framed specimens. Tasligedik et al. (2013) suggested modified details for reducing the damage. First, gaps totaling 40 mm in width, which could accommodate 1.5% drift, were provided at the wall ends and between gypsum boards. Second, the gypsum board was only connected to the studs, and the studs were friction fitted to allow for sliding. The results showed that the gaps closed at about 1.5% drift, and the wall did not sustain any damage until a 2% drift.

Lee et al. (2007b) compared quasi-static and dynamic loading on several configurations of slip-track detailing and revealed that the partition damage is not amplified by dynamic loading comparing to that observed in quasi-static tests. In particular, this study highlighted that the damage was concentrated at the contact perimeter between partitions and ceilings

or other supporting structure. Furthermore, it was demonstrated that the repair of drywall partitions is not required up to drift levels of 0.25%. At drift levels of 2%, the repair costs of drywall partitions equal the initial costs, while at drift levels of 8%, they are twice the initial costs. This observation confirms the importance of partition walls in the resiliency of a building. This study also indicated that the strength of partition walls is not negligible with respect to the structural strength.

Retamales et al. (2013) evaluated the effect of different variables, such as frame thickness, connection type, wallboard thickness, and screw spacing, by both dynamic and quasi-static loading. It was shown that slip-track connections reduced damage associated with drift but increased the damage in the joints between the perpendicular walls compared to full connections. In addition, slip-track connections were associated with damage from studs popping out of tracks. Specifically, this study showed that damage was concentrated around the wall intersecting corners. Furthermore, details for mitigating seismic damage at the corners were developed and experimentally tested. In one of them, a gap is provided between intersecting walls with a sacrificial cornerbead sealing the joint (Figure 2-2). This detail substantially reduced the forces transferred to the partitions. Most of the damage was concentrated in the cornerbead elements, which are classified as DS 1 (easily repairable). However, testing was limited to in-plane, and for practical consideration, evaluations of other design considerations, including bidirectional seismic loading, are required (Retamales et al. 2013).

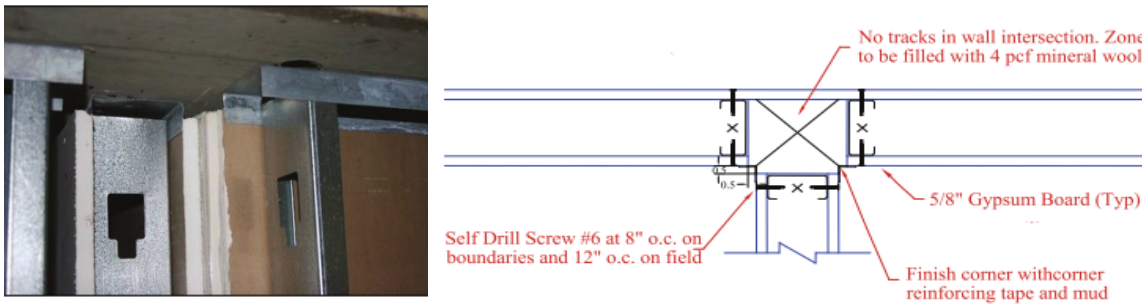

Figure 2-2: Gap detailing (Davies et al. 2011).

Araya-Letelier and Miranda (2012) evaluated the sliding/frictional connection of the wall at the top to the diaphragm for reducing the seismic effect on DPWs. In this connection, the upper track is not directly connected to the slab/beam. Instead, the upper track is placed between a thin plate connected to the upper slab and a square or rectangular short steel tube (Figure 2-3). This connection was shown to isolate the drywall partitions from the lateral structural deformations and increase the drift demands at which damage occurs. Moreover, the repair cost of DPWs with sliding/frictional connections and conventional connections corresponding to specific inter-story drifts were estimated.

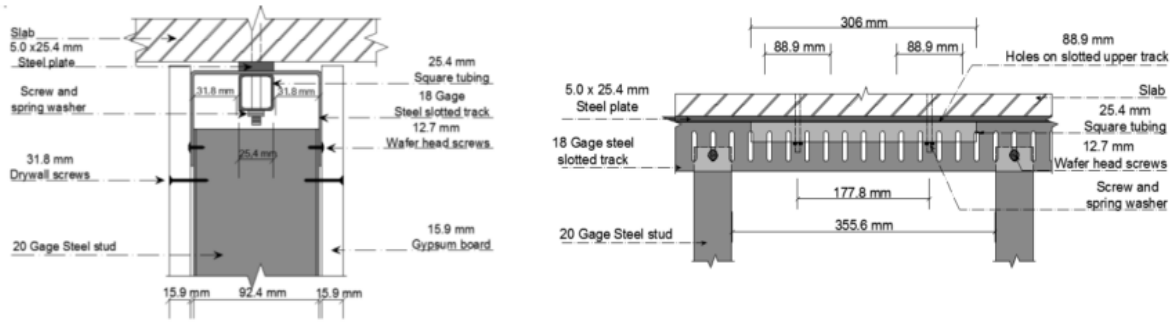

Figure 2-3: Sliding/frictional detailing (Araya-Letelier and Miranda 2012).

2.3.2 System-level tests

Wang et al. (2015) performed shake table tests of a full-scale 5-story building in both base-isolated and fixed-base configurations and with a full collection of nonstructural components and systems. The partition walls in this test were in full connection with a vertical slotted track at the top for accommodating vertical movement. In the base-isolated configuration, damage to the partition walls was minor since the story drift was very low, but in the fixed-based configuration, moderate and severe damage occurred at drift ratios of 0.66%-1.09% and 2.08%-2.75%, respectively.

Soroushian et al. (2016) tested a full-scale 5-story building on the E-Defense shake table, also in base-isolated and fixed-base configurations. In this test, the 4^{th} and 5^{th} floors were completed with a suspended ceiling, sprinkler-piping, and partition walls. DPWs were detailed with full connections on the 4th floor and slip-track connections on the 5th floor. Drifts were low, and horizontal floor accelerations remained below about 1g in all tests; thus, the effect of vertical ground motion dominated the observed damage. For slip-track connections, a new damage state related to vertical shaking was observed. Under large impact forces produced by the vertical motion, the top of the studs moved laterally or "popped out" from their constrained position within the top tracks (Figure 2-4).

Jenkins et al. (2016) performed a series of full-scale experiments on a ceiling-piping-partition system built on a 2-story steel braced-frame testbed. In this test, slip-track, full, and sliding/frictional connections were all considered. Slip track connections were observed to reduce damage in the wall compared to the other two connection types but

caused excessive corner damage. Walls with the sliding/frictional connection experienced damage characteristics of the full connection, such as dislodging of the head of the screw from the plaster coating and plastic hinging of studs.

Figure 2-4: Lateral movement of stud from the top track on slip track partitions (Soroushian et al. 2016).

The studies mentioned previously and others were used to develop DPW fragility functions for loss estimation as part of the FEMA P-58 project (Miranda and Mosqueda 2011). The source data for the fragilities includes (Freeman 1971, 1974, 1976; John A. Blume and Associates 1966, 1968; Lee et al. 2006, 2007b; Restrepo and Bersofsky 2011; Restrepo and Lang 2011; Retamales et al. 2013; Rihal 1982). Recently, the fragilities were updated by Mosqueda (2016), and two recent data sources were added (Chen et al. 2013; Jenkins et al. 2016). Moreover, the damage states were revised since partition wall losses estimated by the software far exceeded those reported in earthquakes. A new DS 0 was added that identifies minor damage that probably would not be repaired, such as hairline cracks or slight screw uplift. The other three damage states now initiate at larger drifts.

To the authors' knowledge, all previous system-level tests were conducted by dynamic loading, and specific interactions of DPWs with the primary structure and other

components were generally not reported. Since the damage in the partition wall is not amplified by dynamic loading (Lee et al. 2007b), quasi-static loading will allow a more careful evaluation of partition walls and their interaction with the structural system at each step. Moreover, most previous tests, both system-level and component level, lack a systematic comparison of in-plane and bidirectional loading of partition walls, which may affect their response considerably.

2.4 Test specimen

A single-story, 2-bay by 1-bay CLT post-tensioned rocking wall system has been designed and will be constructed at the NHERI Lehigh EF. This structure will be tested with and without DPWs to investigate the contribution of DPWs to the whole structure response. For simulating a full-scale realistic specimen, the bay dimensions are 30 ft by 15 ft, and columns are 12 ft high. The rocking wall system is composed of coupled hybrid walls connected by U-shaped flexural plates (UFP) for energy dissipation. The dimensions of each wall panel are 6 ft. x 20 ft in plan and 6.75" thick (Figure 2-5).

Three different test phases are planned, which utilize two different rocking wall to collector beam connections. Connection Type 1, used in Phases I and II, is a round pin through a vertical slot at the CLT wall that doesn't allow for gravity load transfer. Thus, the collector beams and floor diaphragm do not uplift as the CLT walls rock about the foundation. Connection Type 2, used in Phase III, is a pin through a circular hole that allows for gravity load transfer. As a result, the collector beams and floor diaphragm will uplift or distort as

the CLT walls rock about the foundation, which may affect the performance of the partition walls.

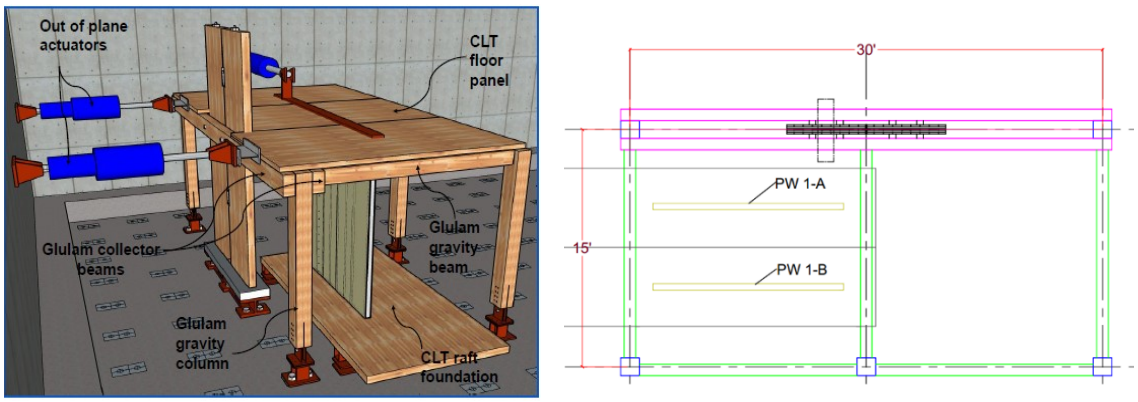

a b

Figure 2-5: (a) 3D rendering, (b) Plan view of phase I test at the NHERI Lehigh EF.

2.5 Partition walls

Each phase will utilize a different configuration and detailing of DPWs to address deficiencies observed in different tests and achieve different goals. In Phase I, the sliding response of a conventional slip-track system and telescoping assembly will be compared in two single walls with no return walls (Figure 2-5(b)). To our knowledge, seismic performance of slip track detailing has been tested using only tracks with standard leg length; Steel Stud Manufacturers Association (SSMA) single deflection track detail uses a deep leg to accommodate the vertical deflections (Figure 2-6(a)). This recommendation will be applied to eliminate the vertical popping out of studs. The Telescoping detailing has mainly been used to accommodate vertical deflection (Figure 2-6(b)). To our knowledge, no tests to date have assessed the seismic behavior of the telescoping detail, although FEMA E-74 (Applied Technology Council 2012) has suggested it for vertical or

lateral movement. It is hypothesized that the telescoping detail will eliminate the damage due to lateral popping out of end studs from the track.

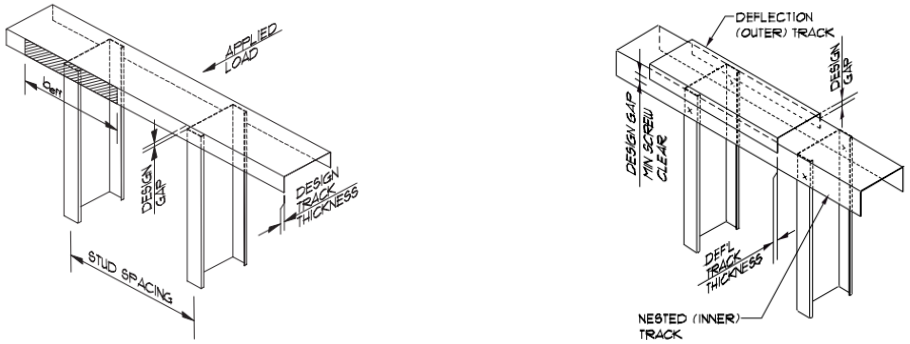

a b

Figure 2-6: (a) Single deflection track (SSMA), (b) Telescoping assembly (SSMA)

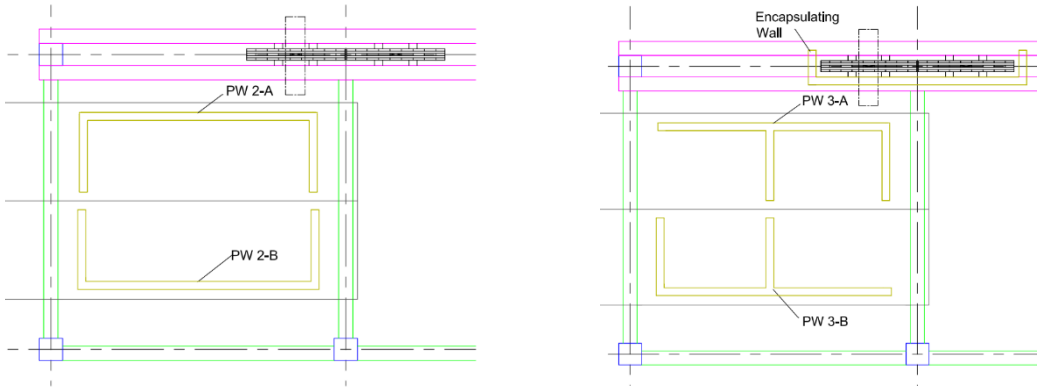

a b

Figure 2-7: Plan view of tests set up with partition wall layout for (a) phase II, (b) phase III.

In Phase II, two different gap details for minimizing damage at wall intersections will be compared in C-shaped walls incorporating traditional slip track detailing (Figure 2-7(a)). Detail A is a concentrated gap at the corner (Davies et al. 2011) that allows the two intersecting walls to penetrate into the corner to prevent damage (Figure 2-8). As mentioned previously, this gap configuration performed satisfactorily during prior unidirectional tests (Retamales et al. 2013), but it has not been studied bi-directionally. In

addition, the first studs were moved 2" away from the corners to prevent the studs from popping out at the corners.

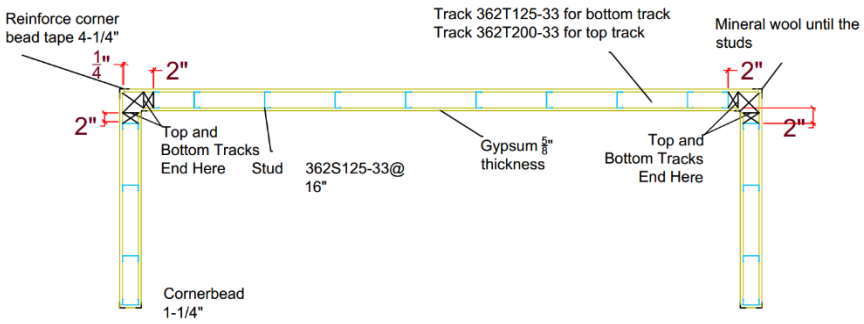

Figure 2-8: DPW A in phase II

Detail B, referred to as the distributed gap, positions 0.5" control joints periodically along the wall (Figure 2-9). The control joints are typically installed to relieve internal stresses due to expansion and contraction; however, it is hypothesized that additional seismic movement can be accommodated by increasing the number of control joints, and they are already standard construction practices. In this specimen, both fire-rated and non-fire-rated expansion joints will be used.

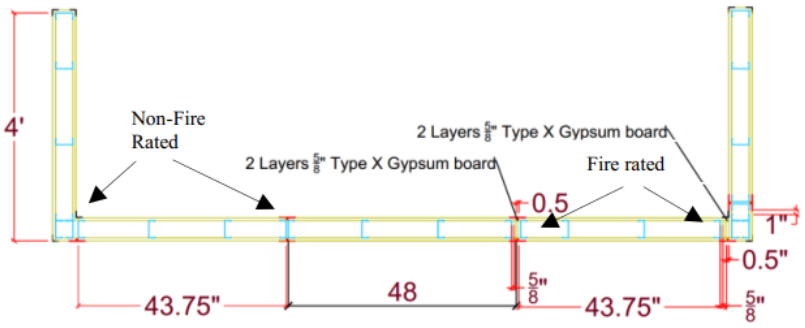

Figure 2-9: DPW B in phase II

Phase III of the experiment will incorporate the best slip detailing from Phase I and the best gap detailing from Phase II in walls with corner and T-intersections (Figure 2-7(b)). Recall that Phase III will incorporate the pin detail that does not allow relative movement between the collector beam and CLT rocking wall; thus, diaphragm deformation is expected. The effect of this diaphragm deformation will be examined by encapsulating the rocking CLT wall with partition walls, as envisioned in practice for fire protection (Figure 2-7(b)).

2.6 Loading protocol

A bidirectional loading protocol has been developed for this test. The path of movement is shown in Figure 2-10 (a). The basis of this loading protocol is FEMA 461 (Applied Technology Council 2007), but the in-plane drift and out-of-plane drift are increased sequentially. Each full cycle commences with an increase in in-plane drift and includes three sub-cycles: in-plane, bidirectional, and bidirectional, with increased out-of-plane drift. The in-plane sub-cycle is repeated to identify deterioration effects on the wall. The bidirectional sub-cycles combine in-plane and out-of-plane drift to trace out a hexagon. For each full cycle, the peak out-of-plane drift corresponds to half of the in-plane drift. The increase in peak in-plane drift in each cycle is shown in Figure 2-10 (b). The drift increment is based on an algorithm generated by Retamales et al. (2008) for in-plane loading.

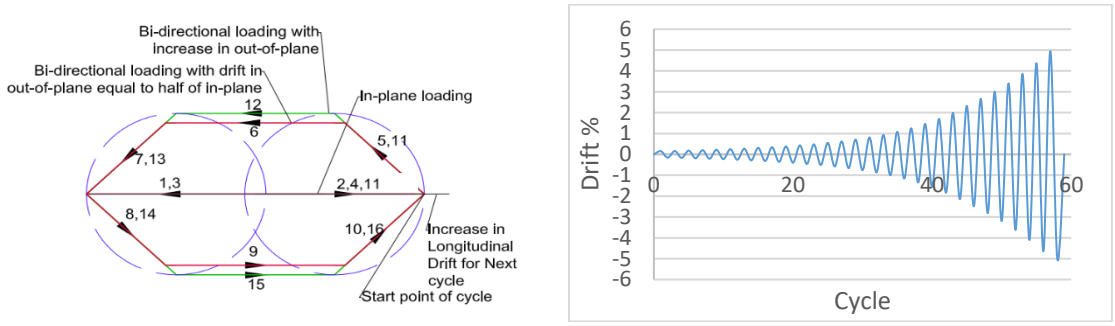

a b

Figure 2-10: (a) Path traced by a full cycle of bidirectional loading with three sub-cycles, (b) Increase of loading in each cycle

2.7 Conclusions

An extensive literature review of previous tests on DPWs has been conducted to understand the state-of-the-art and identify potential opportunities to improve the seismic performance of DPWs. Slip-track connection detailing has produced the best performance, but damage at intersections with return walls still occurs at relatively low drift levels compared to the capacity of CLT rocking walls. Thus, alternative (Telescoping) slip detailing will be investigated, as well as two gap details to reduce the damage at wall intersections. Furthermore, to the authors' knowledge, these will be the first tests to apply controlled bidirectional loading to evaluate the effect of out-of-plane loading on the in-plane resistance of the walls.

Despite the stated intent of previous system-level tests, interactions between nonstructural walls and other components have not been reported. For tall CLT rocking wall lateral systems, the interaction between DPWs and rocking walls is expected due to the local

diaphragm deformation next to the CLT; thus, a system-level test for inspection of this interaction is necessary.

2.8 Acknowledgments

This material is based upon work supported by the National Science Foundation under Grant No. CMMI-1635363 and CMMI-1635227. Any opinions, findings, conclusions, or recommendations expressed in this publication are those of the authors and do not necessarily reflect the views of the National Science Foundation.

2.9 References

Applied Technology Council. (2007). Interim testing protocols for determining the seismic performance characteristics of structural and nonstructural components -FEMA 461.

Applied Technology Council. (2012). Reducing the risks of nonstructural earthquake damage – A practical guide - FEMA E-74.

Araya-Letelier, G., and Miranda, E. (2012). Novel sliding/frictional connections for improved seismic performance of gypsum wallboard partitions. 15th World Conference on Earthquake Engineering, Lisbon, Portugal, 0–9.

Buchanan, A., Deam, B., Fragiacomo, M., Pampanin, S., and Palermo, A. (2008). Multi-storey prestressed timber buildings in New Zealand. Structural Engineering International: Journal of the International Association for Bridge and Structural Engineering (IABSE), 18(2), 166–173.

https://doi.org/10.2749/101686608784218635

Chen, M., Pantoli, E., Wang, X., Astroza, R., Ebrahimian, H., Mintz, S., Hutchinson, T., Conte, J., and Restrepo, J. (2013). BNCS Report #1: Full-scale structural and nonstructural building system performance during earthquakes and post-earthquake fire – specimen design, construction, and test protocol. (December 2013), 1–338. Retrieved from http://bncs.ucsd.edu/resources/BNCS-SSRP-Report2-Final.pdf

Davies, R. D., Retamales, R., Mosqueda, G., and Filiatrault, A. (2011). Experimental seismic evaluation, model parameterization, and effect of cold-formed steel-framed gypsum partition walls on the seismic performance of an essential facility-MCEER-11-0005.

Freeman, S. A. (1971). Third progress report on racking tests of wall panels-Report JAB-99-54. San Francisco, California, U.S.A.

Freeman, S. A. (1974). Fourth progress report on racking tests of wall panels-Report JAB-99-55. San Francisco, California, U.S.A.

Freeman, S. A. (1976). Racking tests of high-rise building partitions. Journal of the Structural Division, Proceedings of the American Society of Structural Engineers, 103(8), 1673–1685.

Ganey, R. S. (2015). Seismic design and testing of rocking cross-laminated timber walls. The University of Washington (Doctoral dissertation).

Jenkins, C., Soroushian, S., Rahmanishamsi, E., and Maragakis, E. M. (2016). Experimental fragility analysis of cold-formed steel-framed partition wall systems. Thin-Walled Structures, 103, 115–127. https://doi.org/10.1016/j.tws.2016.02.015

John A. Blume and Associates. (1966). First progress report on racking tests of wall panels-Report NVO-99-15. San Francisco, California, U.S.A.

John A. Blume and Associates. (1968). Second progress report on racking tests of wall panels-Report NVO-99-35. San Francisco, California, U.S.A.

Lee, T.-H., Kato, M., Matsumiya, T., Suita, K., and Nakashima, M. (2006). Seismic performance evaluation of nonstructural components: drywall partitions. Annals of the Disaster Prevention Research Institute, 177–188. Kyoto University.

Lee, T.-H., Kato, M., Matsumiya, T., Suita, K., and Nakashima, M. (2007). Seismic performance evaluation of nonstructural components: Drywall partitions. Earthquake Engineering and Structural Dynamics, 36, 367–382. https://doi.org/10.1002/eqe.638

Miranda, E., and Mosqueda, G. (2011). Seismic fragility of building interior cold-formed steel framed gypsum partition walls-FEMA P-58/BD-3.9.2. Redwood City, California.

Mosqueda, G. (2016). Interior cold-formed steel framed gypsum partition walls - Background document FEMA P-58/BD-3.9.32.

Restrepo, Jos I., and Bersofsky, A. M. (2011). Performance characteristics of light gage

steel stud partition walls. Thin-Walled Structures, 49(2), 317–324. https://doi.org/10.1016/j.tws.2010.10.001

Restrepo, José I., and Lang, A. F. (2011). Study of loading protocols in light-gauge stud partition walls. Earthquake Spectra, 27(4), 1169–1185. https://doi.org/10.1193/1.3651608

Retamales, R., Davies, R., Mosqueda, G., and Filiatrault, A. (2013). Experimental seismic fragility of cold-formed steel framed gypsum partition walls. Journal of Structural Journal of Structural Engineering, 139(August), 1285–1293. https://doi.org/10.1061/(ASCE)ST.1943-541X.0000657.

Retamales, R., Mosqueda, G., Filiatrault, A., and Reinhorn, A. (2008). New Experimental Capabilities and Loading Protocols for Seismic Qualification and Fragility Assessment of Nonstructural Systems.

Rihal, S. S. (1982). Behavior of non-structural building partitions during earthquakes. Seventh Symposium on Earthquake Engineering, 1, 267–277. University of Roorkee.

Soroushian, S., Maragakis, E. M., Ryan, K. L., Sato, E., Sasaki, T., Okazaki, T., and Mosqueda, G. (2016). Seismic simulation of an integrated ceiling-partition wall-piping system at e-defense . II : evaluation of nonstructural damage and fragilities. 142(2), 1–17. https://doi.org/10.1061/(ASCE)ST.1943-541X.0001385.

Taghavi, S., and Miranda, E. (2003). Response assessment of nonstructural building elements. Report PEER 2003/05, Pacific Earthquake Engineering Research Center,

University of California, Berkeley, 96.

Tasligedik, A.S., Pampanin, S., and Palermo, A. (2012). In-Plane cyclic testing of nonstructural drywalls infilled within RC frames. 15th World Conference on Earthquake Engineering (15WCEE). Lisbon, Portugal.

Tasligedik, Ali Sahin, Pampanin, S., and Palermo, A. (2013). Low damage seismic solutions for nonstructural drywall partitions. Vienna Congress on Recent Advances in Earthquake Engineering and Structural Dynamics (VEESD 2013*)*, 11. https://doi.org/10.1007/s10518-014-9654-5

Wang, X., Elide Pantoli T. C., Hutchinson J. I., Restrepo R. L., Wood M. S., Hoehler P. G., Sesma F. H., and Sesma F. H.. (2015). Seismic performance of cold-formed steel wall systems in a full-scale building. Journal of Structural Engineering 141 (10): 1–11. doi: 10.1061/(ASCE)ST.1943-541X.0001245.

3 Dynamic behavior of mass timber building with cross-laminated timber rocking wall

(This chapter is a standalone manuscript that has been submitted for publication in Earthquake Engineering and Structural Dynamics: "Hasani, H., Ryan, K., Wichman S., Berman, J. (2021) (Submitted) Dynamic behavior of mass timber building with cross-laminated timber rocking wall, *Earthquake Engineering and Structural Dynamics*")

3.1 Abstract

Self-centering rocking wall systems are novel structural systems for seismic regions. Recent studies have reported high-frequency acceleration spikes in the horizontal and vertical direction of rocking wall systems during the impact of the wall base with the foundation. Some have concluded that self-centering rocking walls generally have much larger peak accelerations than more traditional systems. One component that can affect the dynamic behavior of the structure is the diaphragm and its connectivity to the wall. Data from a two-story mass timber building tested at the NHERI@UCSD outdoor shake-table in 2017 shows that although acceleration spikes are observed in cross-laminated timber (CLT) rocking walls, they have been attenuated in the diaphragms. Moreover, this paper demonstrates that modeling assumptions affect the propagation of accelerations through rocking walls and diaphragms. The assumption of rigid diaphragms can predict the fundamental mode, displacement, and acceleration of the structure with acceptable accuracy. However, it cannot predict the high-frequency accelerations resulting from wall

impact. A flexible diaphragm assumption with distributed mass helps to predict the floor acceleration spectra more accurately.

3.2 Introduction

In recent years, mitigating seismic risk has come to include concepts of resiliency against natural hazards. A resilient structure has the ability to quickly recover its functionality after experiencing the effects of an earthquake. To achieve this aim, mitigating damage to both structural and nonstructural components is essential. Considerable research in the past few years has led to new structural systems intended to increase building resiliency. Post-tensioned rocking walls have been proposed as a class of high-performance systems capable of resisting earthquake-induced lateral loads (Priestley et al. 2014) while limiting damage to the structural system. Such walls are detailed to allow unrestrained rocking of the wall at the base. Damage to rocking walls is generally limited to minor damage at the rocking toe. Energy dissipation occurs through the base rocking, and is frequently supplemented by energy dissipation devices, such as U-shaped Flexural Panels (UFP) or other steel energy dissipators. Post-tensioning bars spanning the height of the wall provide a recentering force. The post-tensioned wall concept was originally conceived for precast in concrete systems, and has now been extrapolated to mass timber walls. This study focuses on post-tensioned rocking walls built from cross-laminated timber (CLT) panels. Previous tests have shown great potential for these walls as a resilient lateral load resistant system for buildings in high seismic areas, as they can develop and sustain large drift demands with only minor damage (Buchanan et al. 2008a; Ganey 2015). However, seismic

events over the years have highlighted that even well-designed structures capable of high performance and limited damage to the lateral load resistant system are still susceptible to significant financial losses if the demand on nonstructural elements is high and/or they are poorly designed or detailed.

One rocking wall seismic response feature is a gap opening and closing phenomenon at the wall base, characterized as impact, in a dynamic domain. Some studies have shown that this phenomenon induces short-duration, large-amplitude acceleration spikes in both the horizontal and vertical directions, which is not common in conventional seismic force-resisting systems (Belleri et al. 2014; Marriott et al. 2008; Qureshi and Warnitchai 2016; Schoettler et al. 2009; Toranzo-Dianderas 2002). These acceleration spikes, observed with higher intensity near the rocking joint, appear in the response for a brief time interval with a phase lag following the peak displacement. Although these acceleration spikes are out of phase with displacement response and do not affect the lateral load resisting system, they can cause damage or failure of stiff, acceleration-sensitive nonstructural components (Aragaw and Calvi 2018). In particular, Mayes et al. (2013) performed a comparative numerical study of six different structural systems for a three-story commercial and laboratory building, including a moment frame, buckling restrained braced frame, viscously damped moment frame, Pres-Lam timber coupled-walls, cast-in-place reinforced concrete shear wall, and base-isolated braced frame. The performance of these structures was compared using FEMA P-58, *Development of Next-Generation Performance-Based Seismic Design Procedures for New and Existing Buildings* (FEMA 2012). The Pres-Lam system is a variant of the system considered here, using coupled post-tensioned timber

rocking walls with UFPs and external steel dampers. This numerical study suggested that the Pres-Lam system generates the highest in floor spectral accelerations for periods lower than 0.3 seconds among the six lateral systems considered, which negatively impacts the performance of acceleration-sensitive nonstructural components.

However, accelerations in all rocking wall systems might not be as problematic as suggested in the study. They may depend on both materials, detailing, and propagation of these accelerations to the locations where nonstructural components reside. Therefore, special attention should be given to propagating accelerations through the structure and selecting modeling strategies that accurately reflect it. High amplitude acceleration spikes in the wall may not be transmitted to the nonstructural components depending on the detailing of the wall-diaphragm connection and the diaphragm flexibility; the components are generally attached to floors and thus are somewhat isolated from the walls.

Post-tensioned rocking wall systems have been tested under monotonic, cyclic, and dynamic loading protocols (Buchanan et al. 2008a; Ganey 2015; Marriott et al. 2008; Nazari and Sritharan 2020; Pei et al. 2019; Schoettler et al. 2009). However, only a limited number of these experiments were tested under dynamic loading, and the majority of them were component tests on a single rocking wall (Marriott et al. 2008; Nazari and Sritharan 2020; Toranzo-Dianderas 2002) and cannot provide information about the propagation of system accelerations. While some of the experiments were conducted as system-level tests (Pei et al. 2019; Schoettler et al. 2009), few researchers have specifically evaluated acceleration propagation. Significant high amplitude accelerations associated with high-frequency vibration were observed during the shake table tests of a confined masonry

rocking wall (Toranzo-Dianderas 2002) and a concrete rocking wall (Belleri et al. 2014). In particular, Toranzo-Dianderas tested rocking walls in a confined masonry frame on a shake table and assessed the effect of rocking wall impact on the horizontal diaphragm accelerations; these impacts were found to induce acceleration spikes on the diaphragm. However, the diaphragm was connected to the side of the wall by a hinge. Moreover, the dissipators were found to significantly reduce the effect of impact on the system (Toranzo-Dianderas 2002).

A few studies numerically assessed the dynamic behavior of rocking wall systems (Belleri et al. 2014; Qureshi and Warnitchai 2016; Wiebe and Christopoulos 2010). Belleri et al. (2014) studied the finite element modeling of rocking walls and compared different modeling techniques incorporating 1D to 3D wall elements. The 2D and 3D approaches used plane-stress plate and brick elements, respectively, for the wall and "surface to surface contact" interaction for the wall and foundation connections, while the 1D approach incorporated beam elements with compression-only springs or concentrated rotational springs at the bottom of the wall. The interaction between the rocking wall and the building was neglected in their models. Belleri et al. showed that, among 1D element models, multi compression-only springs lead to the best global response approximation in nonlinear static analysis. In contrast, the model with a concentrated rotational spring does not allow uplift at the base nor capture any pounding effect at the bottom of the rocking wall. Belleri et al. also showed that while the 2D and 3D models can provide results similar to experimental tests with just material damping, the 1D element models are susceptible to global damping assumptions for both response predictions and achieving convergence. Qureshi et al.

(2016) focused on acceleration spikes in a concrete rocking wall building. They found that the acceleration spikes depend on the lateral velocity at impact and the initial contact stiffness, and suggested a velocity-dependent device along with a soft contact for reducing these effects. Wiebe et al. (2010) observed that, numerically, the acceleration spikes are due to abrupt changes in stiffness in the nonlinear system. They developed a mathematical closed-form solution to show that these accelerations originate when stiffness changes from lower values to higher values (gap closure). Moreover, they found that peak horizontal accelerations are reduced when energy dissipaters are included. Ultimately, the wall base contact behavior needs to be modeled to successfully reproduce the impact-induced acceleration spikes.

Another crucial member in the lateral load resisting systems is the diaphragm, which has a vital role in distributing the forces between members. The overall stiffness of the diaphragm is a combination of the diaphragm unit stiffness and the connection deformation between the diaphragm unit and the rocking wall. The effects of diaphragm flexibility are: to determine the distribution of forces between lateral load resisting systems, increase inter-story drift at the diaphragm midspan compared to the wall alone, and potentially induce higher mode effect in dynamic response. Moroder (2016) evaluated post-tensioned timber rocking walls considering the diaphragm flexibility, which was found to increase the building first mode period. Similar findings on other types of structures confirmed the natural period elongation as well (Fleischman and Farrow 2001; Ju and Lin 1999; Lee et al. 2007a).

The connection between the rocking wall and diaphragm can be a pin, pin into a vertical slotted connection, group of bolts, external blocks pushing against the wall, steel angle with slotted holes (Moroder et al. 2014). Moroder et al. (2014) showed that the pin connection could eliminate the rotational incompatibility of the diaphragm and wall, but that a pin into a slotted connection was not successful in eradicating uplift incompatibility due to the existence of friction.

While rocking-induced acceleration effects in the rocking walls and diaphragm flexibility effects have been well studied in isolation, little work has been done to study the combination of these effects. Rocking wall pounding, wall-to-diaphragm connection details, and diaphragm flexibility can affect the propagation of accelerations to the building floor system where they are "felt" by various attached nonstructural components.

The overall objectives of this research are: 1) to evaluate acceleration demands and the propagation of accelerations from the rocking wall to the diaphragm in a full-scale system-level test; 2) to assess the effect of different modeling assumptions, including the diaphragm connection to the lateral load resisting system and diaphragm flexibility, in reproducing these accelerations. For this purpose, this paper describes the experimental results of a shake table test on a full-scale two-story mass timber building with CLT rocking walls conducted at NHERI@UCSD as part of the NHERI TallWood project (“NHERI TallWood-Home” 2021). A simple modeling procedure aimed at predicting accelerations in the rocking walls and diaphragms is developed and validated by the experimental data. In this model, both the differential movement of the slotted connection and the diaphragm flexibility are considered.

3.3 Test program

Pei et al. (2019) tested a full-scale two-story mass timber building; the lateral force-resisting system consisted of two coupled post-tensioned CLT rocking walls. The diaphragms were connected directly to both walls and cantilevered out over both ends while supported by gravity framing. The test specimen was designed for 1D shaking, and in the other direction, braces were used for stability.

Figure 3-1 shows a photo (Figure 3-1a) and 3D rendering (Figure 3-1b) of the test specimen. The rocking walls were connected to the diaphragms using dowel-type steel shear keys (pins). Each dowel was inserted into a vertically slotted hole to transfer shear force between the diaphragm and the rocking wall while isolating the diaphragm from the rocking wall uplift. In this test, horizontal accelerations in the direction of shaking were measured in both the rocking walls and the diaphragms.

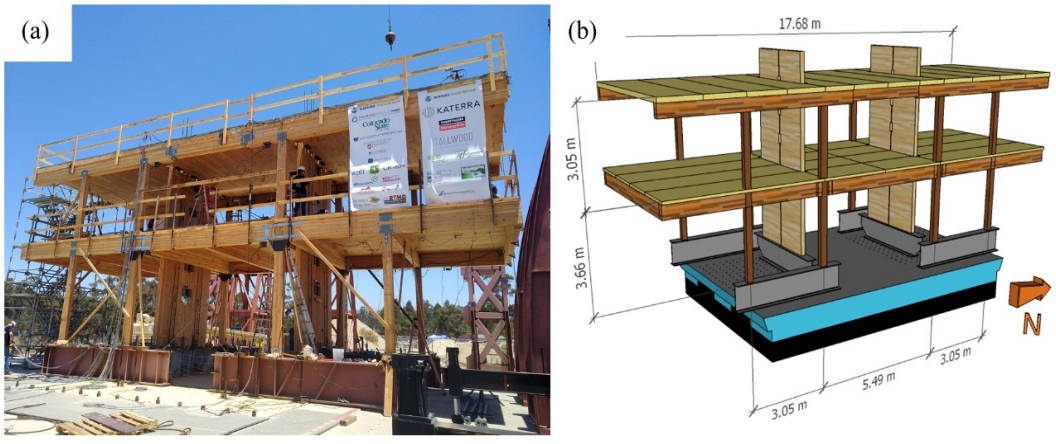

Figure 3-1: Structural test specimen: (a) Photo ("NHERI TallWood-Home" 2021), (b) 3D rendering with dimensions

3.3.1 Test-specimen description

The first and second story heights were 3.66 m and 3.05 m, respectively. The overall footprint of the building was 6.10 m x 17.68 m. Each coupled rocking wall was made from two five-ply 1.52 m x 7.32 m x 0.175 m thick panels, which had an elastic modulus of 8536 MPa and a yield strain of 0.0029. Coupling was achieved with five UFPs, distributed over the wall height for energy dissipation. Each UFP was 10 mm thick, 114 mm wide, and 92 mm in diameter. A 25-mm gap separated the rocking wall panels, and then connected at the UFPs, which were set into wall panel cutouts. Each wall was supported by four 19 mm diameter post-tensioning bars, located eccentrically 127 mm from the centerline of the rocking wall panel. Each bar was post-tensioned with an initial force of 53.4 kN, and the yield strength was 179.7 kN.

The gravity framing, consisting of glulam beams (grade 24F-V4) and columns (grade L2), was designed to accommodate the significant drift demands. The gravity columns in the center of the building were continuous through to the roof (balloon-framed), while the remaining spanned floor-to-floor (platform-framed). The dimensions of gravity columns and beams are tabulated in Table 3-1, and the location of beams is shown in Figure 3-2. Two types of column base connections were used, both of which had a slotted hole that acted as a pin connection. Three types of beam-column joints were included; all were detailed as pin connections in the vibration direction.

The structure was built upon stiffened foundation beams shown in Figure 3-3. The base beams supporting the rocking walls yielded under the toes of each of the rocking walls.

While timber walls are flexible (relative to concrete) to begin with, the base beam yielding is believed to have reduced the impact and related acceleration spikes by softening the transition from no contact to high contact stiffness, while also increasing the displacement of the wall. Figure 3-3 shows the dimensions of the building section and the rocking walls. Further information about the general design procedure and construction can be found in Pei et al. (2019).

Table 3-1: Dimension of gravity beams and columns

Gravity framing	Section dimension
Beam 1-A	171 * 495 mm2
Beam 1-B	222 * 495 mm2
Beam 2-A	222 * 457 mm2
Beam 2-B	222 * 381 mm2
Balloon-framed Columns	222 * 190 mm2
Platform-framed Columns	273 * 190 mm2

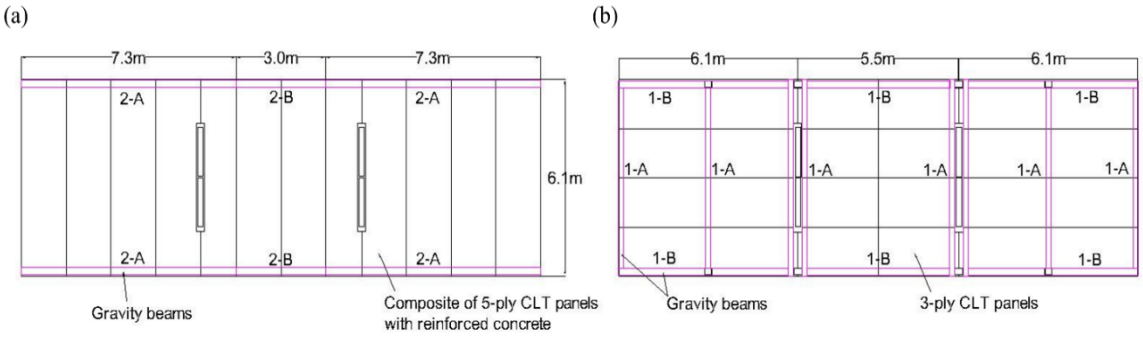

Figure 3-2: Plan view of CLT panels: (a) Floor, (b) Roof

3.3.1.1 Diaphragm design

The layout of the CLT panels and the glulam beams for the floor and roof diaphragms are illustrated in Figure 3-2. The floor diaphragm was constructed from 3-ply CLT panels, while the roof diaphragm was a composite of 5-ply CLT panels and 63.5 mm thick

reinforced concrete. The CLT panels were tied together using surface splines with screws. Chord splices were screwed to the CLT panels. On the roof diaphragm, the concrete was connected to CLT by self-tapping screws inclined at 45 degrees. The floor and roof weighed 428.76 kN and 441.35 kN, respectively, including the mass of diaphragm panels, beams, columns, CLT rocking wall panels, and seismic mass plates. Further information regarding the diaphragms can be found in (Barbosa et al. 2018, 2021).

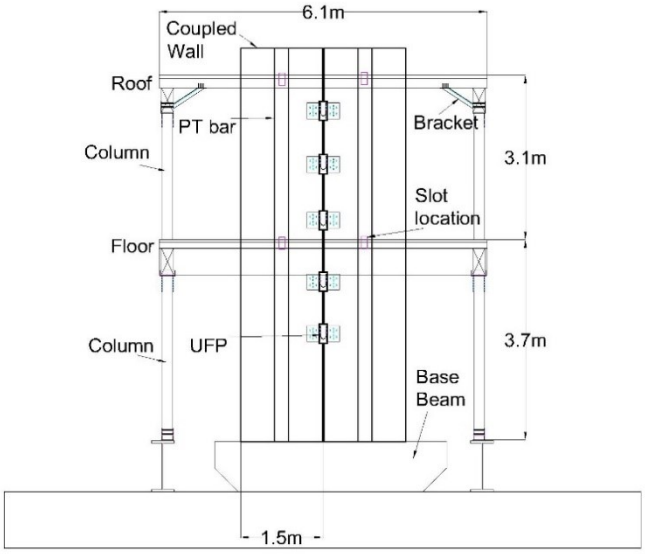

Figure 3-3: Rocking wall elevation with dimensions

3.3.2 Ground motion and instrumentation

The structure was densely instrumented with accelerometers, which facilitated examining the research questions of this study. Accelerometers distributed on the elevation of the rocking wall and over the floor plan and diaphragms are shown in Figure 3-4. A 30 Hz filter was applied to all accelerations presented here for noise-cancellation purposes. The story displacements were measured by string pots spanning from the diaphragms (at

corners and mid-plan) to fixed points off the table, from which story drifts were derived. These measurements also allowed relative diaphragm movements to be evaluated. Linear pots measured the uplift displacements of the rocking wall at the wall base, and movement across each slotted pin connection was measured by a string pot connected to the pin and the wall.

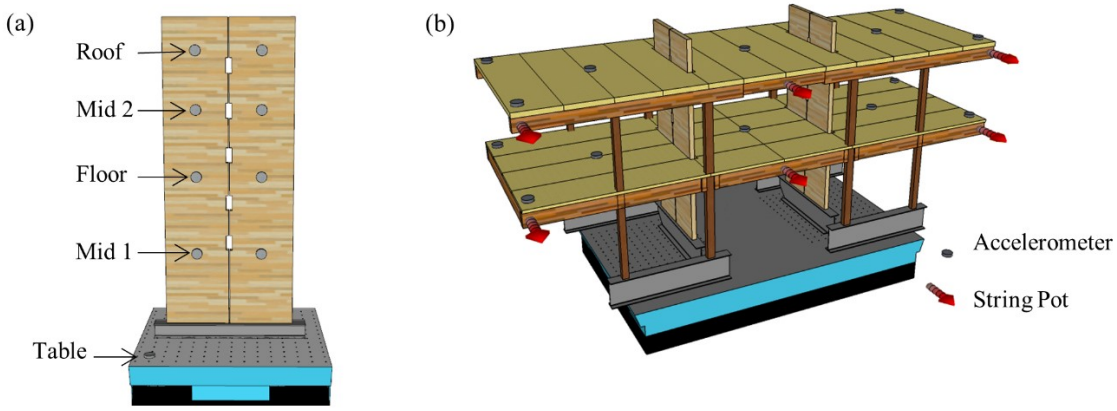

Figure 3-4: Accelerometer plans: (a) Rocking wall, (b) Diaphragm

The test building was subjected to a total of 14 earthquake excitations in the east-west direction, selected to represent three hazard levels for the San Francisco site: (1) service-level earthquake (SLE, i.e., 50% probability of exceedance in 50 years), (2) design-basis earthquake (DBE, 10% probability of exceedance in 50 years), and (3) risk-adjusted maximum considered earthquake (MCE_R, defined by the mapped USGS MCE_R hazard). Ground motion records from past California earthquakes were applied (Table 3-2). The records were scaled to match the spectral acceleration at the approximate natural period of the 2-story wood building estimated using the empirical formula in ASCE 7-10 (American society of civil engineers 2017). In this study, the results of two MCE level excitations are

studied in detail: Northridge-MCE (Record 12) Superstition Hills-MCE (Record 13), referred to hereafter as SH and NR.

Table 3-2: Ground motions

Test	Earthquake	Station	Intensity	PGA (g)	Sa @ 0.9 sec (g)
1	Loma Prieta	Capitola	SLE	0.17	0.16
2	Loma Prieta	Capitola	SLE	0.19	0.16
3	Northridge	Canoga Park	SLE	0.19	0.18
4	Superstition Hills	Poe Road	SLE	0.13	0.12
5	Northridge	Canoga Park	DBE	0.54	0.7
6	Northridge x2	Canoga Park	DBE	0.56	0.76
7	Imperial Valley	Delta	SLE	0.14	0.22
8	Northridge x2	Canoga Park	DBE	0.55	0.76
9	Loma Prieta	Capitola	DBE	0.54	0.50
10	Superstition Hills	Poe Road	DBE	0.48	0.43
11	Loma Prieta	Capitola	MCE	0.66	0.58
12	Northridge	Canoga Park	MCE	0.76	0.92
13	Superstition Hills	Poe Road	MCE	0.68	0.63
14	Northridge	Canoga Park	MCE x1.2	0.89	1.12

3.4 Test results

White noise motions were applied to the building before and after each test to assess changes to the dynamic properties of the structure. The white noise excitation had a PGA of 0.03 g and a duration of 2 min. For the synthesis of data, Fourier-transforms of the white noise motions were calculated. Figure 3-5 shows the Fourier-transform of white noise 17, which was implemented between SH and NR. Based on the synthesis of the data, the natural period was 0.91 seconds (1.1 Hz) and was measured by all sensors at floor, roof, and wall locations. The second mode period was determined to be 0.31 seconds (3.2 Hz), as measured by floor and roof sensors only (Figure 3-5(b, c)). However, this mode was more evident in the roof after Record 7, probably due to minor cracks in the concrete after

a few runs. The third mode period of 0.09 seconds (11.5 Hz) was measured by sensors on the wall only (Figure 3-5a). The wall sensor also suggests a possible fourth mode period at 0.04 sec (25.5 Hz); however, the signal is not distinct enough to be certain.

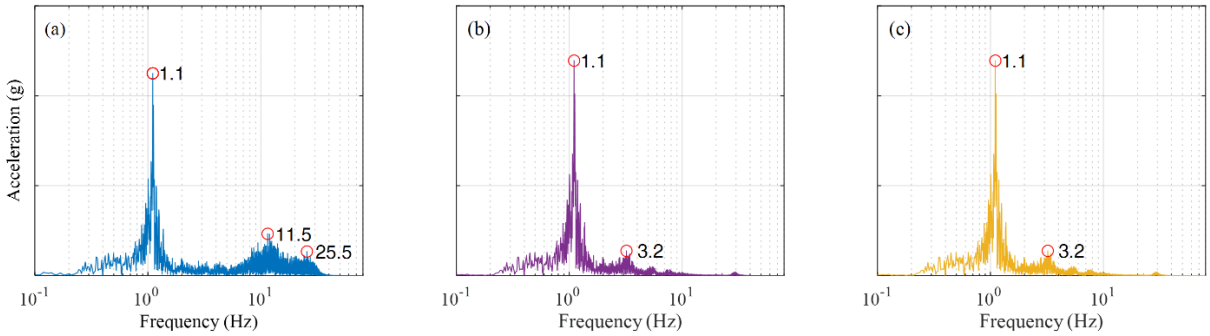

Figure 3-5: Fourier transform of white noise acceleration data recorded on the (a) Wall at roof level, (b) Diaphragm at floor level, and (c) Diaphragm at roof level

3.4.1 Investigation of accelerations in the experiment

Figure 3-6(a, c) shows the recorded wall acceleration histories at approximately mid-height (the elevation of the floor diaphragm) for NR and SH, respectively. Similarly, Figure 3-6(b, d) shows the recorded accelerations of the floor diaphragm for NR and SH, respectively. Figure 3-7 shows the acceleration spectra from the acceleration histories for the wall from acceleration histories for the wall at four levels, namely, midway up the first level (labeled Mid1), at the floor diaphragm, midway up the second level (labeled Mid 2) and at the roof for the NR (Figure 3-7a) and SH (Figure 3-7b) motions. Figure 3-7 also shows the acceleration spectra from the acceleration histories of the shake table and at the center of the floor and roof diaphragms for the NR (Figure 3-7c) and SH (Figure 3-7d) motions. By visual inspection of Figure 3-6, the main vibration frequency is the same for

the wall and floor accelerations. However, the wall accelerations exhibit high-frequency wave packets (Figure 3-6(a, c)). Likewise, the corresponding spectra (Figure 3-7(a, b)) exhibited a peak at a period between 0.03 to 0.04 seconds that increased significantly from the table to the roof level. This is believed to reflect a horizontal acceleration spike due to the pounding effect of the rocking wall. However, these horizontal acceleration spikes were attenuated significantly from the wall to the diaphragms. Visually, the characteristic frequency of the higher frequency wave is much lower in the floor diaphragms (Figure 3-6(b, d)). Furthermore, the peak spectral acceleration at the 0.03-0.04 sec period in the rocking wall ranged from 3g to 6g for the NR motion and from 4g to 10g for the SH motion (Figure 3-7(a, b)); however, there was not any noticeable peak at this period in the spectra for the diaphragms (Figure 3-7(c, d)).

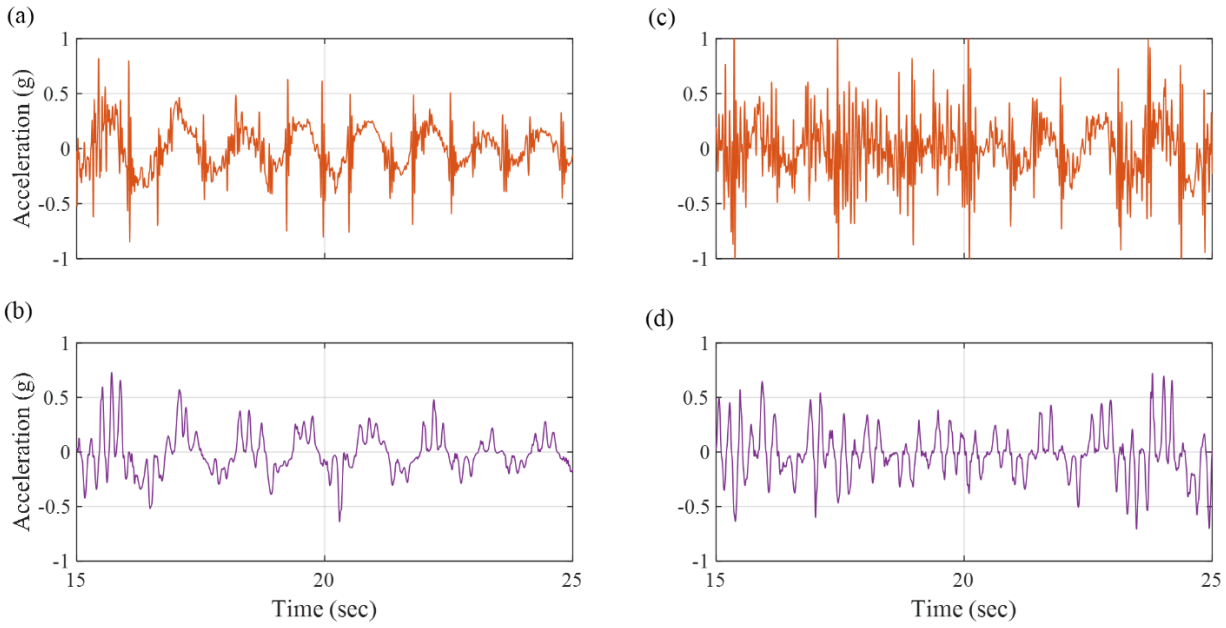

Figure 3-6: Acceleration histories: (a) Wall accelerometers at floor level - NR, (b) Floor diaphragm accelerometers - NR, (c) Wall accelerometers at floor level - SH, (d) Floor diaphragm accelerometers – SH

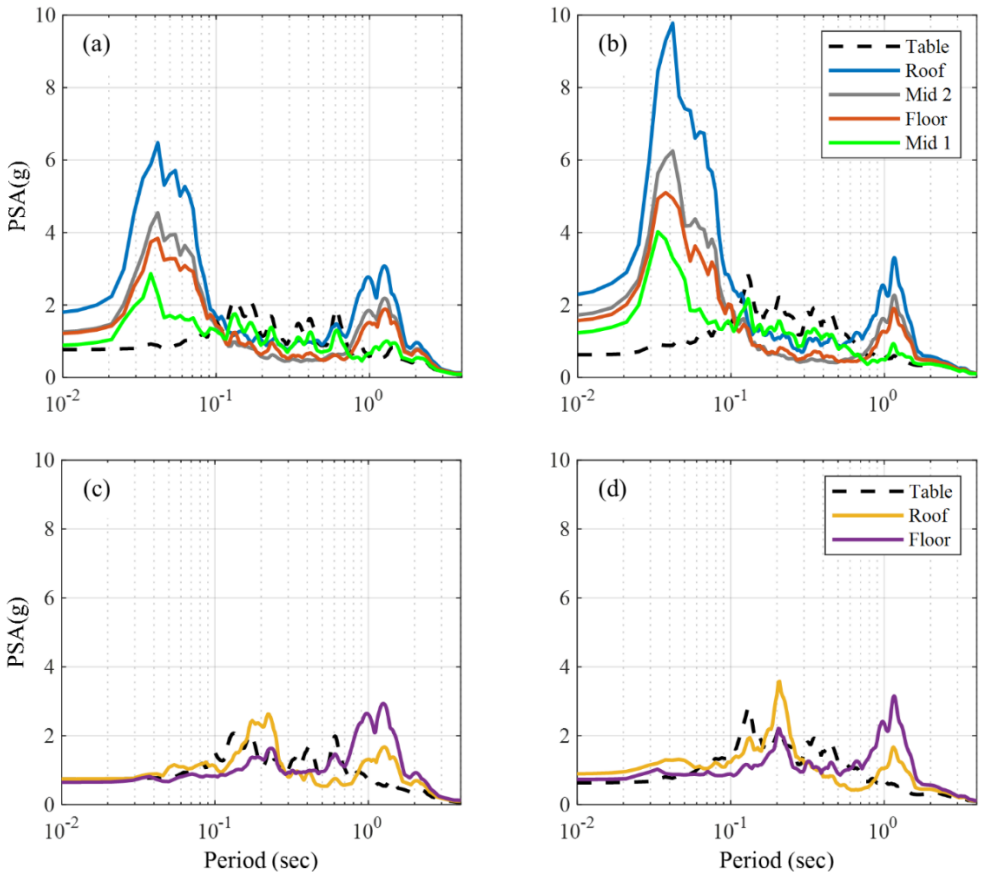

Figure 3-7: Spectral acceleration response (a) Wall accelerometers - NR, (b) Wall accelerometers - SH, (c) Diaphragm accelerometers - NR, (d) Diaphragm accelerometers - SH

It is instructive to evaluate these accelerations with reference to the equation for minimum horizontal seismic design force F_p for nonstructural components in ASCE 7-16 (American society of civil engineers 2017):

$$F_p = \frac{0.4 a_p S_{DS} W_p}{\left(\frac{R_p}{I_p}\right)} \left(1 + 2\frac{z}{h}\right) \quad 3\text{-}1$$

where S_{DS} = spectral acceleration for short period a_p = component amplification factor, I_p = component importance factor, W_p = component operating weight, R_p = component

response modification factor, z = height in the structure of the point of attachment of components with respect to the base, h = average roof height of the structure with respect to the base. Namely, the term $1+2z/h$ specifies a linear increase in the acceleration profile with respect to the height. This equation predicts that accelerations are amplified at the roof compared to the floor, and by a factor of 3 compared to the ground/table. However, based on Figure 3-7(c, d), the peak accelerations (zero period values) on the diaphragms are about the same at every level and do not show much amplification relative to the table. This suggests that despite the impact effect, accelerations in this building (as felt by the components) may actually be less than in a typical structure.

Figure 3-8 shows the spatial variations of the first peak of the spectral acceleration in the rocking walls (Figure 3-8 (a, d)), observed between 0.03 and 0.04 seconds, and diaphragms at the floor and roof levels at the same period (Figure 3-8 (b, e) for the roof and Figure 3-8 (c, f) for the floor) for the previously mentioned NR and SH earthquakes. The accelerations in the diaphragm are uniformly lower than the accelerations in the wall. Moreover, these accelerations are higher in the diaphragm corners than the diaphragm center near the rocking walls, which may be due to a torsional response or diaphragm flapping. However, if the high-frequency accelerations were passed to the diaphragms from the walls, the largest amplitudes would be expected at locations nearest the walls.

Figure 3-9a shows the peak vertical movement across the wall-to-diaphragm vertical connection slots at the floor and roof elevations for Records 7 and beyond. Data before Record 7 has been eliminated for this and similar figures due to observed noises in the data. The movement across the slot is similar to the observed uplift, and suggests that the slotted-

pin design effectively isolates the diaphragm from the vertical movements of the wall. The effective horizontal movement across the slot is also estimated from the vertical movement across the slot acting through the wall rotation (Figure 3-9b). This horizontal movement, which comes largely from the deformation of the pin and its connection to the diaphragm, effectively adds another means of attenuating the accelerations from the wall to the diaphragm.

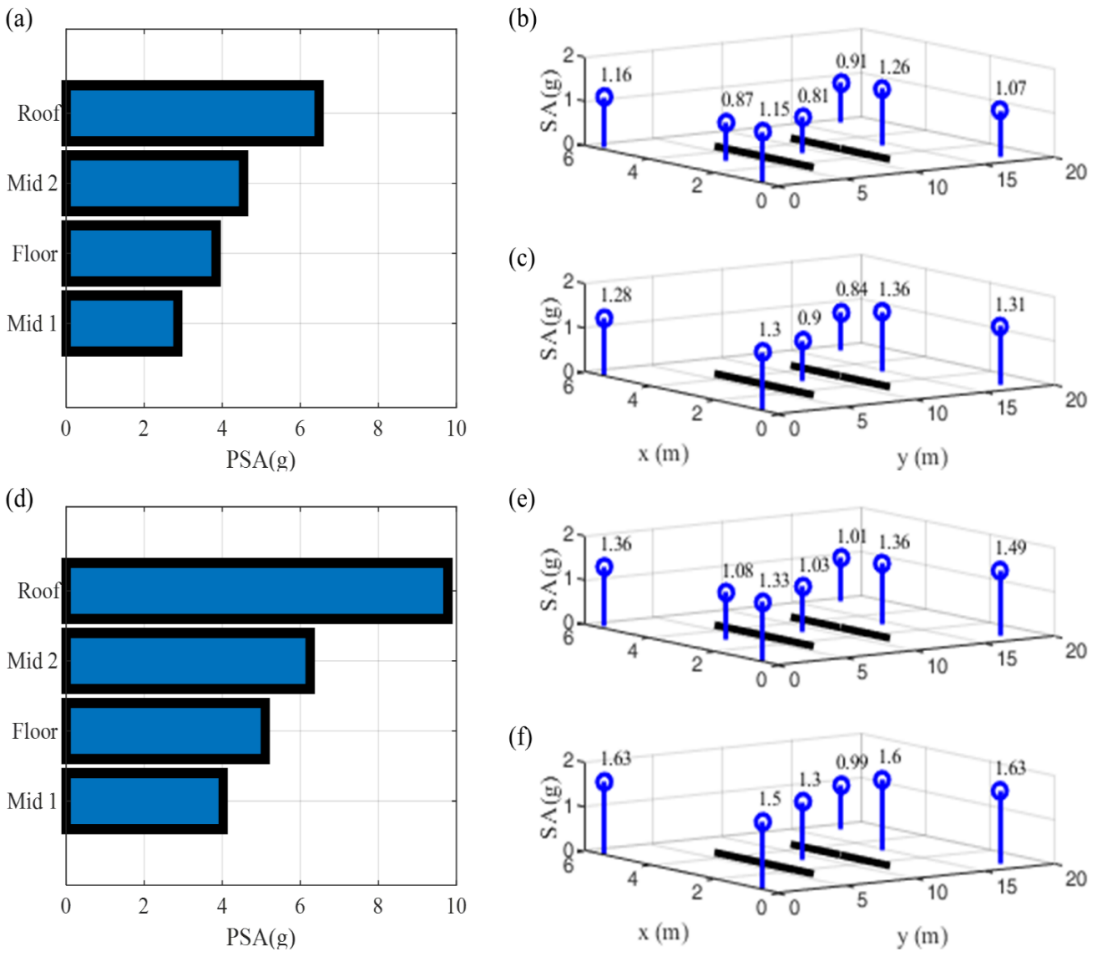

Figure 3-8: Spectral accelerations at 0.04 sec period, representative of acceleration spikes: (a) Wall locations - NR, (b) Roof diaphragm locations - NR, (c) Floor diaphragm locations - NR, (d) Wall locations - SH, (e) Roof diaphragm locations - SH, (f) Floor diaphragm locations - SH

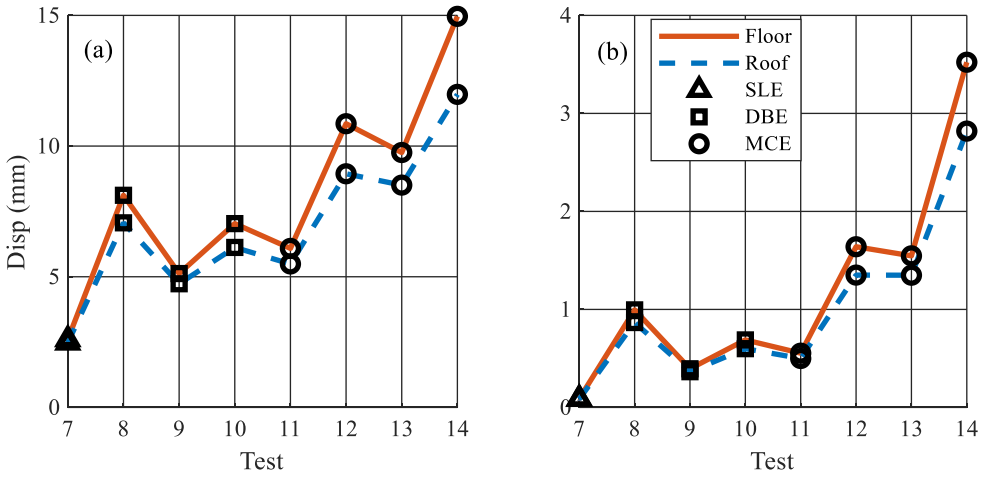

Figure 3-9: Slotted connection behavior for different tests (a) Maximum movement of slot, (b) Mirror of maximum movement in the horizontal direction

Figure 3-10 shows the absolute displacement of the diaphragm taken from the three string potentiometers along the length of the diaphragm (seen in Figure 3-4b) at the instant of peak mid-span diaphragm displacement. The horizontal lines at y=6.10 m and y=11.59 m show the location of the rocking walls, measured from one end of the diaphragm. The displacement pattern confirms that the structure had some torsional response, especially in the last three MCE earthquakes (Tests 12, 13, and 14). However, since the three points are not in a straight line, it also indicates that diaphragm flexibility played a role in the response. The sources of diaphragm flexibility include flexibility of the chords and shear deformation of the CLT panels, as discussed earlier.

In summary, it is believed that the high-frequency accelerations were reduced in the diaphragm compared to the rocking walls for two main reasons: first, the slotted connection provides an isolation effect for the diaphragm at high frequency, and second, the flexibility

of the diaphragm helped to attenuate the high-frequency accelerations that were transferred.

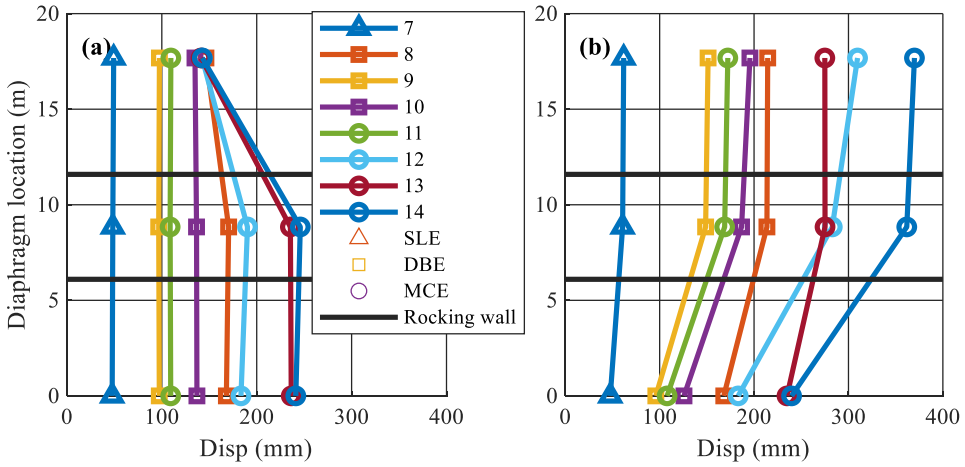

Figure 3-10: Lateral movement of different locations of diaphragms at the instant peak of mid-span diaphragm displacement (a) Floor, (b) Roof

3.4.1.1 Numerical modeling

The test building was designed as a symmetric structure with two sets of coupled walls at the north and south end, providing lateral resistance in the E–W direction. Thus, the dynamic behavior of the structure can be adequately represented by a 2D planar model of only half of the structure (a single set of rocking walls) with a simplified diaphragm model, with the limitation that it cannot represent the torsional response in the system, such as observed in Figure 3-10. Using the computational simulation platform OpenSees (Mazzoni et al. 2007), two different 2D numerical models of the structure were developed to evaluate the effect of diaphragm flexibility on the building accelerations. In the Rigid-Diaphragm model, only the rocking wall was modeled, and all mass (inertia) was assigned directly to

the wall nodes at the story locations. In the Flexible-Diaphragm model, gravity framing was added to the model, and the flexible diaphragm effects were represented by concentrated springs attached to the gravity framing at each floor level. Essentially, the diaphragm flexibility was idealized as a single degree of freedom oscillator (mass on spring) with an equivalent stiffness (Moroder 2016). The gravity frame was attached to the wall with a slotted connection detail, which simulated the flexibility of the slotted connection (Figure 3-11). For both models, the total seismic mass of 4190 kg and 4310 kg was assigned at the floor and roof levels, respectively. In the Rigid-Diaphragm model, the entire mass was attached directly to the wall nodes. In the Flexible-Diaphragm model, the mass was distributed between the wall, frame, and diaphragm, with the majority lumped at the end of the diaphragm springs. Components of the model are described in more detail below.

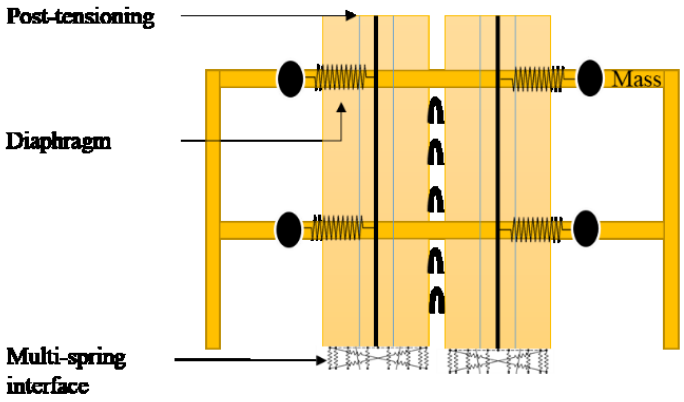

Figure 3-11: The 2D numerical model of CLT rocking wall including gravity framing and mass-spring diaphragm

3.4.2 CLT rocking wall model

The model of the coupled post-tensioned CLT rocking wall consisted of four main components: (1) elastic Timoshenko beam-column wall elements, (2) multi-spring contact elements, (3) post-tensioned (PT) bar truss elements, and (4) UFP spring elements. The wall panels were modeled using a series of elastic Timoshenko beam-column elements spanning between UFP and diaphragm locations. The nonlinear rocking behavior of the panels and the compressive deformation of the CLT were modeled using a multi-spring contact element at the base of each panel, as initially suggested in (Speith et al. 2004). The overall compression stiffness and yield strength of the wall panel were calculated using basic mechanics; the stiffness was found to be 2.4e7 kN/m based on a plastic hinge length of 350 mm (equivalent to twice the wall thickness) (Akbas et al. 2017). The multi-spring contact element was developed with zero-length springs in OpenSees; the distribution of stiffness and spacing to individual springs along the panel base was determined according to Gauss-Lobatto rules. In addition, the flexibility of the base beam in the test was observed to substantially affect the impact/uplift response of the rocking wall. Therefore, springs near the wall corners were replaced by spring units; each spring unit paired a spring to represent the contact stiffness of the wall in series with a second spring to represent the base beam flexibility. Each contact spring or spring unit was attached to the free wall base node on top using a rigid element and fixed at the base directly below. The contact springs were defined with an elastic-perfectly plastic, compression-only material to model the CLT compression behavior and the gap opening at the panel base. All springs or spring units provided stiffness in the vertical direction only. Finally, diagonal shear springs connecting

the corners of each multi-spring contact element were applied to transfer shear at the panel base (Wichman et al. 2018).

The post-tensioning bars were modeled using tension-only truss elements, with a bi-linear hysteretic material model. These elements were fixed at the bottom and connected to a rigid element extending from the top panel beam-column element. An initial strain was applied to the bars to model the initial post-tensioning force. Finally, each UFP was modeled with a zero-length spring with a uniaxial Giuffre-Menegotto-Pinto steel material model with isotropic strain hardening. The stiffness and strength of the UFP material model were calculated based on Baird et al. (2014). Rigid elements were used to link the elastic beam-column wall elements at the center of the panels to the zero-length UFP springs located between the two wall panels (Wichman et al. 2018).

3.4.3 Diaphragm spring model

The diaphragm spring stiffness for the Flexible-Diaphragm model was developed as follows. The stiffness of the CLT diaphragm depends on several parameters, including the orthotropic elastic properties of the panel, the cracked properties of reinforced concrete for CLT concrete-composite diaphragms, the load-slip behavior of the connection between adjacent floor panels, and the load-slip behavior of the connection to the vertical structure (D'Arenzo et al. 2019).

As explained above, diaphragms were represented by a lumped spring-mass system connected to the gravity framing. The diaphragm stiffness was calculated from the diaphragm deflection as a function of story shear. The following formula was applied to

compute the maximum mid-span diaphragm deflection at the location between the two rocking walls:

$$\delta_{dia} = \frac{5vL^3}{8EA_{ch}W} + \frac{0.25vL}{1000WtG_{effCLT}} + CLe_n \quad 3\text{-}2$$

$$C = \frac{1}{2}\left(\frac{1}{P_L} + \frac{1}{P_W}\right) \quad 3\text{-}3$$

where E = modulus of elasticity of diaphragm chords, A_{ch} = area of chord cross-section, W = width of the diaphragm, v = induced unit shear at the edge of the diaphragm ($v = \frac{F_{diaphragm}}{2\times W}$), t =thickness of diaphragm, L = diaphragm length, G_{effCLT} = apparent diaphragm shear stiffness from nail slip and panel shear deformation, e_n = connection slip at the outer edge of the diaphragm under maximum shear load, x = distance from chord splice to the nearest support, and Δ_c = diaphragm chord splice slip. The constant C is defined as shown in Equation 3-3, where P_L and P_W are the length and width of typical panels. Equation 3-2 reflects modifications of the National Design Specifications deflection equation for conventional wood structural panel sheathed diaphragms (American Wood Council 2018) for application to CLT diaphragms (Brenman et al. 2016; Moroder 2016). The first term of Equation 3-2 is the bending deflection (δ_{bend}); the second term is the shear deformation (δ_{shear}), and the third term is deflection due to fastener slip at the panel to panel joints ($\delta_{fastener\ slip}$). The assumed values for all parameters are given in Table 3-3. Since the roof diaphragm is a composite of CLT and concrete, the thickness of the concrete (57 mm) was included in the calculation of $G*t$. The cracked shear of concrete with a value of (2.07e7 kN/m^2) was used due to visible cracks when the NR and SH were tested.

Given the location of rocking walls in the interior of the floor plan, multiple diaphragm segments contributed to the diaphragm flexibility for the 2D model: the diaphragm between the two rocking walls and the cantilevered diaphragms at the end of the building. Stiffnesses were computed separately for the interior and cantilevered portions of the diaphragm, as shown in Table 3-3. The deflection due to bending of the cantilevered portion of the diaphragm was revised to:

$$\delta_{dia} = \frac{vL^3}{0.167EAW} + \frac{0.25vL}{1000AG_{effCLT}} + CLe_n \qquad 3\text{-}4$$

Table 3-3: Diaphragm specifications

	Floor		Roof	
	Center	Cantilever	Center	Cantilever
v	6.2 kN/m		8.2 kN/m	
E	1.1e7 kN/m^2			
W	6.1 m			
A	0.102 m^2		0.102 m^2	
L	5.49 m	6.1 m	5.49 m	6.1 m
$G_{eff\text{-}CLT}$	2.07e5 kN/m^2		2.28e5 kN/m^2	
G^*t (including concrete)	2.17e4 kN/m		1.2e6 kN/m	
P_L	2.74 m	6.1 m	6.1 m	
P_W	1.52 m			
C	0.52 1/m	0.41 1/m	0.41 1/m	
e_n	0.39 mm		0.52 mm	
δ_{bend}	0.09 mm	1.23 mm	0.12 mm	1.64 mm
δ_{shear}	0.39 mm	1.75 mm	0.01 mm	0.04 mm
$\delta_{fastener\ slip}$	1.09 mm	0.97 mm	1.16 mm	1.29 mm
δ_{dia}	1.57 mm	3.95 mm	1.32 mm	2.96 mm
K_d	4.8e4 kN/m	1.9e4 kN/m	7.6e4 kN/m	3.4e4 kN/m
K_{tot}	3.1e4 kN/m		5.3e4 kN/m	

In each segment, the deflection is a linear function for the story force, such that the calculated stiffness (story force divided by the calculated deflection) does not depend on

the story shear. Finally, the resultant spring stiffness was computed as a weighted average of the interior diaphragm and the cantilevered diaphragm stiffnesses. The mass attached to the end of the diaphragm spring included the weight of CLT diaphragm panels, concrete roof decking, and seismic mass plates.

The computed diaphragm stiffness does not reflect additional flexibility resulting from the transfer of horizontal forces across the rotating slotted pin connection between the rocking walls and the diaphragm. Suppose the diaphragm stiffness is $K_{d,}$ and the additional stiffness across the pin connection is K_c. Theoretically, these two springs combine in series and can be replaced with a single spring with equivalent stiffness $K_{eq,c+d}$, as shown in Figure 3-12.

Figure 3-12: Schematic of the contribution of the diaphragm and slotted connection to the overall stiffness (Modified version of Brenman et al. (2016))

For the test building, the calculated diaphragm stiffnesses at the floor and roof were 31333.2 kN/m and 52574 kN/m, respectively. The stiffness of the slotted connection, based on the average force measured across the slot (Pei et al. 2019) divided by the horizontal displacement across the slot (Figure 3-9b), was estimated as 97812 kN/m at the floor and 118173 kN/m at the roof. Thus, the computed equivalent pin-diaphragm stiffness of a single spring – assuming one attached to each of the coupled rocking walls – was 27007.4 kN/m at the floor and 43007 kN/m at the roof. Ultimately, the final stiffnesses used in the

model were calibrated to best match the experimental data; calibrated values are 25393 kN/m for the floor and 21891 kN/m for the roof.

As mentioned previously, the diaphragm spring was connected to the gravity framing. The beams and columns of the gravity frame were modeled with elastic beam-column elements, and only the balloon-framed columns, immediately adjacent to the wall, were considered in the modeling. The connections of gravity framing were modeled as a pin connection. The slotted connection between the gravity framing and the rocking wall was modeled using a spring with Elastic Perfectly Plastic Gap material with a high tangent stiffness in both vertical directions.

The dynamic behavior of the model is very sensitive to damping assumptions, and one crucial factor is the damping associated with the impact phenomenon. Using Rayleigh damping or stiffness proportional damping based on initial stiffness will lead to fictitious forces or moments at the wall base that increases viscous energy and artificially suppresses the response. Alternatively, assigning the damping force proportional to the tangent or current stiffness can lead to an overestimation of the wall response in base shear and base rotation. Rayleigh damping was assumed with damping proportional to the current stiffness, and the coefficients were calibrated to correspond to damping ratios of 2% in the first and second modes to achieve balanced energy dissipation. Moreover, modal damping of 6% in mode 2 was added, which helped suppress spurious vibration for SH earthquakes.

3.5 Comparison of experimental and numerical results

3.5.1 Modal analysis

Modal analysis of the building models was conducted using standard eigenvalue analysis. Mode shapes and natural periods of the Rigid and Flexible-Diaphragm models are indicated in Figure 3-13 and Table 3-4. For the Flexible-Diaphragm model, the lateral system modes are lengthened relative to those in the Rigid-Diaphragm model. Moreover, the Flexible-Diaphragm model includes additional modes, such as those associated with diaphragm deformation (M3 and M4) and a rocking mode with uplift (M5). This is consistent with Lee et al. (2006) finding that an N-story stiff wall and flexible diaphragm structure has N closely spaced modes that primarily represent diaphragm deformation.

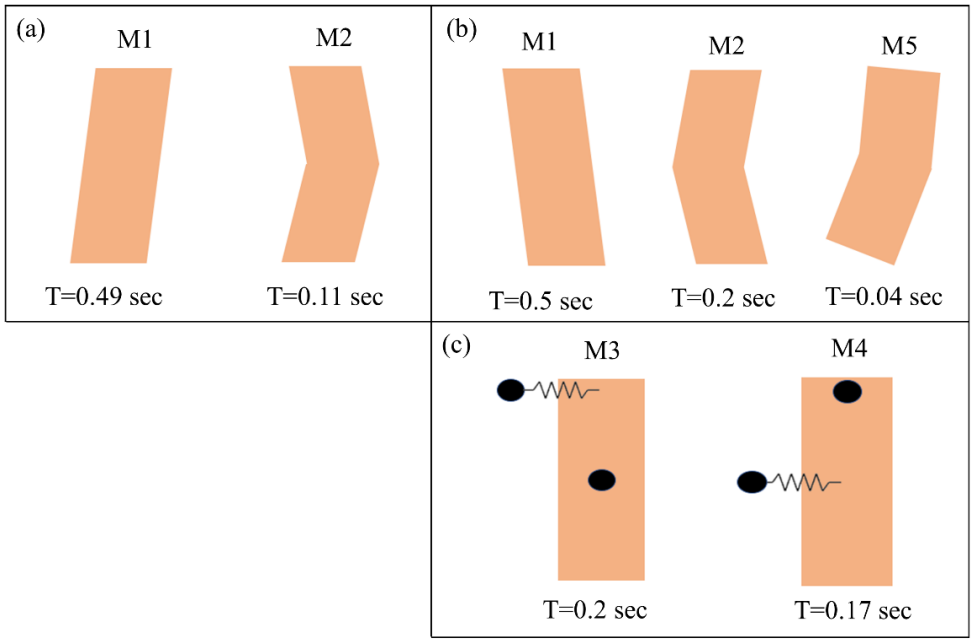

Figure 3-13: Mode shapes and frequencies for (a) Rigid-Diaphragm model, (b) Flexible-Diaphragm model structural modes, (c) Flexible-Diaphragm model diaphragm modes

Table 3-4 compares the experimentally observed periods with those from the Rigid-Diaphragm and Flexible-Diaphragm models. The experimentally observed periods represent effective periods of dynamic response, and are thus lengthened relative to the model periods that are based only on initial stiffness. However, the Flexible-Diaphragm model second and higher modes are more closely aligned with the experimental second and higher modes. Moreover, the experiment only shows one diaphragm mode because of the proximity of the two diaphragm modes.

Table 3-4: Natural periods

Modes	Experiment	Rigid-Diaphragm	Flexible-Diaphragm
1	0.91 sec	0.49 sec	0.5 sec
2	0.31 sec	0.11 sec	0.2 sec
3	0.09 sec		0.2 sec
4			0.17 sec
5	0.04 sec		0.04 sec

3.5.2 Drift and acceleration histories

Figure 3-14 compares story drifts of numerical models with a Rigid and Flexible-Diaphragm to the experimentally determined story drifts for NR and SH earthquakes. The drifts predicted from the model with a Flexible-Diaphragm are slightly higher than those with a Rigid-Diaphragm, but both fall slightly short of the peak experimentally observed peak drifts. The drift histories are used as the benchmark validation for both Rigid and Flexible-Diaphragm models to confirm that both models represent the combined flexural and rocking response of the rocking wall lateral system.

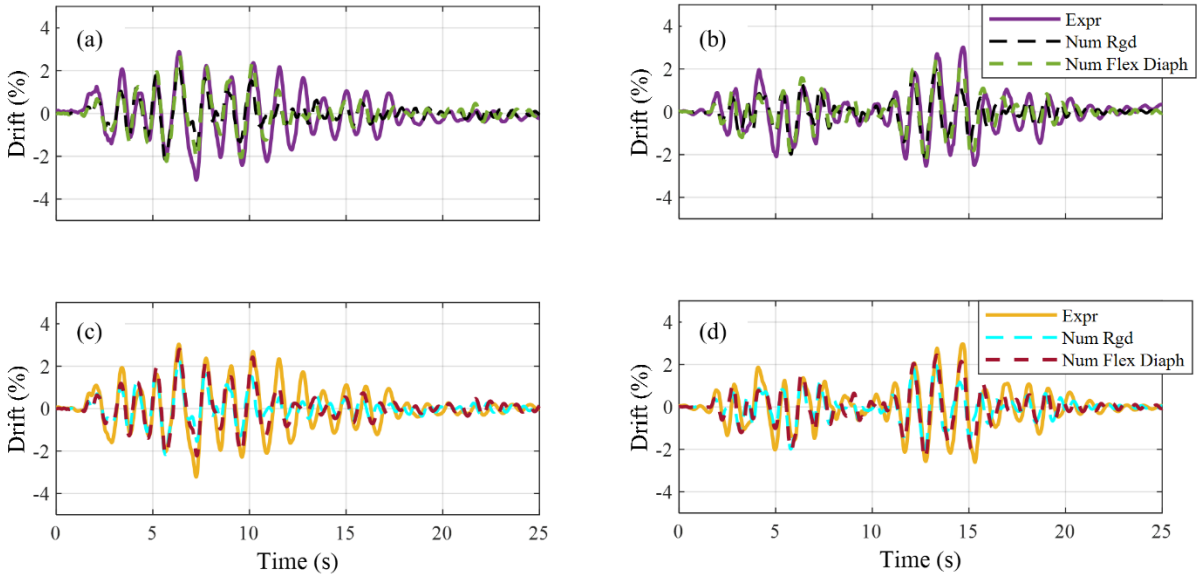

Figure 3-14: Comparison of the drift of experimental results with numerical results (a) Floor - NR, (b) Floor - SH, (c) Roof - NR, (d) Roof - SH

Figure 3-15 shows sample uplift and acceleration histories at the floor level for NR and SH Earthquakes. Only 2 seconds of each ground motion are shown in Figure 3-15 to better illustrate frequency content; however, similar patterns and trends were observed for the motion duration. Figures 3-15a and 15b show the experimentally calculated uplift at the middle of two adjacent walls and, as predicted by the Flexible-Diaphragm model and Rigid-Diaphragm model for NR and SH earthquakes, respectively. Figures 3-15 (c, d) show the experimental acceleration histories on the rocking wall along with those predicted by the Flexible-Diaphragm model and Rigid-Diaphragm model for the NR and SH, respectively. The data shows that high-frequency acceleration pulses are in phase with gap closure or rocking wall impact (Figure 3-15 (a, b)), as Wiebe and Christopoulos mentioned (Wiebe and Christopoulos 2010). Two distinct frequencies can be observed in the wall acceleration history, one associated with the drift and the other associated with the impact

accelerations. The Flexible-Diaphragm model predicts the impact phenomenon well, except the numerical response does not damp out as quickly as the experimental response. Figures 3-15 (e, f) show the experimental, Flexible-Diaphragm model, and Rigid-Diaphragm model acceleration response history on the diaphragm location for the NR and SH, respectively. The high-frequency acceleration pulses in the wall (Figure 3-15 (c, d) are not transmitted to the floor diaphragm, and again the Flexible-Diaphragm model represents this behavior well. In Figure 3-15 (c, d, e, f), the acceleration history of the Rigid-Diaphragm model cannot distinguish between the floor and wall location. These figures confirm that the Rigid-Diaphragm model cannot represent the high-frequency acceleration pulses observed in the wall, and its acceleration response frequency is misaligned with the experimental floor acceleration.

3.5.3 Spectral accelerations

Figure 3-16 shows the acceleration spectral for responses at various locations in the Rigid and Flexible-Diaphragm models as well as experimentally observed for NR (Figure 3-16 (a, c)) and SH (Figure 3-16 (b, d)). Each subplot (floor and roof level) shows distinct spectra at wall and diaphragm locations except for the Rigid-Diaphragm model, which cannot distinguish between the two since they are rigidly connected in the horizontal directions. The Flexible-Diaphragm model replicates the recorded accelerations in the wall and the diaphragm reasonably well. Three peaks are observed in the experimental acceleration spectra that are consistent with modal responses in the structure. The first peak at approximately 1 sec (Table 3-4), observed in spectral accelerations at all wall and

diaphragm locations, is the fundamental mode of the structure. This first mode period is slightly longer than that from modal analysis due to the nonlinear nature of the system response after rocking. The second peak at 0.2 sec is the second mode of the building, closely aligned with the diaphragm mode. The Flexible-Diaphragm model replicates this 0.2 second period at the diaphragm more accurately than the Rigid-Diaphragm model, which is essential for nonstructural components that may be directly susceptible to the

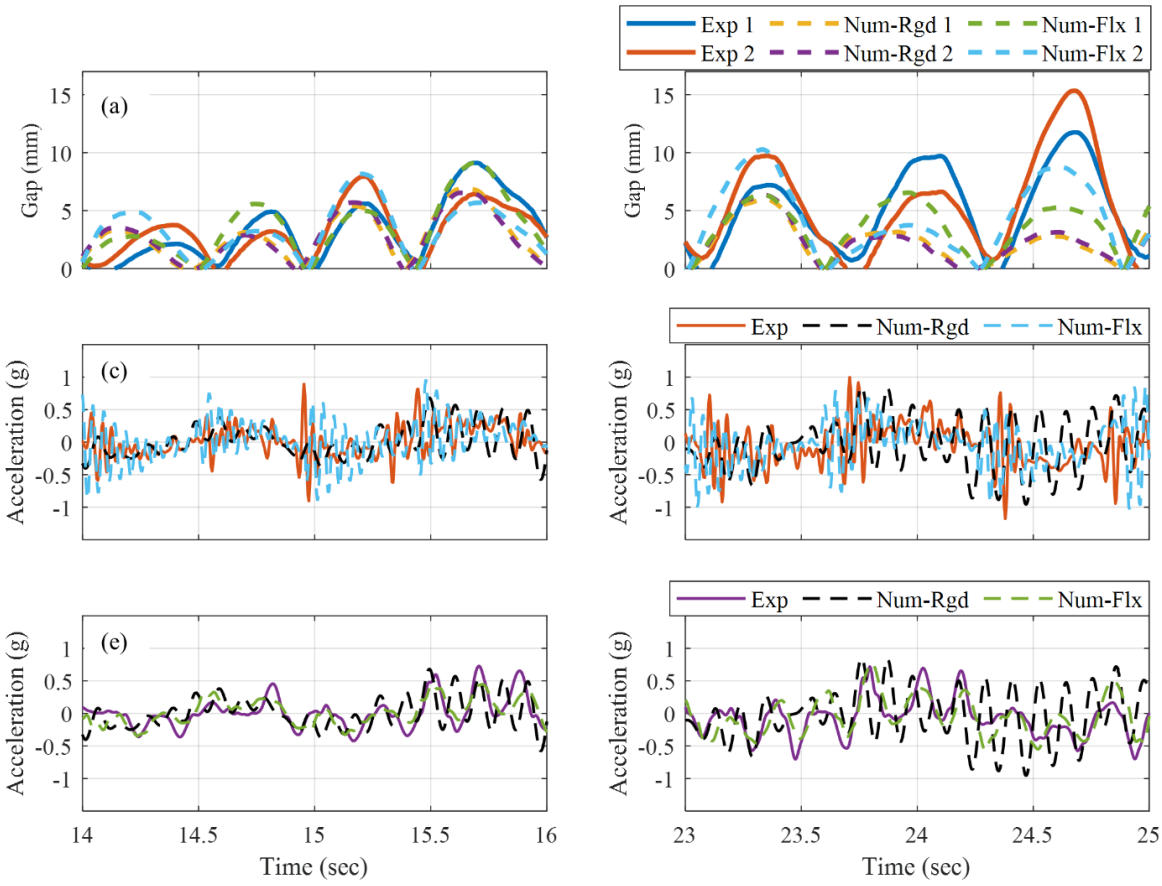

Figure 3-15: For a 2-sec window of the NR and SH earthquake for the floor level: (a) Gap opening - base of the wall - NR, (b) Gap opening - base of the wall - SH, (c) Horizontal acceleration histories - wall - NR, (d) Horizontal acceleration histories - wall - SH, (e) Horizontal acceleration histories - diaphragm - NR, (f) Horizontal acceleration histories - diaphragm - SH

specific frequency content in the floor acceleration. The last peak, observed in the period ranging between 0.03 and 0.04, represents the wall uplift-pounding effect and is only observed in the wall. The Rigid-Diaphragm model with a mass attached to the wall cannot capture this peak due to the pounding behavior of the lightweight wall detached from the rest of the structure. Notably, the Flexible-Diaphragm model does capture this peak in the wall, but consistent with the experimental data, does not reflect this high-frequency content anywhere in the spectral accelerations for the diaphragms.

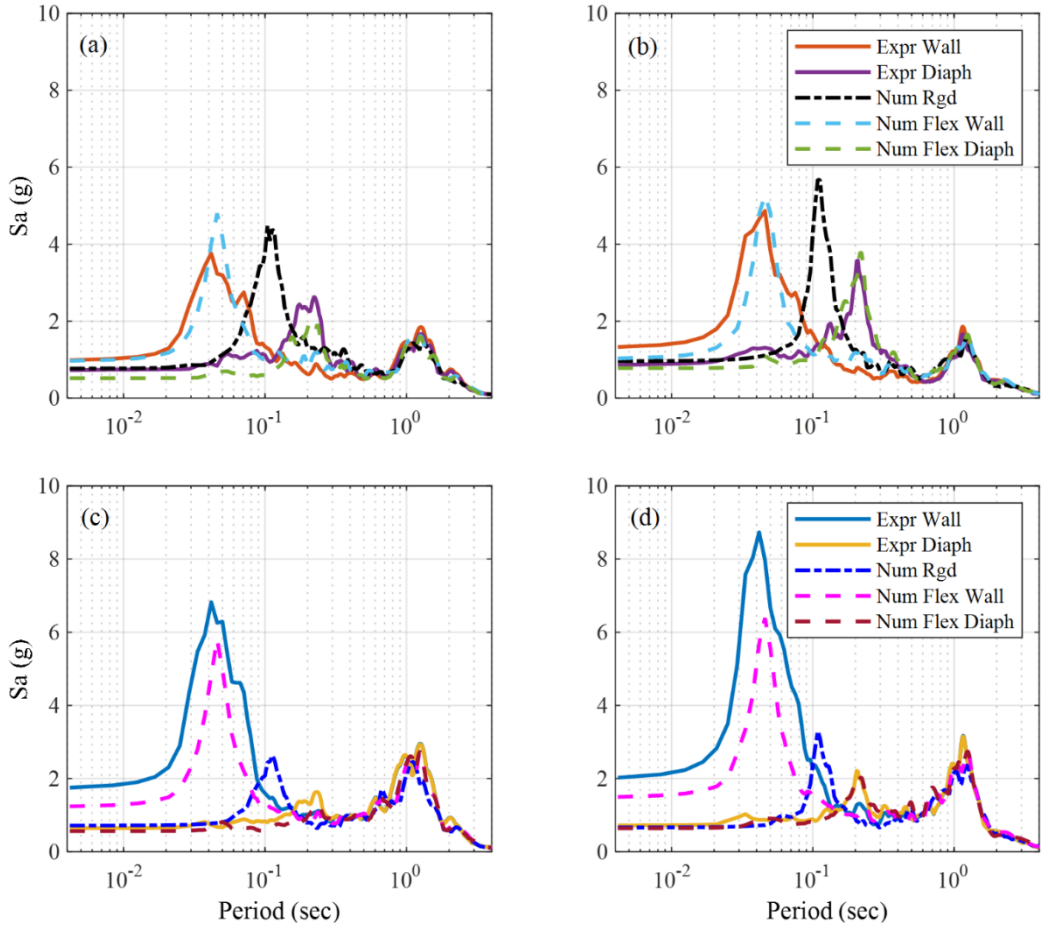

Figure 3-16: Spectral acceleration for Flexible-Diaphragm, Rigid-Diaphragm, and experimental data: (a) NR - floor level, (b) SH - floor level, (c) NR - roof level, (d) SH - roof level

Figure 3-17 compares experimentally observed and numerically computed spectral accelerations at about 0.04 sec in the wall for the first peak over the 14 records imposed in the test program. Although the exact period of the spectral peak varies from record to record, the peak occurred around 0.04 sec in all. As shown, for most records, the Flexible-Diaphragm model more closely matches the 0.04-sec spectral acceleration than the Rigid-Diaphragm model. Although the Flexible-Diaphragm model spectral accelerations more closely match the experimental ones at the floor level and fall short at the roof level, the Rigid-Diaphragm model is low by an order of magnitude and confirms that the Rigid-Diaphragm model cannot begin to capture this effect.

Figure 3-18 shows the peak diaphragm acceleration at the floor and roof level as experimentally observed and predicted by the Rigid-Diaphragm and Flexible Diaphragm models. The Rigid-Diaphragm model predicts higher values compared to the Flexible Diaphragm model. The Rigid Diaphragm model provides more conservative and closer to experimental values in some records. Thus, despite its limitations in representing the actual impact phenomenon in the system, the Rigid-Diaphragm model is a reasonable approach in predicting both peak story drifts and peak diaphragm accelerations, and the suitable model choice should depend on the information needed from the model.

3.5.4 Influence of base beam flexibility

As discussed previously, both the Rigid-Diaphragm and Flexible Diaphragm model included an additional base beam foundation model to represent the steel box girder base

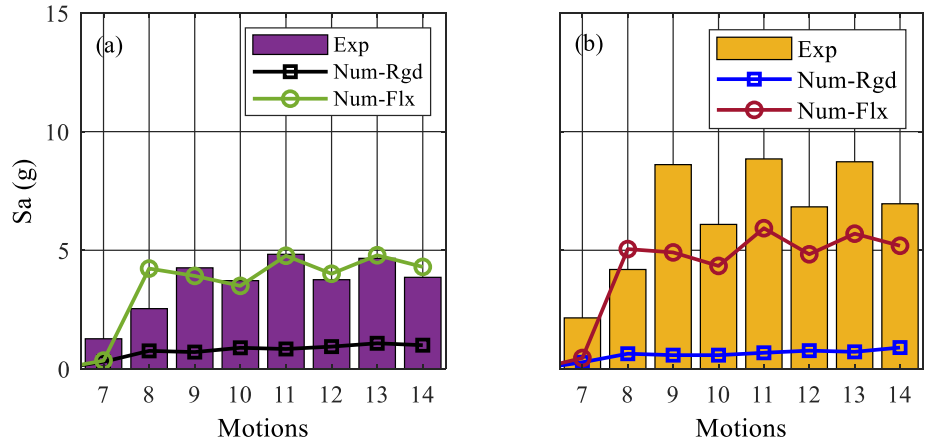

Figure 3-17: Spectral acceleration on the wall at periods of 0.04 sec (a) Floor level, (b) Roof level

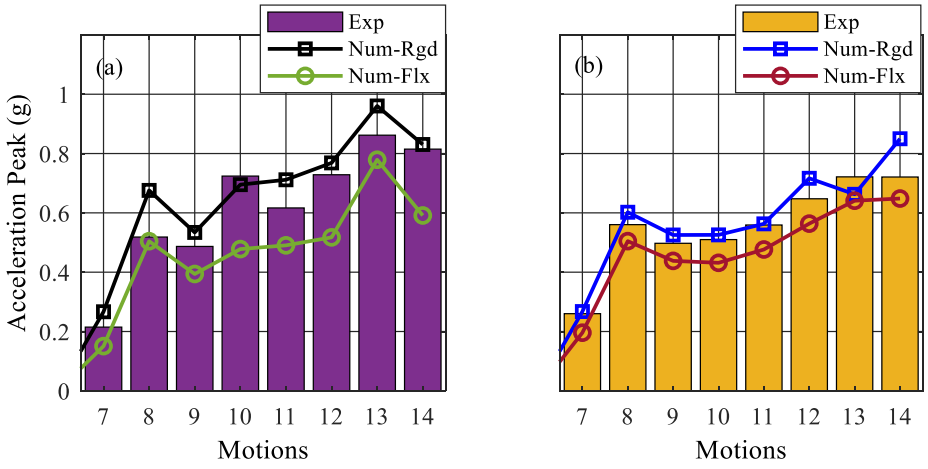

Figure 3-18: Peak diaphragm accelerations (a) Floor level, (b) Roof level.

beam that was present in the experiment as a foundation element for the rocking wall. After repetitive use of the test specimen for different earthquake levels, this base beam yielded and deformed in the top flange in the rocking wall corners (Sarah Wichman 2018). The flexible base beam is unique to this test specimen and would not be present in most situations. In realistic buildings, a stiffer foundation unit would be used. This deformation

of the base beam affected the test building response in different ways, including observations of its period, maximum displacement, and spectral acceleration. In Figure 3-19, the Flexible Diaphragm model of this study (referred to here as Flx-Base) is compared to a comparable model with the box girder base beam effect removed (referred to here as Rgd-Base). Spectral accelerations for these two models are shown for NR (Figure 3-19 (a, c)) and SH (Figure 3-19 (b, d)). As shown, by removing the base beam from the model, the fundamental period of the structure slightly shifted to lower values (from more than 1.0 second to 0.9 seconds), and the values of acceleration spikes in the wall increased significantly (by a factor of 2). This base beam acted as a soft contact element that attenuated the acceleration spikes, as was suggested by Qureshi et al. (2016). Thus, in a more typical base condition, the acceleration spikes due to the pounding effect are even higher, but they still did not transfer to the diaphragm.

3.6 Conclusion and recommendations

This paper addressed concerns about demands imposed on acceleration-sensitive nonstructural components in buildings with post-tensioned CLT rocking wall lateral force resisting systems. The rocking of the walls leads to high acceleration spikes due to the impact behavior of the wall, but the extent to which these accelerations propagate to the diaphragms is not well understood and depends on the detailing. For this purpose, the response of a full-scale two-story mass timber building integrated with CLT rocking walls that was tested on the NHERI UCSD shake table was studied. Acceleration histories of the diaphragms and the rocking walls were analyzed and compared. Afterward, two 2D models

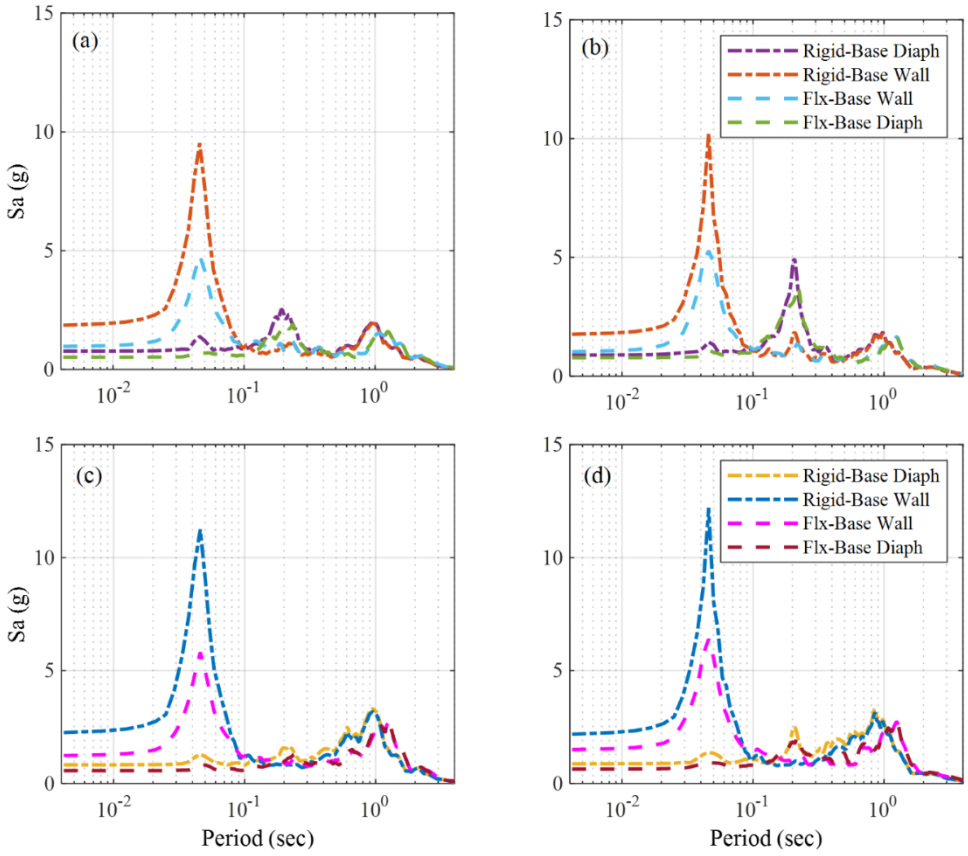

Figure 3-19: Spectral acceleration for Flexible - Diaphragm model with (Flx - Base) and without (Rigid - Base) flexible base beam: (a) NR - floor level, (b) SH - floor level, (c) NR - roof level, (d) SH - roof level

of the building were modeled in OpenSees. In the first model, the diaphragm and its connection to the wall were assumed to be rigid, and all of the mass was assigned to the wall nodes. In the second model, the framing and the diaphragm flexibility were included. The significant findings are summarized as follows:

- The experimental results showed that despite the concern regarding the acceleration spikes in the rocking walls, these high-frequency high-amplitude spikes were

attenuated significantly from the wall to the diaphragm, and they are not a concern for the acceleration-sensitive components. The measured movement across the slotted pin connection showed that diaphragms were isolated from floor uplifts. Moreover, the diaphragm accelerations were considerably lower than ASCE 7 design equations and had almost no amplification over the height of the structure.

- Both the Rigid-Diaphragm and Flexible Diaphragm models predicted the fundamental mode behavior and peak story drifts very well. While both models slightly underestimated the peak drift, the drifts predicted by the Flexible-Diaphragm model were slightly larger.
- The Rigid-Diaphragm model did not predict the higher frequency motion and significantly underestimated the peak wall acceleration due to inaccurate mass distribution that led to a heavy wall. The Rigid-Diaphragm model also produced a spurious period between the rocking mode of the wall and the diaphragm mode.
- Despite somewhat underestimating peak accelerations, the Flexible-Diaphragm model was shown to predict different modes in the wall and the diaphragm and the lateral acceleration spikes with reasonable accuracy.
- Although the Rigid-Diaphragm was limited in estimating the diaphragm and wall spectra, it produced acceptable estimates of the peak diaphragm accelerations at both floor and roof. Moreover, it provided more conservative peak diaphragm accelerations compared to the Flexible-Diaphragm model.
- The flexible base beam in the test structure affected the response of the structure in several ways, including lengthening the fundamental period, increasing the

displacement, and attenuating the severity of acceleration spikes. When the flexible base beam was removed from the model, more similar to a realistic building, the acceleration spikes in the wall increased significantly, but the diaphragm was still isolated from those acceleration spikes.

3.7 Acknowledgments

This material is based upon work supported by the National Science Foundation under Grant Nos. CMMI-1635363, and 1634204. The authors are grateful for this support. Any opinions, findings, conclusions, or recommendations expressed in this publication are those of the authors and do not necessarily reflect the views of the National Science Foundation. The use of the NHERI experimental facility is supported by the National Science Foundation's Natural Hazards Engineering Research Infrastructure (NHERI) Program. The authors would like to acknowledge and thank: (1) the NHERI at UCSD site management and staff, who helped greatly in the construction and testing program; (2) support for the 2-story shake table testing program from industry partners, including TallWood Design Institute, Katerra, Simpson Strong-Tie, Forest Products Laboratory, Softwood Lumber Board, DR Johnson Lumber, and the City of Springfield, Oregon; (3) other collaborators and students who worked on this project, including (in no particular order) Andre R. Barbosa, Reid B. Zimmerman, Eric McDonnell, Hans-Erik Blomgren, Da Huang, Jace Furley, Leonardo Rodrigues, Brian Demeza, Gabriele Tamagnone, Daniel Griesenauer, Ethan Judy, Steven Kordziel, Aleesha Busch, Ali Hansan, Joycelyn Ng, Monica Y. Liu, and Ata Mohseni; (4) the NHERI TallWood project Co-PIs (overall lead

PI Shiling Pei at Colorado School of Mines, John W. van de Lindt at Colorado State University, J. Danel Dolan at Washington State University, James Ricles and Richard Sause at Lehigh University).

3.8 References

Akbas, T., Sause, R., Ricles, J. M., Ganey, R., Berman, J., Loftus, S., Dolan, J. D., Pei, S., Van De Lindt, J. W., and Blomgren, H. E. (2017). Analytical and Experimental Lateral-Load Response of Self-Centering Posttensioned CLT Walls. Journal of Structural Engineering, 143(6), 1–15.

American society of civil engineers. (2017). ASCE/SEI 7-16: Minimum design loads and associated criteria for buildings and other structures. The American Society of Civil Engineers, Reston, Virginia, USA.

American Wood Council. (2018). National Design Specification Design Values for Wood Construction.

Aragaw, L. F., and Calvi, P. M. (2018). Earthquake-induced floor accelerations in base-rocking wall buildings. Journal of Earthquake Engineering, 29.

Baird, A., Smith, T., Palermo, A., and Pampanin, S. (2014). Experimental and numerical Study of U-shape Flexural Plate (UFP) dissipators. New Zealand Society for Earthquake Engineering (NZSEE) Annual Technical Conference, Wellington, New Zealand, 9.

Barbosa, A. R., Rodrigues, L. G., Sinha, A., Higgins, C., Zimmerman, R. B., Breneman, S., Pei, S., van de Lindt, J. W., Berman, J., and McDonnell, E. (2021). Shake-Table Experimental Testing and Performance of Topped and Untopped Cross-Laminated Timber Diaphragms. Journal of Structural Engineering, American Society of Civil Engineers (ASCE), 147(4), 04021011.

Barbosa, A. R., Rodrigues, L., Sinha, A., Higgins, C., Zimmerman, R. B., Breneman, S., Pei, S., Van De Lindt, J., Berman, J., McDonnell, E., Branco, J. M., and Neves, L. C. (2018). Numerical modeling of CLT diaphragms tested on a shake-table experiment. WCTE 2018 - World Conference on Timber Engineering.

Belleri, A., Torquati, M., and Riva, P. (2013). Finite element modeling of 'rocking walls. 4th International Conference on Computational Methods in Structural Dynamics and Earthquake Engineering (COMPDYN 2013). DOI: 10.7712/120113.4706.C1213.

Brenman, S., McDonnel, E., and Zimmerman, R. B. (2016). An approach to CLT diaphragm modeling for seismic design with application to a U.S. high-rise project. WoodWorks.

Buchanan, A., Deam, B., Fragiacomo, M., Pampanin, S., and Palermo, A. (2008). Multi-storey prestressed timber buildings in New Zealand. Structural Engineering International: Journal of the International Association for Bridge and Structural Engineering (IABSE), 18(2), 166–173. https://doi.org/10.2749/101686608784218635

D'Arenzo, G., Casagrande, D., Reynolds, T., and Fossetti, M. (2019). In-plane elastic flexibility of cross laminated timber floor diaphragms. Construction and Building Materials, Elsevier Ltd, 209, 709–724.

FEMA. (2012). Seismic performance assessment of buildings. Volume 1- Methodology. Fema P-58-1, 1, 315.

Fleischman, R. B., and Farrow, K. T. (2001). Dynamic behavior of perimeter lateral-system structures with flexible diaphragms. Earthquake Engineering and Structural Dynamics, 30(5), 745–763.

Ganey, R. S. (2015). Seismic design and testing of rocking cross laminated timber walls. University of Washington (Doctoral dissertation).

Ju, S. H., and Lin, M. C. (1999). Comparison of building analyses assuming rigid and felexible floors. Journal of Structural Engineering, 125(1), 25–31.

Lee, H. J., Aschheim, M. A., and Kuchma, D. (2007). Interstory drift estimates for low-rise flexible diaphragm structures. Engineering Structures, 29(7), 1375–1397.

Marriott, D. J., Pampanin, S., Palermo, a, and Bull, D. (2008). Shake-table testing of hybrid post-tensioned precast wall systems with alternative dissipating solutions. 2008 NZSEE Conference.

Mayes, R. L., Wetzel, N., Tam, K., Weaver, B., Brown, A., and Pietra, D. (2013). Performance based design of buildings to assess and minimize damage and downtime.

Bulletin of the New Zealand Society for Earthquake Engineering, 46(1), 40–55.

Mazzoni, S., Mckenna, F., Scott, M. H., and Fenves, G. L. (2007). Open System for Earthquake Engineering Simulation (OpenSees) OpenSees Command Language Manual.

Moroder, D. (2016). Floor diaphragms in multi-storey timber buildings. University of Canterbury.

Moroder, D., Sarti, F., Palermo, A., and Pampanin, S. (2014). Experimental investigation of wall-to-floor connections in post-tensioned timber buildings. NZSEE Conference.

Nazari, M., and Sritharan, S. (2020). Influence of different damping components on dynamic response of concrete rocking walls. Engineering Structures, Elsevier, 212, 11.

NHERI TallWood-Home. (2021). <http://nheritallwood.mines.edu/> (Apr. 13, 2021).

Pei, S., Van De Lindt, J. W., Barbosa, A. R., Berman, J. W., Mcdonnell, E., Dolan, J. D., Blomgren, H.-E., Zimmerman, R. B., Huang, D., and Wichman, S. (2019). Experimental seismic response of a resilient 2-story mass-timber building with post-tensioned rocking walls. Journal of Structural Engineering, 145(11), 15.

Priestley, M. J. N., Sritharan, S. (Sri), Conley, J. R., and Pampanin, S. (2014). Preliminary results and conclusions from the PRESSS five-story precast concrete test building. PCI Journal.

Qureshi, I. M., and Warnitchai, P. (2016). Computer modeling of dynamic behavior of rocking wall structures including the impact-related effects. Advances in Structural Engineering, 19(8), 1245–1261.

Sarah Wichman. (2018). Large-scale dynamic testing of rocking cross laminated timber walls. University of Washington.

Schoettler, M. J., Belleri, A., Zhang, D., Restrepo, J. I., and Fleischman, R. B. (2009). Preliminary results of the shake-table testing for the development of a diaphragm seismic design. PCI Journal, 100–124.

Speith, H. A., Carr, A. J., Pampanin, S., Murahidy, A. G., and Mander, J. (2004). Modeling of precast prestressed concrete fram structures with rocking beam-column connections. Christchurch, New Zealand.

Toranzo-Dianderas, L. A. (2002). The use of rocking walls in confined masonry structures : a performance-based approach. University of Canterbury.

Wichman, S., Berman, J., Pei, S., Barbosa, A., Dolan, D., Van De Lindt, J., and Zimmerman, R. (2018). NHERI TallWood: dynamic testing and analysis of multi-story rocking cross laminated timberwalls. 11th National Conference on Earthqauke Engineering.

Wiebe, L., and Christopoulos, C. (2010). Characterizing acceleration spikes due to stiffness changes in nonlinear systems. Earthquake Engineering and Structural Dynamics.

4 Experimental cyclic test of reduced damage detailed drywall partition walls integrated with a timber rocking wall

(This chapter is a standalone paper published in Journal of Earthquake Engineering: "Hasani, H., Ryan, K. L. (2021). Experimental cyclic test of reduced damage detailed drywall partition walls integrated with a timber rocking wall. *Journal of Earthquake Engineering*. DOI: 10.1080/13632469.2020.1859005")

4.1 Abstract

Bidirectional quasi-static cyclic loading was applied to a subassembly of drywall partition walls integrated with cross-laminated timber rocking walls. Details aimed to reduce seismic damage to the partition walls were investigated, such as slip connections of partition walls to the diaphragm and gap detailing for the wall intersections. Telescoping detailing eliminated damage to the framing at the wall ends compared to traditional slip-track detailing. The distributed gap wall delayed the damage to about 1% inter-story drift. In the corner gap wall, the sacrificial corner bead opened up at low drifts (0.43%), but the wall was damage-free until more than a 2% drift.

4.2 Introduction

Modern seismic design methodologies are evolving to focus on the overall building performance rather than strength alone. As such, performance-based design approaches are

increasingly used by different design codes (ASCE 2007; FEMA 2000), which allow a level of seismic protection from immediate occupancy (resilience against natural hazards) to collapse prevention. Whole building resilience requires not only the resilience of the structural system but also the resilience of its non-structural systems. In recent earthquakes, the damage to non-structural components has dominated economic losses, as these components comprise the majority of the construction cost and sustain more frequent damage – leading to subsequent downtime – than structural components (Taghavi and Miranda 2003). In general, the economic loss caused by damaged non-structural components alone, the loss of inventory, and the subsequent business downtime may exceed the replacement cost of the building (Villaverde 1997).

A developing approach that has the potential to offer seismic resilience for timber buildings is the use of post-tensioned cross-laminated timber (CLT) rocking walls as the lateral load resisting system (Buchanan et al. 2008; Ganey 2015). Since rocking wall systems lead to larger inter-story drifts compared to traditional shear walls (Zhou et al. 2012), special attention should be given to drift-sensitive non-structural components. Only one system-level test on a timber building incorporated a CLT rocking wall system (Pei et al. 2019). In this test, drift ratios of 1.59% to 2.40% were observed for the design earthquake.

Another aspect of rocking wall systems is the vertical displacement incompatibility between the wall and floor diaphragms. When a rocking wall is subject to lateral load, a portion of the wall uplifts as the bottom of the wall rocks up off the base on one side. This uplift causes a rotation and a vertical displacement incompatibility between the wall and the floor at the location of the wall-to-floor connections. While uplift/rotation is not unique

to the rocking wall system, in a traditional wall, rotation is distributed along the plastic hinge length, while in a rocking wall, the rotation is concentrated at the base joint. This inconsistency has a significant effect on the performance of non-structural components due to the localized diaphragm displacement at the wall-to-floor connection locations.

In general, different wall-to-floor connections can be used, including rigid connections, connections that allow relative rotation, and connections that allow both relative rotation and vertical movement between the floor and the wall. Moroder et al. (2014) investigated several connections for timber rocking walls and their effect on the diaphragm deformation. They showed that a pin-round hole connection could eliminate rotational incompatibility, which minimizes the system strength increase due to connection resistance. A pin-slotted hole connection was used to allow relative vertical movement, but the joint did not move properly because of friction. A connection with an eccentric group of bolts was found to induce higher rotation and uplift in the beam compared to a centered bolt group connection. In shake-table tests that investigated the experimental behavior of building systems with precast concrete rocking walls (Schoettler et al. 2009) and CLT rocking walls (Pei et al. 2019), special slotted connections successfully isolated the floors from the wall uplift to minimize the localized deflection in the diaphragm. However, there is minimal research on how the lessened local diaphragm deformation affects non-structural components.

Drywall partition walls are among the most common non-structural components in building construction and could considerably affect the seismic resilience of buildings. These components are drift sensitive (ASCE 2003) and are susceptible to damage at low shaking intensities. Although wood-framed partition walls have higher ultimate capacity compared

to steel-framed partition walls (Memari et al. 2008), steel-framed partition walls tend to respond in a more ductile manner (Tasligedik et al. 2012). Therefore, many researchers have investigated the seismic response of steel-framed drywall partition walls, referred to hereafter as partition walls (Hasani et al. 2018, Ryan and Hasani 2020). In particular, local connections in partition walls have been tested under monotonic or cyclic loading. Furthermore, component tests of partition walls in isolation have been conducted under monotonic, cyclic, and dynamic loading protocols. System-level shake table tests have been conducted to evaluate the interaction between partition walls, structural systems, and other non-structural components such as ceilings and facades. Table 4-1 summarizes prior experimental studies on partition walls, grouped into local tests, component tests, and system-level tests. Table 4-1 also lists the type of loading, whether the study developed damages states (DS) and fragility functions, and the construction parameters evaluated. These research projects have pursued a variety of objectives and achieved various outcomes, such as:

(1) *Effect of construction details on seismic behavior of partition walls*: Construction details have a fundamental role in the response of partition walls, as even walls built with the same materials and general construction techniques can exhibit different seismic behavior (Retamales et al. 2013). Some of the studied details are as follows: connection detail of wall to the surrounding elements horizontally (CWH) or vertically (CWV); wall discontinuities (WD) such as door frame and window; partial height drywall (PHD); drywall screw (DS), track to diaphragm screw (TDS), and stud to track screw (STS) spacing

and layout; drywall placement (DP) details including dimension, thickness, and type of drywall panels; vertical slotted track (VS); framing properties (FP) such as stud/track gage, size, spacing and material (steel or wood); wall intersection (WI); the gap between stud and track (GST); joint finishing details (JF); wall aspect ratio (AR); partial height walls (PHW); blocking (BE); and reduced damage details in the wall (RDD).

(2) *Definition of damage states and fragility curves*: A few researchers studied damage data to develop damage state definitions and seismic fragilities, such as Rihal (1982), who was a pioneer in this area. The probability of occurrence of a given damage state is usually expressed as a fragility curve function associated with an inter-story drift ratio since the partition walls are drift-sensitive components. Some of the research data has been used for defining general fragility functions for partition walls as part of the FEMA P-58 project (Mosqueda 2016).

(3) *Estimation of repair cost*: Lee et al. (2007) found that partition wall repair was not required for drift levels below 0.25%. At drift levels of 2%, the repair cost of partition walls equaled their initial construction cost, while at drift levels of 8%, repair costs were twice the initial construction costs. Araya-Letelier and Miranda (2012) showed that the expected annual loss of conventional partition walls is eight times larger than the annual loss of partition walls incorporating novel sliding/frictional connections, and even more if the environmental impact is considered. In another study, the partition wall repair costs were estimated to

be up to the initial cost for the serviceability damage state, and up to twice the initial cost for damage beyond serviceability level (Pali et al. 2018; Fiorino et al. 2019).

(4) *Effect of loading protocol*: The number of cycles had only limited effects on the seismic performance of partition wall specimens tested with quasi-static loading (Restrepo and Lang 2011). Based on that, FEMA 461 (ATC 2007), which developed interim loading protocols for seismic qualification tests of components, investigated two loading protocols and found that step increment does not considerably affect the response. Furthermore, partition wall damage was not found to be amplified by dynamic loading compared to quasi-static loading (Lee et al. 2007), and a monotonic test was recommended as a reasonable estimate for the envelope of a cyclic test (Memari et al. 2008; Peck et al. 2012). Fiorino et al. (2019) found that partition walls sustained no damage when subjected to out-of-plane seismic loading alone. However, the literature lacks a systematic comparison of in-plane and bidirectional loading of partition walls for understanding the effect of out of plane loading on in-plane resistance.

(5) *Contribution of non-structural components in structural response*: A few researchers examined the contribution of partition walls to the lateral resistance of the structure. In quasi-static tests, the strength of partition walls was shown to be non-negligible compared to the structure when tested as an infill wall in an enclosed frame of beams and columns, whether using slip-track detailing (Lee et al. 2007) or fixed connections (Tasligedik et al. 2012). Also, the

> influence of partition walls on dynamic properties of buildings was investigated with some dynamic tests on a shake table by measuring secant stiffness, damping, and the fundamental frequency of the building (Mccormick et al. 2008; Matsuoka et al. 2008; Magliulo et al. 2014; Fiorino et al. 2019; Wang et al. 2015; Soroushian et al. 2016). Due to the inherent flexibility of CLT rocking walls, partition walls could contribute significantly to the overall resistance of the building.

While many details have been studied (Table 4-1), the construction details found to most affect the partition wall seismic response are the connection details of the walls to the surrounding elements (Pali et al. 2018). In general, there are two approaches for connecting partition walls to the surrounding structural elements: “fixed” and “slip-track” connections. In fixed detailing, the studs and drywall are connected to tracks on top and bottom. In slip-track detailing, the partition walls are isolated from the inter-story drift by eliminating the connection of studs and drywall to the top track. The slip-track connections reduced damage associated with drift but increased damage at the wall-intersections compared to fixed connections. The slip-track connections were also associated with damage from studs popping out of tracks at the wall ends (Retamales et al. 2013). Moreover, the presence of intersecting walls in slip-track detailing with the slip detail on top and bottom caused partition walls to sustain rocking during in-plane motion (Mccormick et al. 2008).

Table 4-1: Prior studies of partition walls

	Authors	Type of test - direction	DS	Construction parameter
Local Tests	Swensen et al. 2015	monotonic and cyclic - quasi-static - X		DS
	Rahmanishamsi et al. 2016b	monotonic and cyclic - quasi-static - X	Yes	DS, FP
	Rahmanishamsi et al. 2016a	monotonic and cyclic - quasi-static - Y	Yes	GST, FP, STS
	Fiorino et al. 2017	monotonic and cyclic - quasi-static - X		DS, DP
Component Test	John A. Blume and Associates 1966	cyclic - quasi-static - X	Yes	CWH, WD, FP, DP
	John A. Blume and Associates 1968	cyclic - quasi-static - X	Yes	CWH, WD, FP, DP
	Freeman 1971	cyclic - quasi-static and dynamic - X	Yes	CWH, WD, FP, DP, DS, BE
	Freeman 1974	cyclic - quasi-static and dynamic - X	Yes	CWH, FP, DP, WI, DS, BE
	Freeman 1976	cyclic - quasi-static - X	Yes	CWH, FP, DP
	Rihal 1982	cyclic - quasi-static - X	Yes	CWH, WD, PHD, DS, DP, FP, GST, JF
	Lee et al. 2007	cyclic - quasi-static and dynamic - X		WD, WI
	Memari et al. 2008	monotonic and cyclic - quasi-static - X		FP, JF
	Restrepo and Lang 2011	cyclic - quasi-static - X+Y	Yes	
	Restrepo and Bersofsky 2011	cyclic - quasi-static - X	Yes	WD, PHD, DS, DP, VS, FP, WI
	Peck et al. 2012	monotonic and cyclic - quasi-static - X		DS, DP, FP, AR, BE
	Tasligedik et al. 2012	cyclic - quasi-static - X		FP
	Retamales et al. 2013	UB-NCS - X, Y	Yes	CWH, DS, FP, WI, PHW, RDD
	Tasligedik et al. 2013	cyclic - quasi-static - X		FP, RDD
	Magliulo et al. 2014	shake sable - X+Y	Yes	
	Petrone et al. 2015	cyclic - quasi-static - X	Yes	DS, DP, FP
	Petrone et al. 2016	cyclic - quasi-static - Y		FP, DP
	Pali et al. 2018	cyclic - quasi-static - X	Yes	CWH, CWV, DP, FP, JF
	Fiorino et al. 2018	monotonic - quasi-static and dynamic-Y		CWH, AR, FP, TDS
	Araya-Letelier et al. 2019	cyclic - quasi-static - X		CWH, RDD
System-Level Test	Matsuoka et al. 2008	shake table - X+Y	Yes	RDD
	McCormick et al. 2008	shake table - X	Yes	
	Retamales et al. 2011	UB-NCS - X		
	Wang et al. 2015	shake table - X	Yes	
	Soroushian et al. 2012	shake table - X+Y, X+Y+Z		CWH, WD, FP, WI
	Jenkins et al. 2016	shake table - X+Y	Yes	CWH, WD, FP, WI, PHW, RDD
	Fiorino et al. 2019	shake table - X	Yes	CWH, CWV

In this study, to expand the knowledge of the seismic response of partition walls, two sets of partition walls with innovative details aimed at reducing drift-induced damage were

experimentally evaluated using a bidirectional loading protocol. In both phases, partition walls were built within a post-tensioned CLT rocking wall subassembly. The objectives of this study are to evaluate the effect of out-of-plane drift on the partition wall in-plane resisting force, to evaluate the contribution of the partition walls to the overall structural strength and stiffness, and to evaluate the effectiveness of the innovative construction details on damage states. In Phase 1, a telescoping (track-within-a-track) deflection assembly is compared to conventional slip-track detailing in straight walls. Both details permit sliding of the top of the wall relative to the diaphragm, but the telescoping detailing, which has been used mainly for absorbing the vertical deflection of the diaphragm, has not – to the authors' knowledge – been tested under lateral loading (ATC 2012). In Phase 2, two C-shaped walls with details aimed at reducing damage at wall intersections are evaluated. The distributed gap (DG) detail incorporates more frequent expansion joints through the length of the wall to absorb some of the in-plane movement and delay the collision with the intersecting wall. The corner gap (CG) detail incorporates a full gap through the wall intersection to allow intersecting walls to penetrate the corner region without damage. The CG detailing has been proven to reduce damage at the wall-intersection for in-plane loading, but the performance under bidirectional loading has not been investigated (Retamales et al. 2013).

4.3 Test program

As mentioned above, the experimental program consisted of bidirectional tests on full-scale partition walls constructed within a post-tensioned CLT rocking wall subassembly at the

Natural Hazard Engineering Research Infrastructure (NHERI) Lehigh Equipment Facility (EF). This testing was conducted as part of the NSF collaborative NHERI TallWood Research Program ("NHERI TallWood-Home" 2020). The partition wall configurations integrated within the CLT rocking wall subassembly are illustrated in Figure 4-1. In particular, Phase 1 consisted of two straight partition walls (Figure 4-1 (a)), and Phase 2 consisted of two C-shaped wall assemblies (Figure 4-1 (b)).

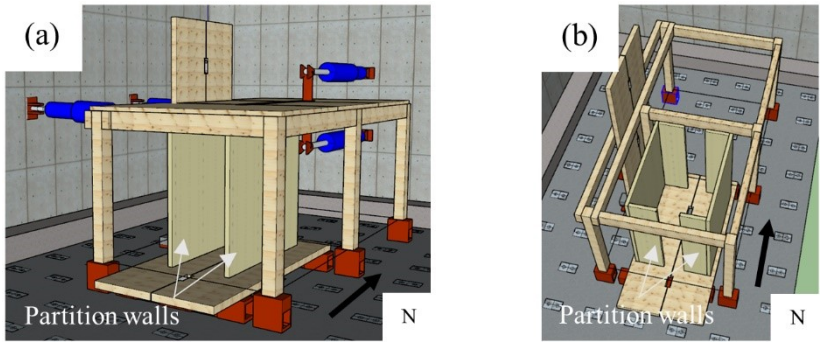

Figure 4-1: Configurations of partition walls: (a) Phase 1, (b) Phase 2

4.3.1 Test-bed setup

The structural test-bed specimen, designed by Lehigh University (Bond et al. 2018; Clay et al. 2019), was a post-tensioned CLT rocking wall subassembly. The test-bed was used to impose bidirectional cyclic loading on partition walls installed between the CLT base and floor diaphragms. Figure 4-2(a) shows the different parts of the test-bed specimen. U-shaped flexural plates connected coupled post-tensioned CLT rocking walls for energy dissipation. Each wall was constructed from a 5-layer (175 mm thick) Spruce-Pine-Fir South (SPF-S) CLT panel with dimensions 1.52 m long by 6.1 m high, and was post-tensioned with an 806 mm^2 steel to the foundation at the center of the panel to produce a

self-centering response. Two 222 mm x 419 mm Douglas-Fir (DF) glulam collector beams were connected to the CLT rocking wall from both sides to deliver the lateral forces from the 3-layer SPF-S CLT floor diaphragm to the CLT rocking wall. The collector beam to the CLT rocking wall connection was a round pin through a vertical slot at the wall (Figure 4-2(b)). The connection was designed so that the collector beam and floor diaphragm do not uplift when the CLT rocking wall rocks up off the foundation. Out-of-plane rubber bearings, sliding on the Teflon surface, were designed to transfer the out-of-plane loading from the floor diaphragm to the CLT rocking wall and to brace the CLT rocking wall in the out-of-plane direction. The gravity load system consisted of 140 mm x 305 mm DF glulam beams and 311 mm x 381 mm DF glulam columns with pinned bases. The base diaphragm consisted of two separate five-ply CLT panels placed on friction Teflon pads, which allowed the forces in each partition wall to be measured by axial load cells (Figure 4-2 (c)).

The partition wall tests followed a series of tests on the structural test-bed performed by Lehigh University. Prior to the partition wall tests, the CLT rocking walls were repaired (Figure 4-2 (d)) by attaching steel plates with wood screws to the corner of each wall panel.

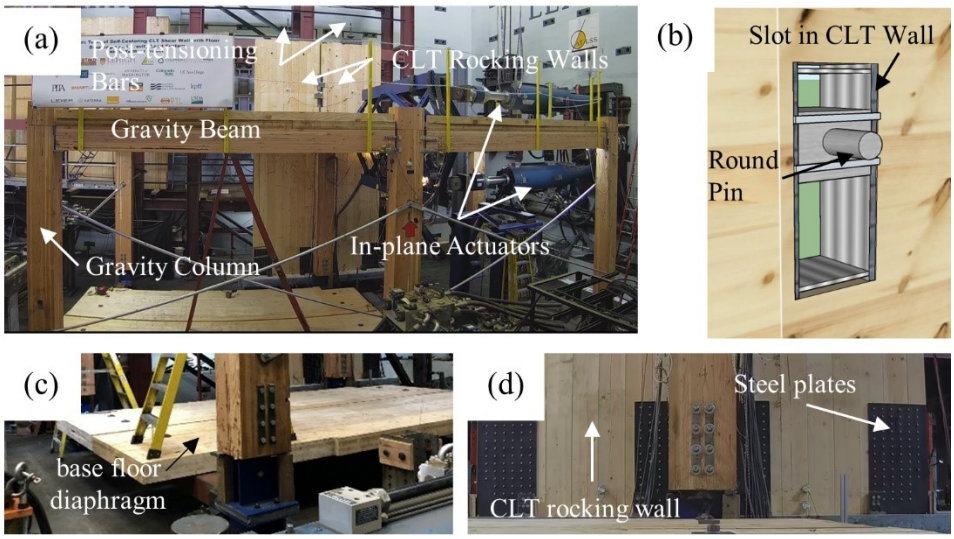

Figure 4-2: Structural test specimen; (a) Test specimen, (b) Collector-beam-to- CLT rocking wall connection, (c) Base floor diaphragm, (d) Repaired CLT rocking wall

4.3.2 Test-specimen detail

Partition wall dimensions are illustrated in Figure 4-3. The partition walls for Phase 1 were 3.69 m long (Figure 4-3 (a)). For Phase 2, the clear lengths of the walls between return walls were 3.45 m for the CG wall and 3.49 m for the DG wall. The return walls (intersecting walls) were 0.92 m long and 0.85 m long respectively (Figure 4-3 (b)). Discrepancies in wall lengths were due to differences in the gap detailing. All walls were 3.81 m high.

The partition walls adopted in both phases were built according to common construction practice for institutional slip track detailing, and the wall design was checked against out-of-plane deflection limits for a horizontal load of 0.24 kN/m^2 (IBC 2012; SSMA 2000a; SSMA 2000b). Figure 4-4(a) illustrates the partition wall components, and Table 4-2 lists the framing and material specifications for the partition walls. The walls were framed from

steel with a nominal minimum yield strength of 227.53 MPa, and the studs were spaced at 406 mm o.c. The framing was sheathed with a 15.9 mm thick standard drywall. Self-drill screws were used for all stud-to-track connections (4.8 mm diameter screws) and drywall-to-stud connections (3.5 and 4.2 mm diameter screws). The studs and drywall were generally fixed to the bottom tracks (Figure 4-4 (b)). Corner-bead sticks with 35.1 mm legs were generally used for outside corners. All walls were taped and painted according to standard finishing procedures.

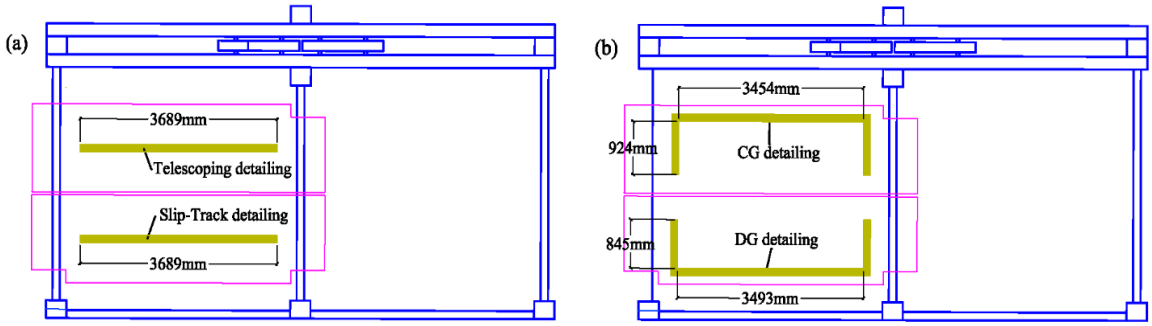

Figure 4-3: Placement of walls in the test-bed structure and dimension of walls; (a) Phase 1, (b) Phase 2.

Figure 4-5 shows the proposed details for damage reduction considered in this study. As mentioned previously, two details for connecting the partition wall to the floor diaphragm were considered in Phase 1: slip-track detailing (Figure 4-5 (a)) and telescoping detailing (Figure 4-5 (b)). In the slip-track detailing, the studs and drywall were not connected to the top track, allowing the studs to slip relative to the top track. In telescoping detailing, the sliding occurred between an inner track nested within an outer track, while all the studs and the drywall were connected only to the inner track.

Table 4-2 Nominal dimensions and material properties of partition walls

Studs	362S125-33	92.08 mm width x 31.75 mm leg height x 0.84 mm thickness
Tracks	362T125-33	92.08 mm width x 31.75 mm leg height x 0.84 mm thickness
	362T200-33	92.08 mm width x 50.8 mm leg height x 0.84 mm thickness
	362T250-43	92.08 mm width x 63.5 mm leg height x 1.09 mm thickness
	375T200-54	95.25 mm width x 50.8 mm leg height x 1.37 mm thickness
Track to diaphragm screws	SDS Heavy-duty connector screw 6.35 mm Ø x 76.2 mm @ 305 mm, and 152 mm at corner zone	
Frame screws	#10 SMS Self Drill Screw	
Drywall to frame screws	Self-Drill Screw #6 at 203 mm o.c. on boundaries and 305 mm o.c. on the field (#8 for 2 or 3 layers attachments)	
Finishing	Joints	Paper tape attached with plaster-based compound and covered with two coats of plaster-based compound
	Fasteners	Covered with three coats of plaster-based compound
	Expansion joints	PVC "V" expansion joints with the allowable movement of 9.5 mm attached with spray adhesive
	CG angles	Covered with flexible corner bead with a leg width of 57.2 mm
	Exterior angles	Covered with corner-bead sticks with the 35.1 mm legs

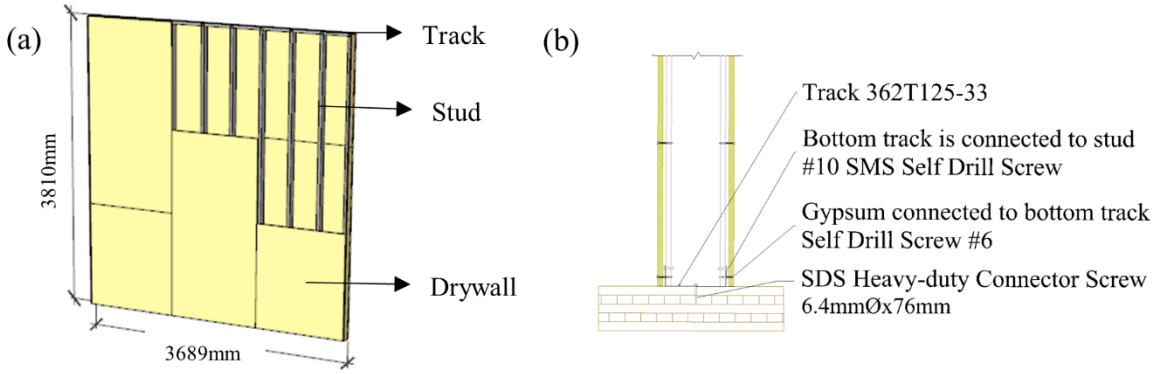

Figure 4-4: (a) Partition walls components - 3D view, (b) Detail of connection of walls to the bottom diaphragm

Phase 2 incorporated the DG detailing and CG detailing into conventional slip-track walls to reduce damage at the wall intersections. Expansion joints are usually limited to the mid-wall region, but in the DG detailing tested here, expansion joints were also located adjacent to the return walls. Both non-fire-rated (Figure 4-5(c-d)) and fire-rated (Figure 4-5(e-f)) expansion joints were incorporated adjacent to the wall intersection and in the wall interior,

respectively. In the fire-rated expansion joints, two layers of drywall were added within the joint to prevent fire intrusion. PVC "V" expansion joints with an allowable movement of 9.5 mm were attached with spray adhesive. The drywall was not screwed at the bottom of the DG wall to provide a hinge connection and better accommodate the movement permitted by the expansion joints.

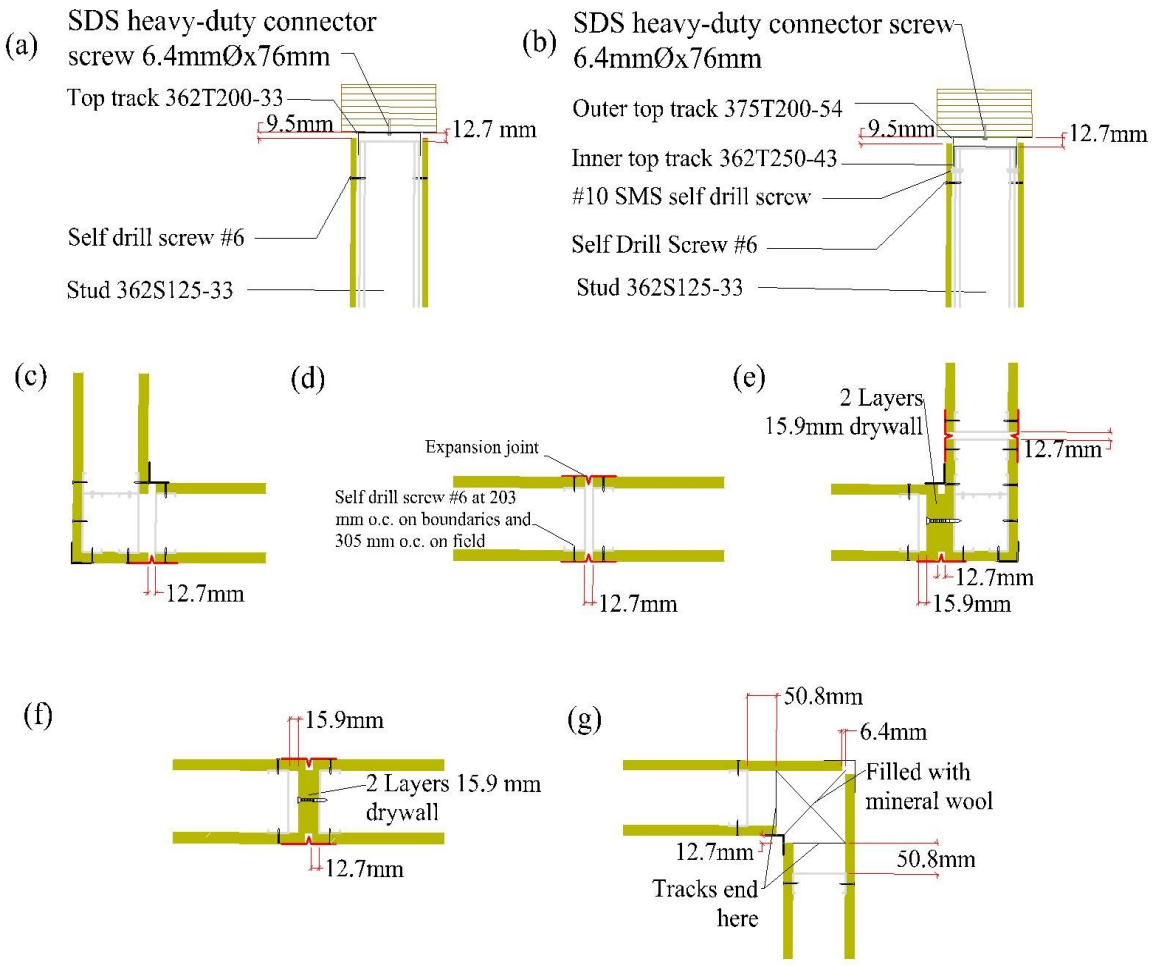

Figure 4-5: Details adopted in phases 1 and 2 for damage reduction; (a) Slip-track connection, (b) Telescoping connection, (c) Wall intersection non-fire-rated expansion joint, (d) Interior non-fire-rated expansion joint, (e) Wall intersection fire-rated expansion joint, (f) Interior fire-rated expansion joint, (g) Corner gap detail

In the CG wall, tracks and studs were not extended into the corner region, to allow slip movement of the walls to penetrate the intersection (Figure 4-5(g)). The corner region was filled with mineral wool for fire protection. Moreover, the angles of the CG wall were covered with a flexible corner bead with a leg width of 57.2 mm.

4.3.3 Loading protocol and instrumentation

Photos of relevant instrumentation for the structural specimen are shown in Figure 4-6. Plastic slides at the bottom of the CLT rocking wall measured its uplift, and string pots connected to the collector beam (only attached in Phase 2) measured its vertical movement (Figure 4-6(a)). Load cells attached at the end of each actuator measured the total lateral force in the subassembly (Figure 4-6(b)). String potentiometers measured the structure-physical node (SPN) displacement (Figure 4-6(c)).

The layouts of the partition wall instrumentation for Phases 1 and 2 are provided in Figure 4-7(a) and Figure 4-7(b), respectively, while pictures of instrumentation are shown in Figure 4-8. Figure 4-8(a) shows plastic slides that measure the slip of the bottom track and rocking of walls in Phase 1 (PSE1, PSE5, PSE4, PSE8, PSW1, PSW5, PSW4 and PSW8 in Figure 4-7(a)). Figure 4-8(b) shows a unidirectional load cell attached to the bottom diaphragm. Figure 4-8(c) shows an example of a plastic slide used to measure the vertical gap at the top of the walls (PSW2, PSW3, PSE2 and PSE3 in Figure 4-7(a), and PSW1, PSW4, PSW5, PSW8, PSE1, PSE4, PSW7, and PSE10 in Figure 4-7(b)). Figure 4-8(d) shows the cameras that are used for continuously following the damage, and some of the videos are available online (“NHERI TallWood Research Tasks” 2020).

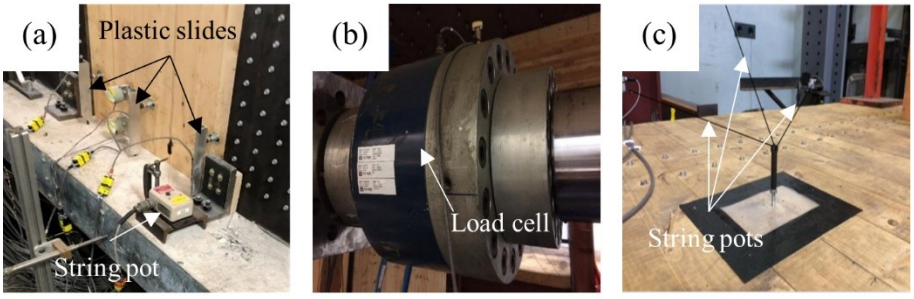

Figure 4-6: Instruments on the structural specimen; (a) String pot and plastic slide to measure uplift in collector beam and wall, (b) Load cells on actuators to measure the force in the building, (c) String pot connected to the SPN

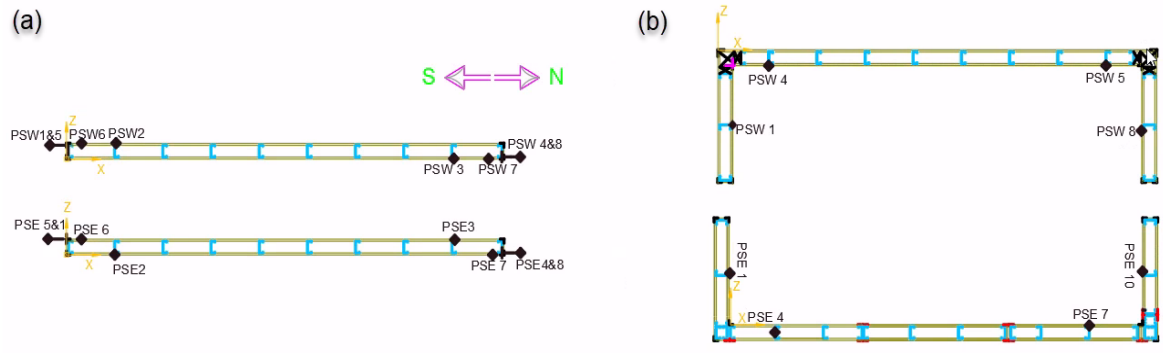

Figure 4-7: Schematic view with the indication of the adopted instrumentations; (a) Phase 1, (b) Phase 2

The test specimen was subjected to displacement-controlled bidirectional loading imposed by actuators connected to the CLT floor diaphragm of the subassembly. Loading in the direction of the lateral load resisting system (in-plane) was applied by two in-plane actuators and in the out-of-plane direction by two out-of-plane actuators. The movement of the test subassembly was controlled by the SPN, wherein displacement commands were imposed through a relationship between the SPN and the actuators.

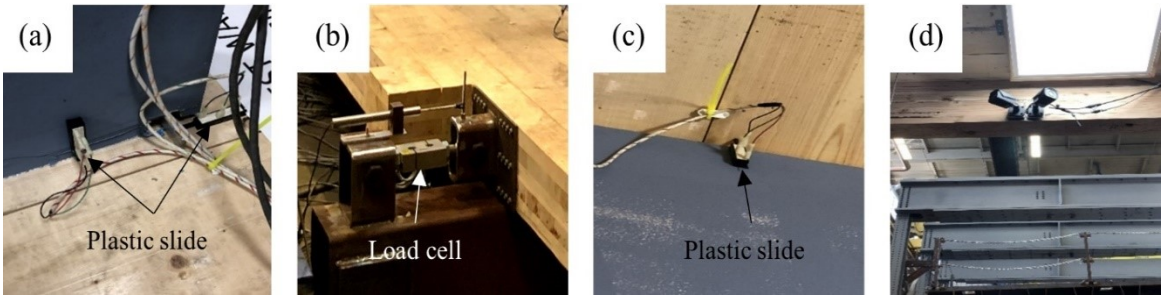

Figure 4-8: Instrumentation; (a) Plastic slides for measuring track slide and rocking of partition wall, (b) Load cell for measuring the force in the partition wall, (c) Plastic slide for measuring gap at the top of the wall, (d) Cameras

A cyclic drift loading protocol was used for this test. The loading protocol specified a bidirectional path of movement, with three sub-cycles in each stage: in-plane, bidirectional hexagonal, and bidirectional hexagonal with an increase in out-of-plane drift (Figure 4-9(a)). The magnitude of peak in-plane drift was increased in each stage, as shown in Figure 4-9(b). The Phase 1 walls were loaded to 5% drift and the Phase 2 walls to 4% drift. This loading protocol was designed to evaluate the effect of the out-of-plane drift on the in-plane resistance of the partition wall. The loading protocol was based on FEMA 461 (ATC 2007) but with additional cycles in each stage. After the first two stages, the amplitude was increased by a factor of 1.25 in each stage. These modifications were introduced to capture the wall damage for both minimal and high drift ratios. Table 4-3 shows the drift, displacement, and loading rate of each cycle. The displacement-controlled test procedure varied the displacement rate between 15 to 40 mm/min (Table 4-3). The data were recorded with a sampling frequency of 8 Hz.

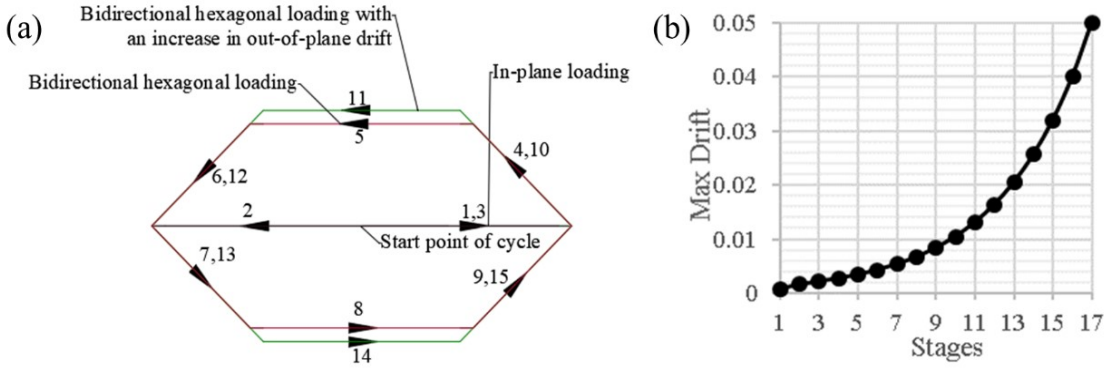

Figure 4-9: (a) Path of movement of the bidirectional load step, (b) Peak in-plane drift amplitude in different stages

Table 4-3: Loading protocol

Stage	In-plane Wall Drift at Floor Level % (mm)	Out-of-plane plane Wall Drift at Floor Level % (mm)	Cycles	Loading Rate (mm/min)
A	0.08 (3)	0.04 (2)	3	15
B	0.16 (6)	0.08 (3)	3	15
C	0.22 (8)	0.11 (4)	1	15
D	0.27 (10)	0.14 (5)	1	20
E	0.34 (13)	0.17 (7)	1	20
F	0.43 (16)	0.21 (8)	1	20
G	0.54 (21)	0.27 (11)	1	20
H	0.67 (26)	0.33 (13)	1	30
I	0.84 (32)	0.42 (16)	1	30
J	1.05 (40)	0.52 (20)	1	30
K	1.31 (50)	0.65 (25)	1	30
L	1.64 (57)	0.82 (29)	1	30
M	2.05 (78)	1.02 (39)	1	35
N	2.56 (98)	1.28 (49)	1	35
O	3.2 (122)	1.6 (61)	1	35
P	4 (152)	2 (76)	1	40
Q	5 (191)	2.5 (96)	1	40

4.4 Test results

4.4.1 Damage observations

The seismic performance of the partition walls was evaluated through observation of the damage mechanisms. The primary damage measures observed in the partition wall specimens in both phases are shown in Figure 4-10. In this figure, T refers to telescoping detailed, and ST refers to slip-track detailed Phase 1 walls, while CG refers to the corner gap, and DG refers to distributed gap Phase 2 walls. In Figure 4-10, Images 1 and 2, respectively, depict detachment of the corner bead and warping of the drywall, which were observed in both the slip-track and telescoping walls when the track leg pushed against the end drywall. Images 3-5 depict the opening of the corner bead, bending of the end stud, and bending of the track leg, which were all observed only in the slip-track wall. These occurrences corresponded to a significant increase in the resisting force of the wall when the end stud passed the end of the track and could not slide back into place upon cyclic reversal.

At a drift of 0.43%, the sacrificial corner beads detached from the CG wall due to the incompatible movement of in-plane and out-of-plane drywall (Image 6). Damage to the track leg in the CG wall (Image 7) was similar to that observed in Image 5. Damage to the end stud (Image 8) and permanent movement of the CG return wall (Image 9) were observed in post-test inspections after the drywall was removed. This damage was believed to have occurred at 78 mm (2.05%) drift after the end stud slid past the end of the track. Note that this drift corresponded to approximately the length of the track beyond the stud

(50.8 mm) plus the stud leg length (31.8 mm). The first damage observed in the DG wall was the detachment, or opening of the expansion joint when its limit was reached (Image 10). After the expansion joint closed, the track leg of the return wall opened or bent (Image 11), and the studs of the main wall pushed against the return wall. In Images 12 and 13, the wall completely separated at the expansion joint due to the repeated cyclic opening and closing of the joint, causing extensive damage to the stud and track. The introduction of expansion joints on both walls immediately adjacent to the wall intersection (fire-rated detailing) led to a stability issue because, as both joints opened, a small wall section at the corner detached and became isolated. Post-test inspections of the DG wall after removal of drywall showed the permanent movement of the return wall (Image 14) similar to Image 9 and damage to the studs and tracks (Image 15) due to the impact of the main wall and the return wall.

Figure 4-11 (a)-(d) shows the force versus drift hysteresis loops in each partition wall. The likely occurrences of the damage measures in Figure 4-10 are indicated on the hysteresis loops with corresponding numbers 1-14. Some damage to the slip track wall (Images 3 and 5) occurred during the bidirectional loading, which indicates that bidirectional loading contributed to the initiation of damage. These damage occurrences corresponded to sudden increases in force on the hysteretic loops. Since the slip-track (Figure 4-11(a)) and telescoping walls (Figure 4-11(b)) have similar slip behavior, the magnitude of forces generated in each wall was similar. Because the CG wall did not have studs and tracks in the wall intersection that allowed the walls to penetrate the intersection, its resisting force was similar to the Phase 1 walls without return walls (Figure 4-11(c)). However, the DG

wall experienced significant resistance from the collisions at the wall-intersection after the expansion joints closed (Figure 4-11(d)). The differences in the response of different walls, including the resistance and stiffness, are summarized in Figure 4-11(e), which shows the backbone curves of in-plane cycles of all wall specimens. Although these backbone curves did not capture peaks that occurred during out-of-plane cycles, they are useful for the relative comparison of walls.

For each wall specimen, the strength was evaluated by calculating the average value of the maximum and minimum values of resisting force from the backbone curves (Figure 4-12(a)), and the stiffness as the peak-to-peak stiffness between these two points (Figure 4-12(b)). The strength and stiffness values (0.8 kN and 68.1 kN/m for slip-track compared to 1.0 kN and 81.2 kN/m for telescoping) suggest that even with a similar slip behavior at the top, the friction was slightly higher in the telescoping detailing. The average maximum force that developed in the DG wall was much higher than in the CG wall (6.0 kN compared to 1.5 kN) because the DG detailing led to typical resistance at the intersection walls after the expansion joints closed, while the CG wall responded similarly to the Phase 1 walls without return walls. The difference in the secant stiffness was much less than the difference in the strength (173.1 kN/m for DG compared to 99.0 kN/m for the CG) because of the peak force in the DG wall occurred at a larger drift.

1. T: Detachment of corner bead (0.43% drift)

2. ST: Warping of drywall (0.67% drift)

3. ST: Opening of corner bead due to bending of stud (0.84% drift)

4. ST: Bending of end stud (2.56% drift)

5. ST: bending of leg of track (3.2% drift)

6. CG: Detachment of corner bead (0.43% drift)

7. CG: Damage to the leg of track (2.56% drift)

8. CG: Damage to end stud (after test)

9. CG. Permanent movement of return wall (after test)

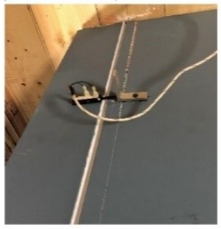

10. DG: Detachment of expansion joint (0.84% drift)

11. DG: Opening of leg of track (1.05% drift)

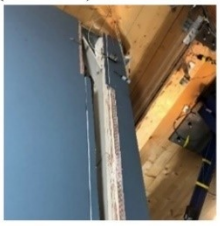

12. DG: Big opening at expansion joint fire-rated (2.56% drift)

13. DG: Big opening at expansion joint non-fire-rated (after test)

14. DG: Permanent movement of return wall (after test)

15. DG: Damage to the studs and tracks (after test)

Figure 4-10: Observed damages to partition walls at various stages of testing: T = Telescoping, ST = Slip-track, CG = Corner gap, DG = Distributed gap

The hysteresis loops of the entire sub-assembly (CLT rocking walls and partition walls) are compared to those of the structural sub-assembly alone in Figure 4-13 for both test phases. For Phase 1, there is not a noticeable difference when the resistance of the partition walls is included in the hysteresis loops (Figure 4-13(a)). For Phase 2, only a slight difference between the two curves is visible (Figure 4-13(b)). Specifically, in Phase 1, the partition walls contributed 0.6% to the whole subassembly force (1.8 kN of 292.8 kN) and 10% to the whole subassembly stiffness (149.3 kN/m of 1516.9 kN/m). In Phase 2, the partition walls contributed less than 3% to the total force (7.5 kN of 266.1 kN) and about 16% to the stiffness (272.1 kN/m of 1719.4 kN/m) of the whole subassembly. The resistance of partition walls in Phase 2 increased due to the impeding effect of the return walls, but their contribution to the subassembly resistance was still minor. Note that the peak forces in the partition walls occurred at low drifts (average of 1.2 percent), but the peak force of the subassembly was observed at the peak drifts. Therefore, the partition walls contribute more significantly to the initial resistance than to the limit state responses.

Even after repairs were made to the CLT panels of the rocking walls, there was still stiffness degradation due to localized bearing, spalling of the concrete footings at the corners, and deformation in the connection between the steel plates and the CLT wall panels. Thus, assuming the lateral system is initially undamaged, the resistance of the partition walls likely need not be accounted for in the lateral system design for a large earthquake. However, the numbers provided here could be used to estimate the inter-story stiffness and strength contributions of partition walls based on total wall length in each direction.

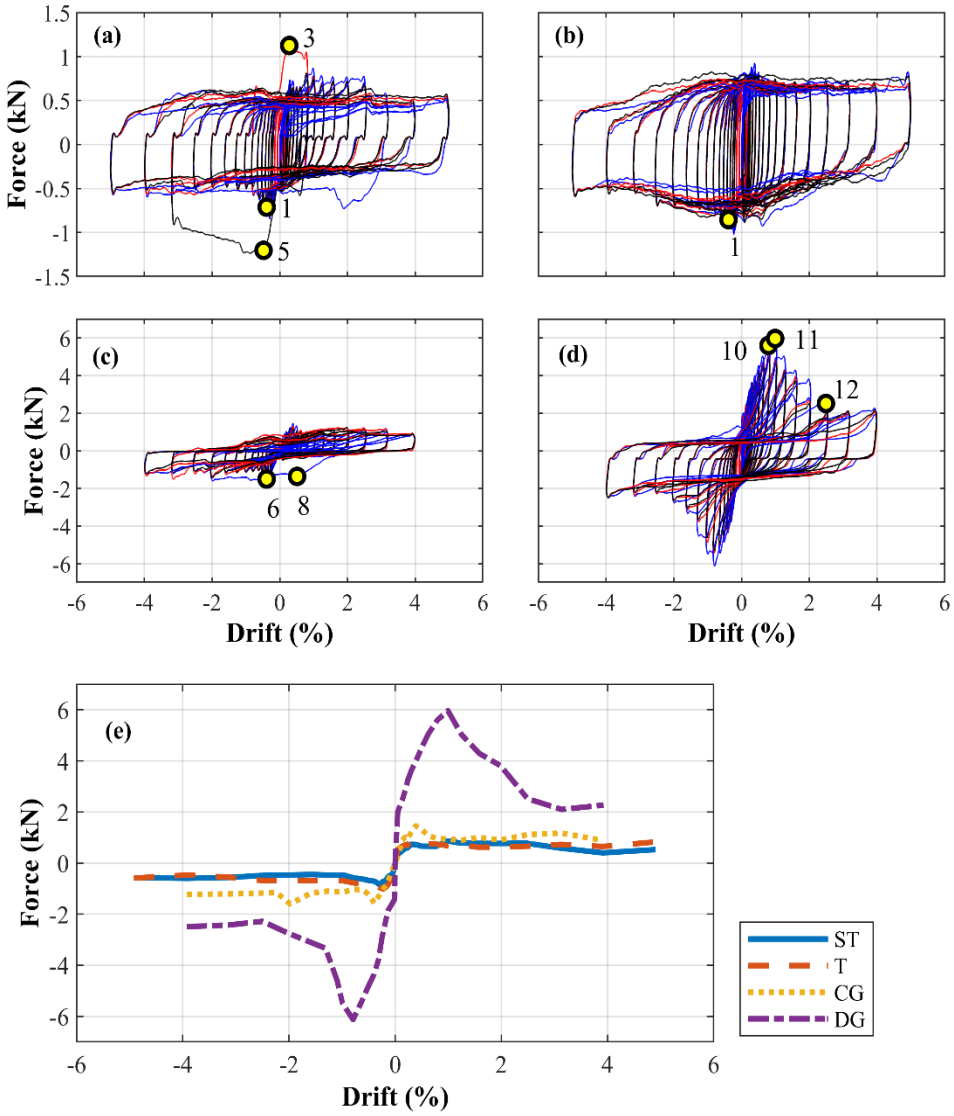

Figure 4-11: Experimental load versus inter-story drift with an indication of damage progression; (a) Slip track, (b) Telescoping, (c) Corner gap, (d) Distributed gap; blue = in-plane cycle, red = bidirectional cycle 1, black = bidirectional cycle 2, (e): backbone

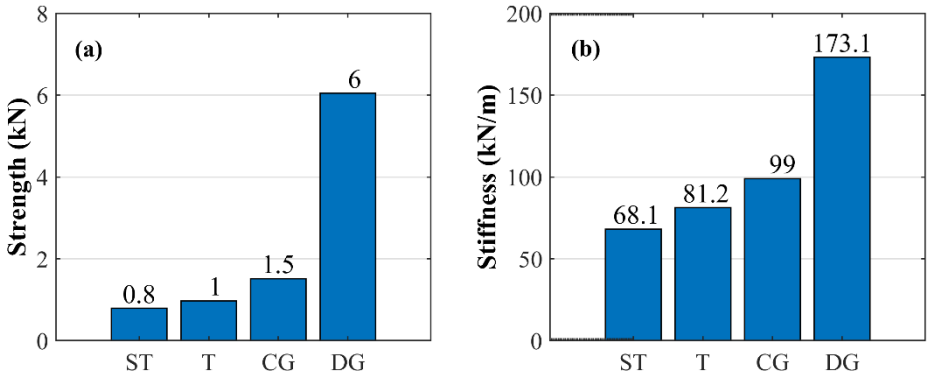

Figure 4-12: (a) Peak strength and (b) Corresponding secant stiffness of each partition wall

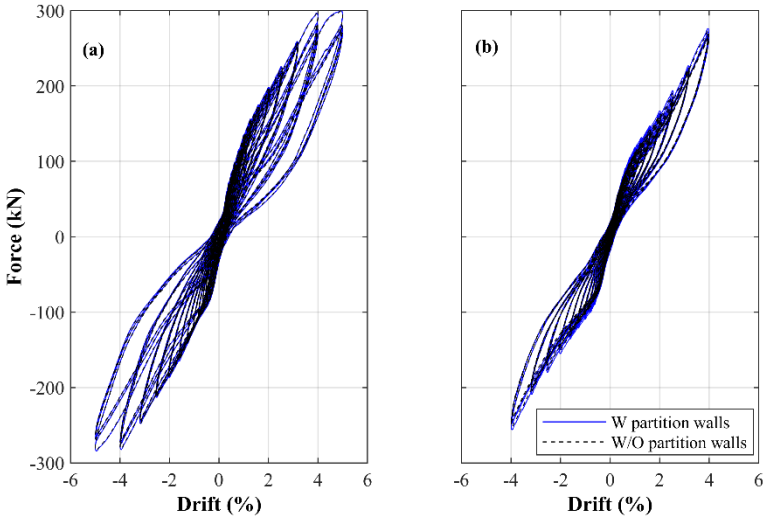

Figure 4-13: Hysteresis of building in the in-plane direction; (a) Phase 1, (b) Phase 2

4.4.2 Correlation between damage limit states and drifts

Next, the damage observations in these tests are correlated to standard damage states characterized by damage observation class and, most importantly, required repair actions. Based on the FEMA-P58 background document for partition walls (Mosqueda 2016), in Damage State 1 (DS 1), the wall needs minor drywall patching, taping, and painting. A DS

2 wall needs more drywall patching, taping and painting, and replacement of a few boundary studs. In DS 3, at least half of the wall requires replacement, and the whole wall requires repainting. Table 4-4 also presents the drift ratio at which each damage state was observed in each test specimen. For some walls, multiple damage observations can be interpreted as DS 3, but for evaluation purposes, the first observation (minimum drift) corresponding to a defined DS was selected. Furthermore, Table 4-5 and Table 4-6 compare drift ratios corresponding to partition wall DSs for Phase 1 and Phase 2 walls, respectively, to other prior experimental studies of similarly configured walls. Prior studies in Table 4-5 are restricted to institutional slip-track detailing, with a similar stud to bottom track connections as the Phase 1 walls here. Note that while efforts have been made to be consistent, discrepancies in DS drifts may occur due to different loading protocols, experimental setup, detailing, or even interpretation of the DS definition.

Table 4-4: Inter-story drift ratio (IDR) levels recorded at different damage states

DSs and Damage Phenomena		**ST(%)**	**T(%)**	**CG(%)**	**DG(%)**
DS1	Medium/severe opening of corner bead	0.43	0.43	0.43	0.84
DS2	Bending of end stud	0.84	-	2.05	1.05
DS3	Bending of the leg of the track	3.20	-	2.56	1.05
	Large opening at expansion joint	-	-	-	2.56
	Permanent movement of the return wall	-	-	4.00	4.00

Table 4-5: Comparison of drift ratios for straight walls (no return walls) with institutional slip track detailing

Damage state	**DS1 (%)**	**DS2 (%)**	**DS3 (%)**
Davies et al. 2011	0.53	0.81	1.66
Jenkins et al. 2016	2.07	2.07	-
Phase 1-ST	0.43	0.84	3.2
Phase 1-T	0.43	-	-

Besides the two Phase 1 walls, two other studies evaluated institutional slip-track detailing without return walls: Davies et al. (2011) and Jenkins et al. (2016). The telescoping detail examined in this study (Phase 1-T) was observed to eliminate damage to the framing of partition walls caused by the separation of the end studs from the track at large drifts that occurred in the other walls (Table 4-5). Thus, DS 2 and beyond were never observed in the Phase 1-T wall, while studies of traditional slip track detailing observed DS 2 at drifts ranging from 0.81%-2.07%. DS 1 and DS 2 were observed at larger drifts in Jenkins et al. (2016) compared to the Phase 1-ST wall; the reason is unclear, but perhaps these wall ends were better detailed to avoid damage during sliding, and only the Phase 1-ST wall was subjected to bidirectional loading. DS3 was not observed in one of the specimens in Davies et al. (2011), but it was observed in the two other specimens with an average of 1.66%.

Table 4-6 focuses on reduced damage detailing for wall intersections and is restricted to C-shaped/T-shaped walls with return walls. Besides the Phase 2 CG and DG walls, studies included in Table 4-6 are Mosqueda (2016), Retamales et al. (2013), and Araya-Letelier et al. (2019). Mosqueda (2016) represents the average based on fragility functions for typical slip track detailing. Retamales et al. (2013) tested a CG detailing similar to the Phase 2 CG wall, and a double slip-track detailing. In double slip-track (DST) detailing, nail fasteners of the top and bottom track to the slabs are eliminated within 1200 mm of intersecting walls, and the out-of-plane flexibility of the transverse walls is relied on to reduce the contact forces. Araya-Letelier et al. (2019) evaluated a different detail to allow the partition wall to slip relative to the diaphragm above called the “sliding/frictional connection.” In this connection, the upper track is placed between a thin plate connected to the upper slab

and a short square or rectangular steel tube. The upper track has 88.9 mm circular holes centered around anchors that clamp the tube to the slab above. The clamping force is specified to control the friction, and the holes allow movement in both directions so that intersecting walls can move together. In both of these tests, the specimens were subjected to in-plane loading only.

Table 4-6: Comparison of drift ratios for intersecting walls with various low damage detailing

Damage state	DS 1 (%)	DS 2 (%)	DS 3 (%)
Mosqueda 2016	0.4	1.1	1.9
Araya-Letelier et al. 2019	1.5-2.1	1.5-2.1	3
Retamales et al. 2013-CG	0.6	-	-
Retamales et al. 2013-DST	1.00	1.35	1.84
Phase 2-CG	0.43	2.05	2.56
Phase 2-DG	0.84	1.05	1.05

In the Phase 2-CG wall tested here, the sacrificial corner bead detached (DS 1) at low drifts, similar to slip-track detailing with typical intersection details. However, DS 2 and DS 3 were not observed until after 2% drift. By comparison, the CG detail tested in Retamales et al. (2013) never sustained DS 2 or DS 3 but was subjected only to in-plane loading. The Retamales et al. (2013)-DST detailing was successful in delaying DS 1 up to 1% story drift; however, the DS 2 and DS 3 occurred in the same drift range as typical slip-track detailing. In the Phase 2-DG wall evaluated here, expansion joints helped to delay DS 1 to about 1% story drift (Table 4-6). Only the expansion joints adjacent to the wall intersections were effective in reducing the damage. Also, Araya-Letelier's sliding/frictional connection was shown to successfully isolate the partition walls from any damage up to a displacement of 37 mm (drift = 1.5%). Damage occurred shortly after reaching the free sliding limit of 32 mm, which was determined by the size of the circular hole in the track. Jenkins et al. (2016)

reported on additional experimental tests of the sliding/frictional connection incorporated in a building test-bed. Damage to the walls initiated at drifts less than 1% in these experiments, which is partially explained by the fact that the free sliding limit (constant at 32 mm) corresponded to a lower drift due to the increased story height. At larger drifts, Jenkins et al. (2016) reported damage characteristics similar to a fixed connection, such as dislodging of the screw head from the plaster coating and plastic hinging of studs. However, noticeable reductions in tape damage and cracks in the wall corners were observed.

In comparing the connections, the sliding/frictional connection (Araya-Letelier et al. 2019) was most successful in delaying the onset of damage (DS 1), but this connection will be less effective for taller story heights. However, the range of drift percentages observed in DS 2 and DS 3 was comparable for the Phase 2-CG wall and the sliding/frictional connection. The Phase 2-DG wall was shown to be another possible approach to delay the initiation of damage; however, total damage (DS 3) occurred at only incrementally larger drifts.

Another study worth mentioning is Tasligedik et al. (2013), but it was not included in Table 4-6 because the setup did not incorporate return walls. The study explored gap details similar in concept to the Phase 2-DG wall. First, gaps totaling 40 mm in width, which could accommodate 1.5% drift, were provided at the wall ends and between drywall panels. Second, the drywall was only connected to the studs, and the studs were friction fitted to allow for sliding. The partition walls were tested as an infill wall within a concrete frame. The performance of this detail was much better than the Phase 2-DG wall. However, the

structural integrity of this detail might be challenged when implemented with typical return wall configurations rather than bound by a rigid frame, and fire protection remains an issue.

4.4.3 Influence of rocking wall uplift on partition wall response

In this test, the collector beam was connected to the CLT rocking wall by an eccentric round pin through a vertical slot at the wall. The intended behavior of the connection is that the collector beam and floor diaphragm do not uplift when the CLT wall rocks up off the foundation.

Figure 4-14 presents several measurements to quantify the impact of rocking wall uplift during the tests. For the Phase 1 walls at a drift cycle of 3.2%, Figure 4-14(a) shows the uplift of the south wall at the location of the pin. Since the pin was located eccentrically on the rocking walls, the uplift was asymmetric. Figure 4-14(b) shows movement across the vertical gap at the top of the partition walls at various sensor locations (PSE 2, PSE3, PSW2, and PSW3 in Figure 4-14(b)). Notably, the movement of the diaphragm was not sufficient to close the vertical gap of 9.5 mm (depicted as negative in Figure 4-14(b)) or open the gap (depicted as positive in Figure 4-14(b)) enough to cause the stud and track (overlapping by 41.3 mm) to pull apart. There was no real correlation between movement across the gap and proximity to the rocking wall, which suggests that these partition walls were not affected by localized diaphragm deformation.

Figure 4-14(c) is analogous to Figure 4-14(a) for Phase 2 tests, except that the vertical displacements of the adjacent collector beam at the pin and near the column, which were only measured in Phase 2, are also shown. The relative movements across the partition wall

vertical gap are shown in Figure 4-14(d) and Figure 4-14(e) at the main wall sensor locations (PSW4, PSW5, and PSE7) and return wall sensor locations (PSW1, PSW8, PSE1, and PSE10), respectively. The uplift was reduced significantly from the wall to the collector beam due to the introduction of the slotted connection (Figure 4-14(c)). However, this connection did not completely prevent the vertical movement of the collector beam at higher drifts, probably due to increased friction as the wall rotated. The collector beam started to displace upward at about 2% drift, and its displacement was comparable to the wall uplift thereafter. The provided gap at the top of the partition wall was again sufficient to accommodate the movement of the diaphragm for Phase 2 walls, even though the main CG wall was in much closer proximity to the rocking wall. Moreover, the relative vertical movement across the partition walls gap was more significant for wall locations near the south end of the diaphragm (PSW4, PSW1, and PSE1) than at other locations. Larger vertical movements were believed to occur at these locations due to proximity to the collector beam or end of the diaphragm, and the corners being less restrained by gravity load.

Figure 4-15 shows the maximum and minimum value of vertical displacement/movement across the gap in the in-plane cycle of each stage. The maximum values correspond to the opening of the gap (Figure 4-15(a)), and the minimum values correspond to the closing of the gap (Figure 4-15(b)). As noted earlier, after 2% drift, a greater portion of the wall uplift transferred to the collector beam both near the column and at the pin location. Moreover, this vertical movement of the collector beam more significantly affected partition wall locations at the end of the diaphragm (south sensors), so these locations experienced a

significant increase in the vertical movement across the gap after a 2% drift compare to other locations.

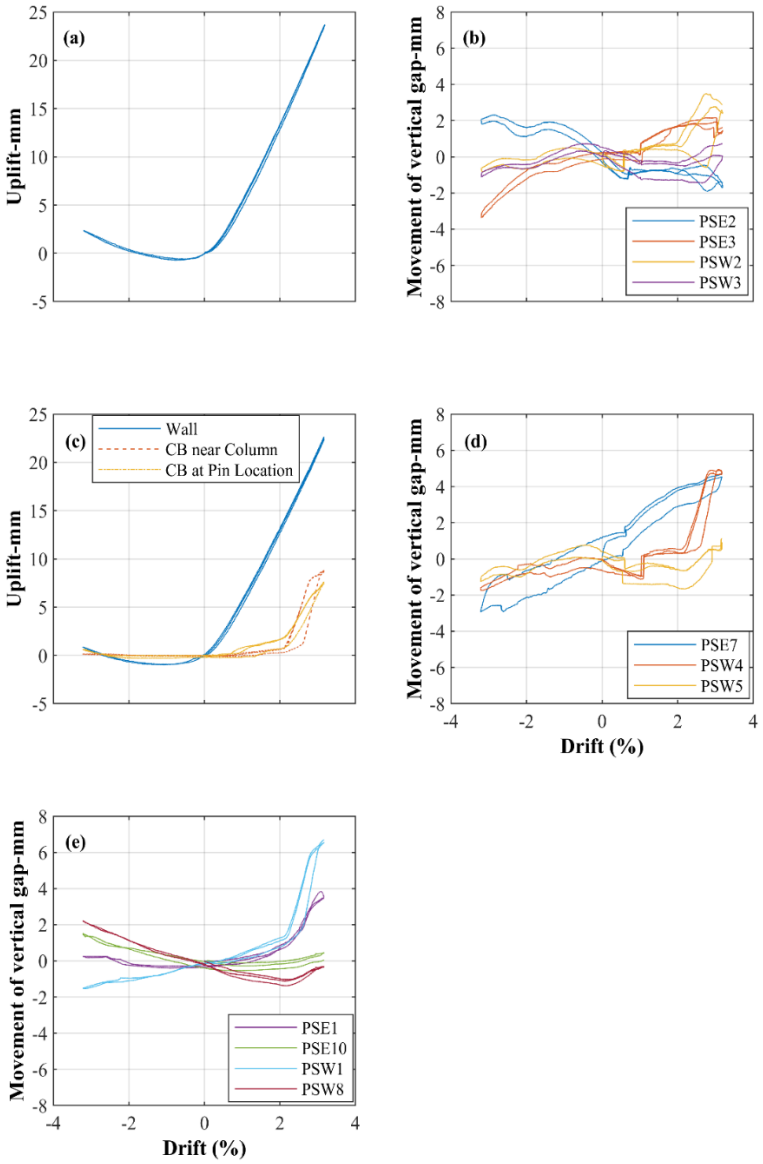

Figure 4-14: Phase 1: (a) Uplift at the wall-pin location, (b) Relative vertical movement of gaps at the top of partition walls; Phase 2: (c) Uplift at the wall-pin location and vertical movement of collector beam, and relative vertical movement of gaps at the top of the (d) Main walls, and (e) Return walls

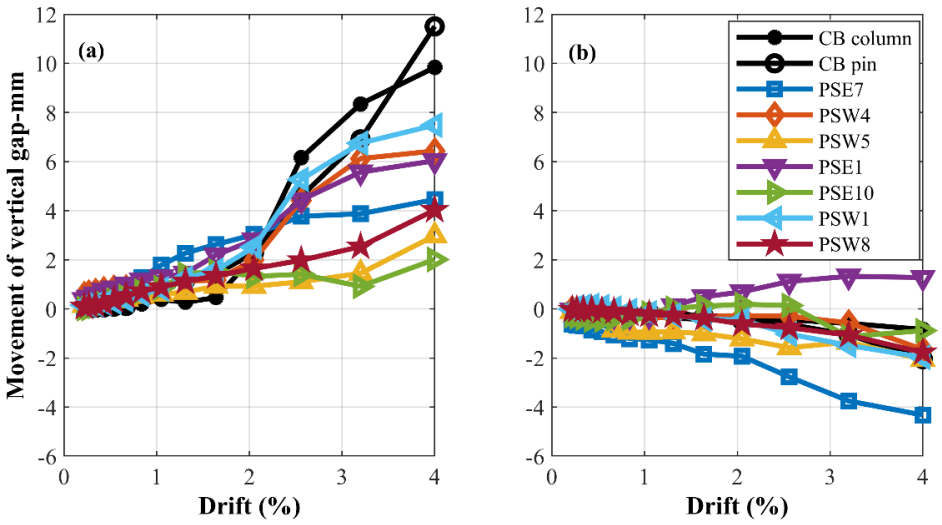

Figure 4-15: Movement of vertical gaps - positive values: opening - negative values: closing; (a) Maximum value in a stage, (b) Minimum value in a stage

4.5 Conclusion

This paper has addressed concerns about demands imposed to non-structural components in buildings using the CLT rocking wall as a resilient lateral system, such as large inter-story drifts and diaphragm deflection due to the uplift of the rocking wall. Experiments of partition walls integrated into a CLT rocking wall subassembly subjected to quasi-static bidirectional loading were performed at the NHERI Lehigh EF. Different configurations of partition walls were selected to study the effect of different construction details for reducing the drift induced damage in the partition walls. Phase 1 focused on the seismic performance of partition walls detailed to slip/slide, wherein a telescoping detail was compared to a traditional slip-track connection detail in two straight walls. Phase 2 incorporated return walls and investigated details aimed at isolation/separation of intersecting walls to reduce impact. A CG detail and DG detail were incorporated into C-

shaped walls to reduce the damage that occurs at the wall intersections. The major findings are summarized as follows:

- In Phase 1, the telescoping detailing proved to be more favourable than traditional slip track detailing, as it was observed to eliminate damage to the framing of partition walls caused by the separation of the end studs from the track at large drifts.
- In the Phase 2 DG wall, expansion joints helped to delay the onset of damage to about 1% story drift. Only the expansion joints adjacent to the wall intersections were effective in reducing the damage. However, the introduction of expansion joints on both walls adjacent to a corner is not recommended due to a potential stability issue at large drifts. As the joints on both walls opened, a small corner section of the wall detached from the rest and posed a local collapse risk.
- In the Phase 2 CG wall, the sacrificial corner bead detached at low drifts, but DS 2 and DS 3 occurred at much higher drifts compared to other C-shaped walls detailed without the CG. This approach has promise as a low damage detail and should be explored in additional configurations; however, it still needs evaluation of fire resistance and acoustic transmission.
- The contribution of partition walls to the lateral resistance may be significant in flexible mass timber construction. Based on the results, however, stiffness and strength of all wall details were negligible except the DG wall, which behaved like the traditional wall-intersection after the closure of the expansion joints. The

strength of partition walls was insignificant compared to the whole subassembly in both phases.

- For all partition walls, out-of-plane drift did not affect the in-plane resistance, but some of the damage phenomena initiated specifically during the out-of-plane cycles and, as a result, at lower drifts than in comparable prior studies. For example, in contrast to previous studies, DS 3 was observed in the slip track wall without return walls due to damage to the track legs, which may have been caused by out-of-plane loading. Furthermore, in the CG wall, DS 2 and 3 were observed despite not having been observed in previous studies.
- Furthermore, providing a stud-track and gypsum-diaphragm gap is fundamental for accommodating the diaphragm deflection. However, the vertical movement of the diaphragm due to the influence of the rocking wall uplift was insignificant up to 2% drift, and after that, a portion of uplift transferred to the collector beam and the adjacent diaphragm. In general, the provided gap at the top of the partition walls was sufficient for accommodating this movement.
- Minimizing the damage that occurs at the corners of the partition walls has proven challenging. However, in the CG wall detail, damage to the framing was associated specifically with the slip-track detailing. The authors hypothesize that combining telescoping tracks and the CG detail will be the best option for reducing the damage at wall intersections. This configuration and others will be explored in an upcoming shake-table test on a ten-story CLT rocking wall building at NHERI@UCSD.

Industry consultants will provide input to verify that these innovative details are constructible and satisfy fire rating and acoustic requirements.

4.6 Acknowledgment

This material is based upon work supported by the National Science Foundation under Grant Nos. CMMI-1635363, and 1635227. Any opinions, findings, conclusions, or recommendations expressed in this publication are those of the authors and do not necessarily reflect the views of the National Science Foundation. The authors are grateful for wall fabrication provided by Duggan and Marcon Inc and their suppliers and are especially indebted to Ken Loush of Eastern Exterior Wall Systems Inc, who coordinated the entire effort. The authors recognize Lehigh University collaborators and laboratory personnel who assisted with aspects of testing, especially Alia Amer, Darrick Fritchman, Thomas Marullo, Chad Kusko, James Ricles, and Richard Sause.

4.7 References

Applied Technology Council. (2007). Interim testing protocols for determining the seismic performance characteristics of structural and nonstructural components -FEMA 461.

Applied Technology Council. (2012). Reducing the risks of nonstructural earthquake damage – A practical guide - FEMA E-74.

Araya-Letelier, G., and Miranda, E. (2012). Novel sliding/frictional connections for improved seismic performance of gypsum wallboard partitions. 15th World

Conference on Earthquake Engineering. Lisbon, Portugal.

Araya-Letelier, G., Miranda, E., and Deierlein, G. (2019). Development and testing of a friction/ sliding connection to improve the seismic performance of gypsum partition walls. Earthquake Spectra, 35(2), 653–677. https://doi.org/10.1193/123117EQS270M

ASCE. (2003). American Society of Civil Engineers: ASCE/SEI 41-13: Seismic evaluation of existing buildings. Reston, Virginia: American Society of Civil Engineers.

ASCE. (2007). American Society of Civil Engineers: ASCE/SEI 41-06: Seismic rehabilitation of existing buildings. Reston, Virginia: American Society of Civil Engineers.

Blume, J. A., Associates. (1966). First progress report on racking tests of wall panels-report NVO-99-15. San Francisco, CA: URS/John A. Blume and Associates Engineers.

Blume, J. A., Associates. (1968). Second progress report on racking tests of wall panels-report NVO-99-35. San Francisco, CA: URS/John A. Blume and Associates Engineers.

Bond, R. B., Amer, A., Sause, R., and Ricles, J. (2018). PRJ-2054: Undergraduate research experience (REU), NHERI 2018: Self-centering cross-laminated timber walls erection and instrumentation plan. DesignSafe-CI, doi:10.17603/DS2GT2M

Buchanan, A., Deam, B., Fragiacomo, M., Pampanin, S., and Palermo, A. (2008). Multi-storey prestressed timber buildings in New Zealand. Structural Engineering

International, 18(2), 166–173. https://doi.org/10.2749/101686608784218635

Clay, A., Amer, A., Sause, R., and Ricles, J. (2019). PRJ-2487 undergraduate research experience (REU), NHERI 2019: Seismic tests of self-centering CLT shear wall with floor diaphragm and gravity load system. DesignSafe-CI, doi: 10.17603/ DS2NFDPXE86

Davies, R. D., R. Retamales, G. Mosqueda, and A. Filiatrault. 2011. Experimental seismic evaluation, model parameterization, and effect of cold-formed steel-framed gypsum partition walls on the seismic performance of an essential facility-MCEER-11-0005. New York: University at Buffalo, State University of New York.

FEMA. (2000). Prestandard and commentary for the seismic rehabilitation of buildings (FEMA 356). Washington, DC: Federal Emergency Management Agency.

Fiorino, L., Bucciero, B., and Landolfo, R. (2019). Evaluation of seismic dynamic behaviour of drywall partitions, façades, and ceilings through shake table testing. Engineering Structures, 180 (November 2018), 103–123. https://doi.org/10.1016/j.engstruct.2018.11.028

Fiorino, L., Pali, T., Bucciero, B., Macillo, V., Teresa Terracciano, M., and Landolfo, R. (2017). Experimental study on screwed connections for sheathed CFS structures with gypsum or cement based panels. Thin-Walled Structures, 116(January), 234–249. https://doi.org/10.1016/j.tws.2017.03.031

Fiorino, L., T. Pali, and R. Landolfo. (2018). “Out-of-plane seismic design by testing of

non-structural lightweight steel drywall partition walls.”. Thin-Walled Structures 13: 213–30. doi: 10.1016/j.tws.2018.03.032.

Freeman, S. A. (1971). Third progress report on racking tests of wall panels-report (JAB-99-54). California, U.S.A: San Francisco.

Freeman, S. A. (1974). Fourth progress report on racking tests of wall panels-report (JAB-99-55). California, U.S.A: San Francisco.

Freeman, S. A. (1976). Racking tests of high-rise building partitions. Journal of the Structural Division, 103 (8): 1673–85.

Ganey, R. S. (2015). Seismic design and testing of rocking cross laminated timber walls. University of Washington (Doctoral dissertation).

Hasani, H., K. L. Ryan, A. Amer, J. M. Ricles, and R. Sause. 2018. Pre-test seismic evaluation of drywall partition walls integrated with a timber rocking wall. In Proceeding of the US National Conference on Earthquake Engineering. Los Angeles, California, 11. doi:10.1002/eqe.

International Building Code Council. (2011). 2012 International building code (IBC). Country Club Hills, IL: ICC.

Jenkins, C., Soroushian, S., Rahmanishamsi, E., and Maragakis, E. M. (2016). Experimental fragility analysis of cold-formed steel-framed partition wall systems. Thin-Walled Structures, 103, 115–127. https://doi.org/10.1016/j.tws.2016.02.015

Lee, T.-H., Kato, M., Matsumiya, T., Suita, K., and Nakashima, M. (2007). Seismic performance evaluation of non-structural components: Drywall partitions. Earthquake Engineering and Structural Dynamics, 36, 367–382. https://doi.org/10.1002/eqe.638

Magliulo, G., Petrone, C., Capozzi, V., Maddaloni, G., Lopez, P., and Manfredi, G. (2014). Seismic performance evaluation of plasterboard partitions via shake table tests. Bulletin of Earthquake Engineering, 12(4), 1657–1677. https://doi.org/10.1007/s10518-013-9567-8

Matsuoka, Y., Suita, K., Yamada, S., Shimada, Y., and Akazawa, M. (2008). Non-structural component performance in 4-story frame tested to collapse. The 14th World Conference on Earthquake Engineering, 8. Beijing, China.

Mccormick, J., Matsuoka, Y., and Nakashima, M. (2008). Evaluation of non-Structural partition walls and suspended ceiling systems through a shake table study. 2008 Structures Congress – Structures Congress 2008: Crossing the Borders, Vancouver, BC, Canada, 314. doi:10.1061/41016(314)223.

Memari, A. M., Kasal, B., Manbec;, H. B., and Adams, A. R. (2008). Experimental cyclic racking evaluation of light-frame wood stud and steel stud wall systems. PHRC Research Series Rep, 107.

Moroder, D., Sarti, F., Palermo, A., and Pampanin, S. (2014). Experimental investigation of wall-to-floor connections in post-tensioned timber buildings. NZSEE Conference, Auckland (pp 21–23).

Mosqueda, G. (2016). Interior cold-formed steel framed gypsum partition walls - Background document FEMA P-58/BD-3.9.32.

NHERI TallWood Research Tasks. (2020). Accessed April 21, 2020. http://nheritallwood.mines.edu/task3.html

NHERI TallWood-Home. (2020). Accessed April 13, 2020. http://nheritallwood.mines.edu/

Pali, T., Macillo, V., Terracciano, M. T., Bucciero, B., Fiorino, L., and Landolfo, R. (2018). In-plane quasi-static cyclic tests of nonstructural lightweight steel drywall partitions for seismic performance evaluation. Earthquake Engineering and Structural Dynamics, 47(6), 1566–1588. https://doi.org/10.1002/eqe.3031

Peck, Q., Rogers, ; N, and Serrette, R. (2012). Cold-formed steel framed gypsum shear walls: In-Plane response. Journal of Structural Engineering 138 (7): 932–41. doi: 10.1061/(ASCE)ST.1943-541X.0000521.

Pei, S., J. W. van de Lindt, A. R. Barbosa, J. W. Berman, E. Mcdonnell, J. Daniel Dolan, H.-E. Blomgren, R. B. Zimmerman, D. Huang, S. Wichman, et al. (2019). Experimental seismic response of a resilient 2-story mass-timber building with post-tensioned rocking walls. Journal of Structural Engineering 145 (11): 04019120. doi: 10.1061/(ASCE)ST.1943-541X.0002382.

Petrone, C., Magliulo, G., Lopez, P., and Manfredi, G. (2015). Seismic fragility of plasterboard partitions via in-plane quasi-static tests. Earthquake Engineering and

Structural Dynamics, 44(14), 2589–2606. https://doi.org/10.1002/eqe.2600

Petrone, C., Magliulo, G., Lopez, P., and Manfredi, G. (2016). Out-of-plane seismic performance of plasterboard partition walls via quasi-static tests. Bulletin of the New Zealand Society for Earthquake Engineering, 49(1), 125–137. https://doi.org/10.5459/bnzsee.49.1.125-137

Rahmanishamsi, E., Soroushian, S., and Maragakis, M. (2016a). Evaluation of the out-of-plane behavior of stud-to-track connections in nonstructural partition walls. Thin-Walled Structures, 103, 211–224. https://doi.org/10.1016/j.tws.2016.02.018

Rahmanishamsi, E., Soroushian, S., and Maragakis, M. (2016b). Cyclic shear behavior of gypsum board-to-steel stud screw connections in nonstructural walls. Earthquake Spectra, 32(1), 415–439. https://doi.org/10.1193/062714EQS091M

Restrepo, J. I., and Lang, A. F. (2011). Study of loading protocols in light-gauge stud partition walls. Earthquake Spectra, 27(4), 1169–1185. https://doi.org/10.1193/1.3651608

Restrepo, J. I., and Bersofsky, A. M. (2011). Performance characteristics of light gage steel stud partition walls. Thin-Walled Structures, 49(2), 317–324. https://doi.org/10.1016/j.tws.2010.10.001

Retamales, R., Mosqueda, G., Filiatrault, A., and Reinhorn, A. (2011). Testing protocol for experimental seismic qualification of distributed nonstructural systems. Earthquake Spectra, 27(3), 835–856. https://doi.org/10.1193/1.3609868

Retamales, R., Davies, R., Mosqueda, G., and Filiatrault, A. (2013). Experimental seismic fragility of cold-formed steel framed gypsum partition walls. Journal of Structural Engineering, 139(August), 1285–1293. https://doi.org/10.1061/(ASCE)ST.1943-541X.0000657.

Rihal, S. S. (1982). Behavior of non-structural building partitions during earthquakes. Seventh Symposium on Earthquake Engineering, 1, 267–277. University of Roorkee

Schoettler, M. J., Belleri, A., Zhang, D., Restrepo, J. I., and Fleischman, R. B. (2009). Preliminary results of the shake-table testing for the development of a diaphragm seismic design. PCI Journal 54: 100–24. doi: 10.15554/pcij.01012009.100.124.

Soroushian, S., Ryan K. L., Maragakis M., Wieser J., Sasaki T., Sato E., Okazaki T., et al. (2012). NEES/E-defense tests: Seismic performance of ceiling/sprinkler piping nonstructural systems in base-isolated and fixed base building. 15th World Conference on Earthquake Engineering. (15WCEE), Lisbon, Portugal

Soroushian, S., Maragakis M., Ryan K. L., Sato E., Sasaki T., Okazaki T., Mosqueda G. (2016). Seismic simulation of an integrated ceiling-partition wall-piping system at E-Defense. II: Evaluation of nonstructural damage and fragilities. Journal of Structural Engineering 142 (2): 1–17. doi: 10.1061/(ASCE)ST.1943-541X.0001385.

SSMA (Steel Stud Manufacturers Association). (2000a). Single deflection track selection.

SSMA (Steel Stud Manufacturers Association). (2000b). Track within a track deflection assembly.

Swensen, S., Deierlein, ; G G, and Miranda, E. (2015). Behavior of screw and adhesive connections to gypsum wallboard in wood and cold-formed steel-framed wallettes. Journal of Structural Engineering 142 (4). doi: 10.1061/(ASCE)ST.1943-541X.0001307.

Taghavi, S., and Miranda, E. (2003). Response assessment of nonstructural building elements. Report PEER 2003/05, Pacific Earthquake Engineering Research Center, University of California, Berkeley, 96.

Tasligedik, A.S., Pampanin, S., and Palermo, A. (2012). In-Plane cyclic testing of non-structural drywalls infilled within RC frames. 15th World Conference on Earthquake Engineering (15WCEE). Lisbon, Portugal.

Tasligedik, A. S., Pampanin, S., and Palermo, A. (2013). Low damage seismic solutions for non-structural drywall partitions. Vienna Congress on Recent Advances in Earthquake Engineering and Structural Dynamics (VEESD 2013), 11. Vienna, Austria. doi:10.1007/s10518-014-9654-5.

Villaverde, R. (1997). Seismic design of secondary structures: State of the art. *Journal of Structural Engineering* 123 (August): 1011–19. doi: 10.1061/(ASCE)0733-9445(1997)123:8(1011).

Wang, X., Elide Pantoli T. C., Hutchinson J. I., Restrepo R. L., Wood M. S., Hoehler P. G., Sesma F. H., and Sesma F. H.. (2015). Seismic performance of cold-formed steel wall systems in a full-scale building. Journal of Structural Engineering 141 (10): 1–

11. doi: 10.1061/(ASCE)ST.1943-541X.0001245.

Zhou, Y., Li, R., and Lu, X. L. (2012). Earthquake-resilient tall buildings using rocking walls. 15th World Conference on Earthquake Engineering, 10.

5 Effect of partition walls on the seismic response of mass-timber buildings with a post-tensioned rocking wall system

(This chapter is a standalone manuscript submitted for publication to Engineering Structures: "Hasani, H., Ryan, K. L. (2021). (Submitted) Effect of partition walls on the seismic response of mass-timber buildings with a post-tensioned rocking wall system. *Engineering Structures*.")

5.1 Abstract

The popularity of mass-timber as a building material is increasing among engineers, investors, and building owners. Using cross-laminated timber (CLT) rocking walls as the lateral load resisting system in mass timber buildings can offer seismic resiliency. Due to the flexibility of mass-timber building with post-tensioned CLT rocking wall and a wide variety of partition wall responses in terms of stiffness and strength, partition walls could affect the dynamic response and resiliency of these buildings significantly. In this paper, a parametric study was conducted to evaluate the effect of the inclusion of partition walls on the seismic demand of mass-timber buildings with post-tensioned CLT rocking walls.

Representative 5-story and 12-story mass-timber buildings were selected and modeled in OpenSees. Moreover, concentrated spring models were developed to represent effective force-deformation for four different variations of partition wall detailing, and applied to the building models to represent wall densities associated with apartment and hospitality

occupancies. Eigenvalue, pushover, and time-history analysis were performed on 2D models of the bare structure structures and those with partition wall variations. It is concluded that partition walls with fixed connection details considerably affect the dynamic properties and response and should be included in models, whereas those with deformation-compatible details have little influence.

5.2 Introduction

Recent advancements in structural engineering have led to new structural systems that can reduce earthquake-induced damage and promote seismic resilient responses. However, damage to nonstructural elements has dominated the economic losses in recent earthquakes. Such elements are susceptible to damage – contributing to downtime – at low shaking intensity, and comprise the majority of construction cost (Taghavi and Miranda 2003). Therefore, to achieve a resilient structure, the resilience of both structural and nonstructural components is essential.

Partition walls are one of the most common nonstructural components within a building – connected floor-to-floor – that are subjected to the seismic loading of the building. Specifically, they are subjected to the differential displacement demands or inter-story drifts, which vary throughout the building. Partition walls are prone to initial damage at inter-story drifts as low as 0.1% (Mosqueda 2016). Partition walls are usually not anticipated to contribute to the primary load-bearing or lateral load resisting system of the building and are not accounted for in the design. However, when partition walls are stiff, they can alter the response of the structure. They tend to generate their highest stiffness

and strength before being damaged, and thus most likely to influence the overall response in low-level earthquakes. Alternative drift-compatible details intended to reduce seismic damage are being developed; walls with alternative detailing may have much lower stiffness and strength than conventional partition walls.

Previous research has shown that accounting for the stiffness and strength of partition walls can influence the dynamic characteristics and seismic response of the structure. A few experimental studies examined the contribution of partition walls in the seismic response of structures. For example, Lee et al. (2007) and Tasligedik et al. (2012) performed quasi-static testing of partition walls built as infill walls within a moment frame, and showed that the strength of partition walls is not negligible compared to the frame alone. In addition, some studies evaluated the effect of partition walls on the dynamic behavior of structural subassemblies or buildings during shake table testing (Fiorino et al. 2019; Magliulo et al. 2014; Matsuoka et al. 2008; McCormick et al. 2008; Soroushian et al. 2016; Wang et al. 2015). Finally, some numerical studies examined the effect of partition walls as well. For example, partition walls were shown to decrease the fundamental period up to 14% in a hospital building with a steel moment frame (Wood and Hutchinson 2012), and a 10% reduction in a 10-story reinforced concrete building occurred due to partition walls (Tasligedik et al. 2013).

Self-centering systems have emerged as a promising class of lateral systems for advanced seismic protection, but such systems are flexible and may have more significant drift than conventional systems due to reduced hysteretic damping (Chancellor et al. 2014). For example, buildings with post-tensioned reinforced concrete rocking walls were shown to

have longer periods and larger inter-story drifts than buildings with traditional reinforced concrete walls (Zhou et al. 2012). Post-tensioned rocking walls built from mass timber components, such as cross-laminated timber (CLT) panels, have been developed as a lateral system for mass timber buildings. Combining a flexible post-tensioned rocking wall system and the inherent flexibility of timber compared to concrete can result in a building with considerable flexibility. Previous tests have shown the potential for post-tensioned CLT rocking walls as a resilient lateral load resistant system for tall buildings in high seismic areas, as they can develop and sustain large drift demands with minor damage (Buchanan et al. 2008b; Ganey 2015). Furthermore, since mass timber buildings with post-tensioned CLT rocking walls are pretty flexible, the stiffness contribution of different partition walls might significantly affect the seismic response of these types of buildings.

For mass timber buildings with post-tensioned CLT rocking walls, this research aims to 1) understand how the partition wall detailing affects the structure-nonstructure interaction, such as dynamic properties of the structural system, and 2) determine whether these nonstructural walls should be considered part of the overall building resistance and accounted for in the design. For this purpose, different partition wall models were applied to two mass timber building archetype models; the seismic response of the bare structure and combined models were evaluated to determine the effect of different partition walls on the overall system response.

5.3 Modeling of partition walls

5.3.1 Partition wall details

Interior partition walls are framed with horizontal tracks at the top and bottom and vertical studs connected to the tracks, then covered with drywall (Figure 5-1(a)). The framing can be timber or steel; however, steel framing is more common than timber framing in modern buildings due to its higher ductility (Tasligedik et al. 2012). Therefore, steel-framed partition walls are considered in this study.

Many construction details can affect the performance of partition walls, but the details of connecting the partition walls to the structural system have the most effect on their seismic response (Pali et al. 2018). In general, there are two approaches for connecting partition walls to the surrounding structural elements: “fixed” and “slip-track” connections. In fixed detailing, the studs and drywall are connected to tracks on top and bottom. In slip-track detailing, the partition walls are isolated from the inter-story drift by eliminating the connection of studs and drywall to the top track. Walls with fixed connections are observed to have much higher stiffness and strength than those with slip-track connections. However, basic slip-track detailing leads to damage at the intersecting or return walls, as the slip of the in-plane wall causes it to collide with the intersecting out-of-plane wall. For slip-track detailed walls, this interaction with return walls increases the stiffness and strength relative to those with no return walls. In addition, details intended to reduce damage at return walls are under development, leading to lower stiffness and strength.

The seismic response of interior partition walls with full connections and slip track connections (with and without return walls) was characterized during a series of tests at the State University at New York, University at Buffalo (UB) (Davies et al. 2011) (Figure 5-1(b)). Recorded responses of specimens from this program were used to develop numerical models (Wood and Hutchinson 2012). Select models have been adapted to represent the general response of fixed and slip track connections when return walls are present. The partition wall specimens were 3.6 m long by 3.5 m high (main in-plane wall dimension), built from lightweight steel framing, and used institutional detailing. Institutional detailing specifies 0.75 mm minimum thickness framing, 406 mm minimum stud spacing, and extra reinforcement through the corners. Moreover, in slip-track detailing, there was a stud and gypsum connection to the bottom track. Half of the track-to-concrete shot pin connectors were spaced at 305 mm for the fixed connection, and the other half spaced at 610 mm. More details can be found in Wood and Hutchinson (2012).

In addition, two other wall configurations with innovative details intended to reduce the drift-induced damage at the intersecting slip-track partition walls are considered in this study. The numerical responses of these walls were generated in an experimental test of C-shaped walls performed at NHERI Lehigh EF in 2019 (Figure 5-1(c)). The first distributed gap (DG) detail incorporated frequent expansion joints through the length of the wall, while the second corner gap (CG) detail incorporated a full gap through the intersection of the wall. Although the DG and CG walls were subjected to a bi-directional quasi-static reversed cyclic test, the models developed for this study were based on the in-plane response. The main in-plane walls were 3.8 meters long by 3.5 meters high, and built with

an institutional-grade construction (0.88 mm thickness framing and 406 mm stud spacing) and slip-track detailing. More details can be found in Hasani and Ryan (2021).

Figure 5-2 presents the backbone curve force versus displacement, used for numerical models, of walls with each of the four considered details. The fixed connection detail offers more than twice the resistance of any of the other details, while novel details have lower resistance than traditional slip track detail. Specifically, the CG detailing generates almost no resistance, and its response is similar to the slip-track detailing without return walls. Full experimental hysteresis loops for each detail can be found in Wood and Hutchinson (2012) and Hasani and Ryan (2021).

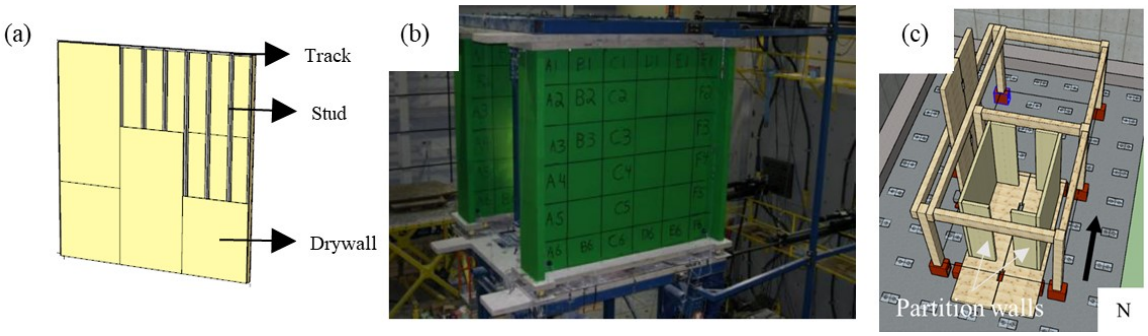

Figure 5-1: (a) Lightweight steel drywall partition wall components (b) Experimental test at UB (c) Experimental test at NHERI@Lehigh

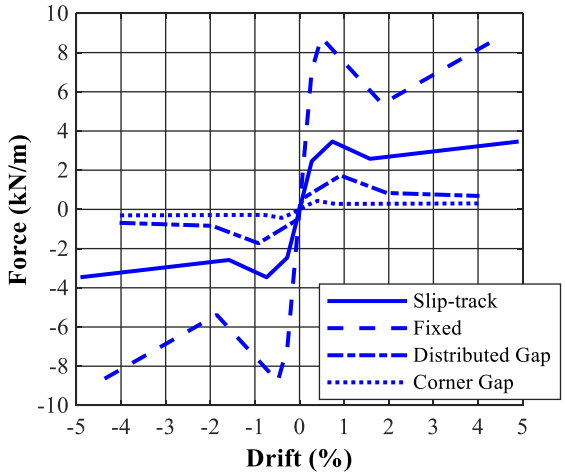

Figure 5-2: Backbone curves of different partition walls

5.3.2 Partition wall modeling

To date, two classes of models have been developed for predicting partition wall cyclic response. In the first or finite element approach, all components and connections of partition walls are represented by separate elements. This approach is used to study the effect of specific details and configurations of partition walls and develop the fragility curves (Rahmanishamsi et al. 2016). In the second or simplified approach, concentrated spring elements represent the total partition wall response, and the global hysteretic force-deformation response of the designated length of the partition wall is assigned to a single spring. The simplified approach is helpful in high-level building simulations incorporating structure-nonstructural interaction (Davies et al. 2011; Magliulo et al. 2014; Shakeel et al. 2020; Tasligedik et al. 2013; Wood and Hutchinson 2012). In addition, this approach facilitates implementing numerous partition walls within a building while maintaining a fast and efficient analysis.

Due to the aims of this research, the concentrated spring model approach was used for modeling the nonlinear hysteretic response of partition walls, and the models were generated in OpenSees (Mazzoni et al. 2007). In general, the hysteretic response of this class of partition walls is characterized by a pinching force-displacement cyclic behavior, where each cycle shows degradation in strength and stiffness compared to the previous cycle. Therefore, the available pinching material in OpenSees (Figure 5-3) is used to model the partition wall by calibrating the material model to the observed force-deformation backbone curves in the experiments. The calibrated hysteretic response of each wall is shown in Figure 5-4. These models have been normalized by wall length; thus, the force should be multiplied by the wall length for application in a building model.

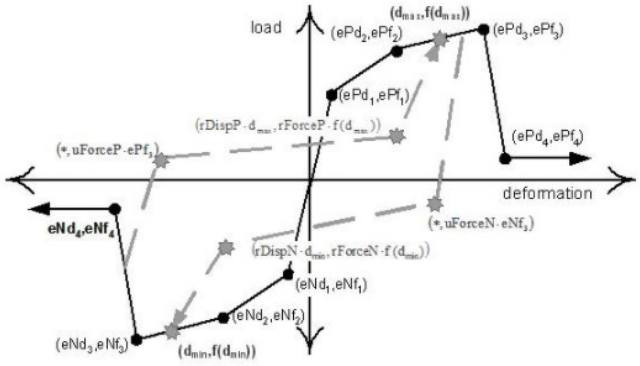

Figure 5-3: Pinching material (Mazzoni et al. 2007)

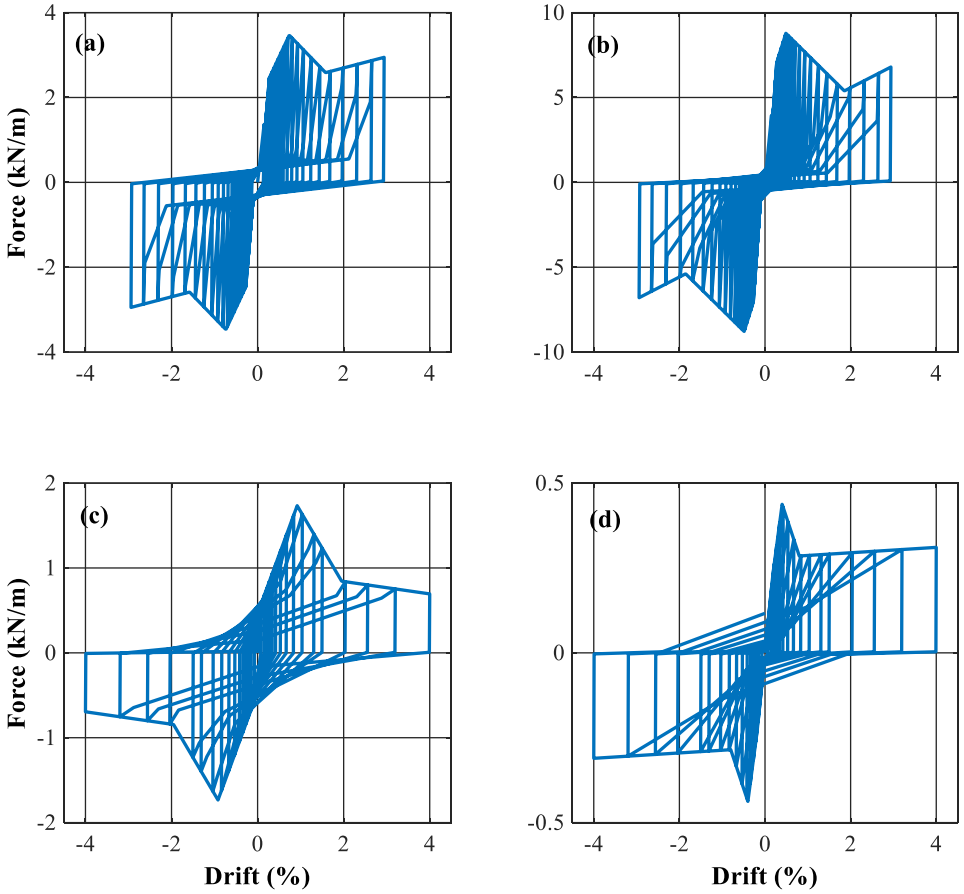

Figure 5-4: Hysteresis loops using calibrated models of partition walls (a) Slip-Track (b) Fixed (c) Distributed Gap (d) Corner Gap

5.4 Development of the structural model

Next, 5-story and 12-story archetype buildings with post-tensioned CLT rocking wall lateral systems are modeled to evaluate the influence of various partition walls on their overall seismic response. These buildings, designed by Wilson (2018), are made of CLT

panels and other mass timber components, with lateral resistance provided by the CLT rocking walls.

5.4.1 Building design specifications

Figure 5-5 depicts the buildings that were modeled in this research. The 5-story building, shown in Figure 5-5(a), is 19.81 m tall with 3.96 m story heights and floor dimensions of 27.5 m by 51.1 m. The 12-story building (Figure 5-5(b)) measures 45.72 m tall with story heights of 3.81 m, and floor dimensions of 27 m by 74.25 m. Post-tensioned CLT rocking walls are distributed throughout both buildings in both directions, as shown in Figure 5-6. These buildings were designed for the South Lake Union neighborhood of Seattle (coordinate: 47.6222° N, -122.3346° W), risk category II, and site class D (Wilson 2018).

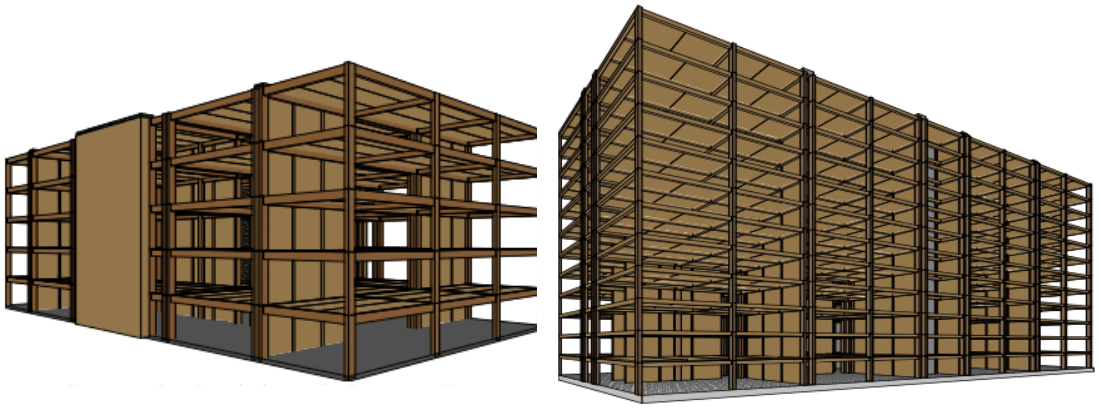

Figure 5-5: (a) 5 story building (b) 12 story building (Wilson 2018)

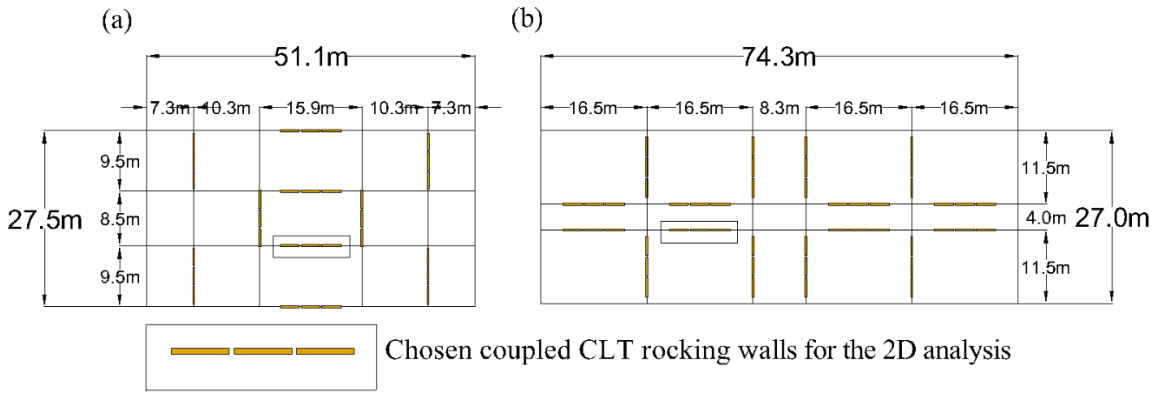

Figure 5-6: Prototype building plans showing CLT coupled rocking walls: (a) 5-story (b) 12-story building

The five-story building had 6 and 4 coupled rocking wall units in the N-S and E-W direction, respectively, while the 12-story building had eight coupled rocking wall units in each direction. Each coupled rocking wall unit consisted of three adjacent wall panels coupled with U-shaped flexural plates (UFP) for energy dissipation. The rocking wall panels were 9-ply (315 mm thick) CLT panels, 3.05 m in length, except for the 5-story in N-S direction, for which the panels were 2.75 m in length. Two UFPs connected each adjacent set of panels on each floor, with a total of 4 UFPs per floor per coupled wall unit. Post-tensioning (PT) rods extended from the tops of the walls down to the foundation in each building; each wall panel was post-tensioned with four bars with a total area of 6193 mm^2 centered on the wall panel (both buildings). The total initial PT forces of 530 kN and 1800 kN were applied to PT rods per wall panel in 5-story and 12-story, respectively. There was assumed to be a mechanism for transferring shear at the base of the rocking wall.

The coupled rocking walls were connected to the gravity framing with a slotted pin connection. Thus, the rocking walls were isolated from the gravity loading of the rest of the building and carried only their self-weight. Some of the material properties of buildings can be found in Table 5-1. More information can be found in Wilson (2018).

Table 5-1: Material properties of structural components

Material	**CLT**			**PT (rods)**			**UFP**
Property	E (MPa)	G (MPa)	f_y (MPa)	E (MPa)	f_y (MPa)	f_u (MPa)	f_y (MPa)
Value	4215	219	37	200000	882	1034	413

5.4.2 Structure model

Two-dimensional (2D) models of a coupled rocking wall unit with the standard 3 m wall panel length were developed in OpenSees for each building. One-fourth and one-eighth of the mass of the buildings were assigned to each model for the 5-story and 12-story, respectively. The models consisted of a few main components, including elastic Timoshenko beam-columns for wall panels, multi-spring contact elements for base rocking, truss elements for PT bars, and zero-length spring elements for UFPs.

The wall panels were modeled using a series of elastic Timoshenko beam-column elements spanning between UFP and floor locations. The nonlinear rocking behavior of the panels and the compressive deformation of the CLT were modeled using a multi-spring contact element at the base of each panel. The contact stiffness was calculated using the following equation:

$$K_s = \frac{AE}{L_p} \tag{5-1}$$

where A and E are the cross-sectional area and elastic modulus of the CLT panels, and L_p is the plastic hinge length of the wall. The assumed plastic hinge length was 254 mm, which resulted in a stiffness of 2.0e8 kN/m. This stiffness was distributed to 80 zero-length springs for each wall panel, spaced according to Gauss-Lobatto rules. A compression-only elastic, perfectly plastic gap material (ElasticPPGap in OpenSeees) was assigned to the zero-length springs to model the compression response and gap opening. Finally, corotational truss elements were applied to transfer shear at the base of rocking walls.

The PT bars were modeled using tension-only corotatonal truss elements with a bi-linear hysteretic material model. These elements were fixed at the bottom and connected to the top panel beam-column element at the roof. An initial strain was applied to these truss elements using an initial strain material (InitStrainMaterial in OpenSees), combined with a MinMax material to track the ultimate strain of the PT bars. For the UFPs, a uniaxial Giuffre-Menegotto-Pinto steel material model with isotropic strain hardening was assigned to zero-length spring elements, and the material specifications were determined by Baird et al. (2014). Rigid elements were used to link the elastic beam-column wall elements at the center of the panels to the zero-length UFP springs located between the two wall panels. The main dimensions of UFPs and calculated specifications for the material models can be found in Table 5-2. At the floor levels, the adjacent rocking wall panels were connected by rigid links (very stiff truss elements) that represented the diaphragms.

Table 5-2: UFP specifications

Dimensions	b_u **(mm)**	D_u **(mm)**	t_u **(mm)**	F_y **(kN)**	K_0 **(kN/m)**	R
Value	279	102	12.7	91.63	20577	14.7

5.5 Coupled structure-partition wall model

The concentrated spring elements representing the resistance of the partition walls were added to the 2D building model, as shown in Figure 5-7. As discussed previously, partition wall resistance was represented by translational spring elements, and the force-displacement relations of different partition walls (Figure 5-4) were assigned to these translational springs. The spring elements were connected to nodes at mid-height that were slaved to structural nodes at the top and bottom of the story in all degrees of freedom. As a result, the partition wall hysteretic responses were lumped at the story mid-height.

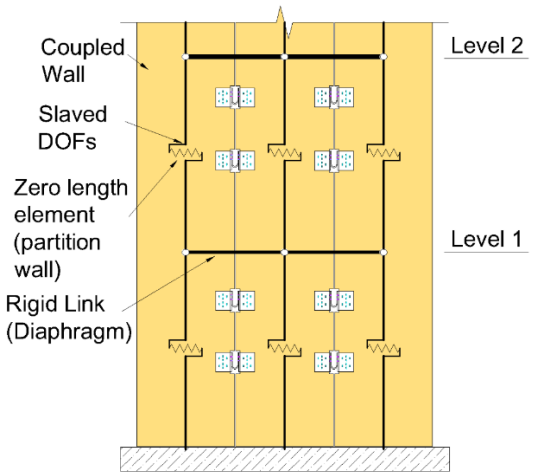

Figure 5-7: Partition wall implementation into lateral load resisting system

Partition wall indices were used to determine representative wall length in the building. The partition wall index is defined as the total length L of partition walls per story floor divided by the plan area A of the floor (with units 1/Length). Two partition wall indices were chosen from eight available occupancies in the FEMA P-58, Normative Quantity Estimation Tool (FEMA 2012). Apartment occupancy represents an upper bound partition

wall density, with a partition wall index of 0.12. Hospitality occupancy represents an average partition wall density, with a partition wall index of 0.06. Since partition walls run in both directions, one-half of the density was applied to the 2D models. Table 5-3 tabulates the calculated total partition wall lengths and the partition wall length assigned to each coupled rocking wall in the 2D model per floor. In the 2D model, the partition wall lengths were distributed between the three rocking wall panels.

Table 5-3: Partition wall length

Buildings		**Apt.**		**Hsp.**	
		Total	Coupled rocking wall	Total	Coupled rocking wall
5-story	Partition Length (m)	276.5	69.1	138.3	34.6
12-story	Partition Length (m)	347.6	43.5	173.8	21.7.

5.6 Effects of partition walls on the response of mass timber building

Eight different variations of partition walls were considered: hospitality (Hsp) and apartment (Apt) partition wall densities, combined with four different partition wall types: fixed (F), slip track (ST), distributed gap (DG), and corner gap (CG). For both the 5-story and 12-story structures, the bare rocking wall structure model (no partition walls) and each partition wall variation model were subjected to eigenvalue analysis, pushover analysis, and time history analysis to assess the inclusion of partition walls in a mass timber building.

5.6.1 Eigenvalue analysis

Using eigenvalue analysis, vibration periods of the first five modes were obtained. Table 5-4 shows the periods for the bare structures and the eight variations mentioned above. To facilitate the comparison, the percent change in the period ΔT_i is calculated to display the period shift when considering the addition of partition walls.

$$\Delta T_i^n = \frac{(T_i^n - T_i^{bare})}{T_i^{bare}} \times 100 \qquad 5\text{-}2$$

where T_i^n is the period of the structure with the partition wall and T_i^{bare} is the period of structure without a wall for i[th] mode. A negative ΔT_i indicates a decrease in the period. These period shifts are illustrated in Figure 5-8.

Table 5-4: Periods of mode shapes

			ST		**F**		**DG**		**CG**	
	Mode	Bare (sec)	Hsp. (sec)	Apt. (sec)	Hsp. (sec)	Apt. (sec)	Hsp. (sec)	Apt. (sec)	Hsp. (sec)	Apt. (sec)
5 story	1	0.91	0.84	0.79	0.74	0.65	0.86	0.81	0.90	0.89
	2	0.28	0.26	0.25	0.24	0.21	0.27	0.25	0.28	0.27
	3	0.15	0.15	0.14	0.14	0.12	0.15	0.14	0.15	0.15
	4	0.11	0.11	0.11	0.10	0.09	0.11	0.11	0.11	0.11
	5	0.10	0.09	0.09	0.09	0.08	0.09	0.09	0.10	0.10
12 story	1	2.15	1.96	1.81	1.71	1.48	2.00	1.87	2.12	2.10
	2	0.62	0.58	0.55	0.52	0.47	0.59	0.56	0.61	0.61
	3	0.31	0.30	0.28	0.28	0.25	0.30	0.29	0.31	0.31
	4	0.20	0.19	0.19	0.18	0.17	0.20	0.19	0.2	0.20
	5	0.15	0.14	0.14	0.14	0.13	0.15	0.15	0.15	0.15

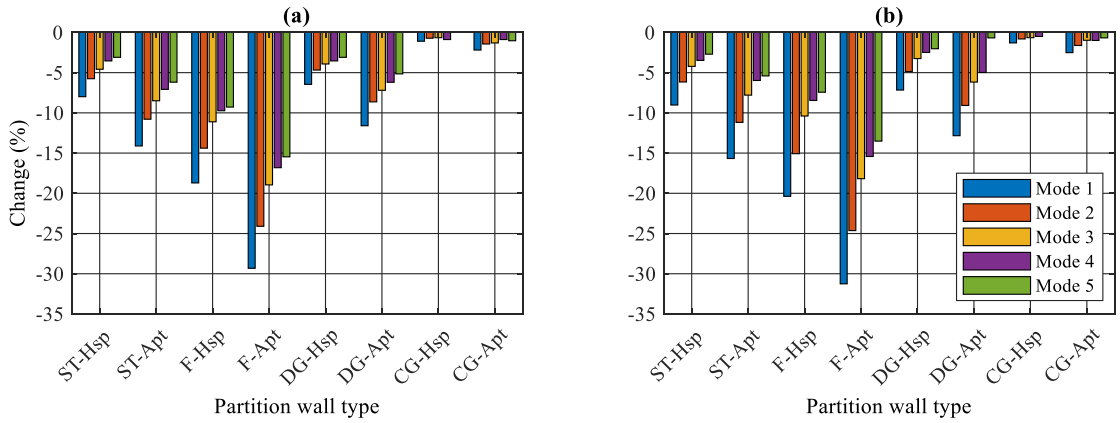

Figure 5-8: Partition wall effect on periods (a) 5-story (b) 12-story

By including the partition walls, all periods were observed to decrease due to the stiffening of the structure. The partition wall type influenced the modal periods more than partition wall density. The most significant period shift of about 30% was observed for the first mode of F-Apt in both buildings, and the effect of CG detailing was minor. Remarkably, in CG-Apt, the first mode periods of 5-story and 12-story buildings were reduced by only 2.2% and 2.5%, and the effect was even less in other modes. The period shifts for other details were somewhere in between these two extremes. Assuming Hsp density caused the modal periods to reduce on average by 40% to 51% and 40% to 52% compared to the reductions for Apt density in the 5-story and 12-story buildings.

In all cases, the first mode period shift was the largest among all modes. Among all the partition walls, only the Fixed (F) detailing reduced the period by more than 20%, suggesting that it is likely to affect the response significantly. In similar studies for a concrete moment frame building (Wood and Hutchinson 2012), the period shift was limited

to 8%. This comparison suggests the importance of including partition walls in the analysis due to the flexibility of mass-timber building compared to a concrete structure.

5.6.2 Nonlinear pushover analysis

Nonlinear static pushover analyses were performed to assess the shear capacities of buildings. This analysis provided an estimation of the force-deformation characteristics of the buildings and the relative contribution of the partition walls to stiffness and strength. Figure 5-9 presents pushover curves of 5 story and 12 story buildings for all partition wall types and densities to illustrate the significance of partition walls in global responses of buildings. The pushover curves are calculated for one coupled rocking wall unit. The results are presented as base shear coefficient V/W (i.e., lateral force V normalized by weight W collected by that wall unit) versus roof drift as a height percentage. In general, the pushover curves can be divided into three specific regions: 1) initial stiffness (at the start of pushover analysis), 2) second stiffness (when lowest stiffness occurred), and 3) final stiffness (at the drift of 3%). Variations in stiffness and base shear coefficient were computed as follows:

$$\Delta K_i = \frac{(K_i - K_{bare})}{K_{bare}} \times 100 \tag{5-3}$$

$$\Delta(\frac{V}{W})_i = \max(\left(\frac{V}{W}\right)_i - \left(\frac{V}{W}\right)_{bare}) \tag{5-4}$$

where K_i and $\left(\frac{V}{W}\right)_i$ are the stiffness and base shear coefficient of the structure with partition walls and K_{bare} and $\left(\frac{V}{W}\right)_{bare}$ are the stiffness and base shear coefficient of the structure

with no partition walls. The stiffness variation (Equation 5-3) represents a percentage change and was applied to the initial stiffness $(\Delta K_1)_i$, second stiffness $(\Delta K_2)_i$, final stiffness $(\Delta K_f)_i$. The variation in base shear coefficient (Equation 5-4) represented an absolute change and was taken at the drift level that maximized building strength. These coefficients are tabulated for all buildings in Table 5-5.

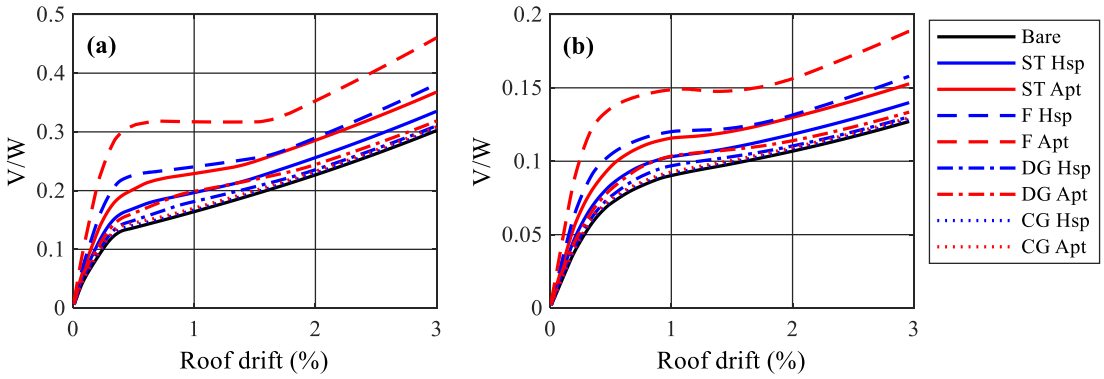

Figure 5-9: Pushover curves of buildings including the partition walls (a) 5-story (b) 12-story

For the 5-story building (Table 5-5), the initial stiffness increased by 2.56% for the CG-Hsp (negligible) to 112.93% for the F-Apt (more than doubled). Similar stiffness increase ranges were seen for the 12-story building (3.06% to 133.09%). For the 5-story building, the maximum increase in base shear coefficient ranged from 0.028 for the CG-Hsp to 0.272 for the F-Apt. These maximums occurred between roof drifts of 0.39% to 0.89%, where the base shear coefficient of the bare structure was about 0.15. For the 12-story building, the maximum increase in base shear coefficient ranged from 0.002 (negligible) for the CG-Hsp density to 0.065 for the F-Apt, relative to a bare structure base shear coefficient of about 0.08 in the roof drift range (0.38% to 0.97%) where the maximums occurred. The

maximum increase in base shear coefficient in both buildings occurred below 1% roof drift since partition walls yield at drifts well less than 1%. Each partition wall type has a negative stiffness region somewhere after yielding (see the backbone curves in Figure 5-2), reducing its relative effect on the total base shear coefficient.

Table 5-5: Pushover statistics

		Slip-Track		**Fixed**		**Distributed Gap**		**Corner Gap**	
		Hsp.	Apt.	Hsp.	Apt.	Hsp.	Apt.	Hsp.	Apt.
5-story	$(\Delta K_1)_i$	20.08	39.84	57.26	112.93	15.75	31.26	2.56	5.09
	$(\Delta K_2)_i$	-21.71	-43.28	-51.33	-102.62	-16.44	-32.74	-0.01	0.14
	$(\Delta K_f)_i$	3.99	8.27	20.01	40.16	-1.18	-2.20	-0.10	0.04
	$\Delta(\frac{V}{W})_i$	0.036	0.071	0.090	0.175	0.018	0.036	0.004	0.009
12-story	$(\Delta K_1)_i$	23.87	47.25	67.78	133.09	18.76	37.13	3.06	6.07
	$(\Delta K_2)_i$	-33.33	-63.98	-81.07	-150.10	-22.01	-49.319	0.54	0.03
	$(\Delta K_f)_i$	6.11	12.50	29.18	58.35	-1.55	-2.81	0.01	0.20
	$\Delta(\frac{V}{W})_i$	0.014	0.027	0.033	0.065	0.007	0.013	0.002	0.003

The second stiffness occurred in the mid-drift range where some parts of the coupled rocking wall, mainly UFPs, and all partition walls are yielded. In this region, the negative stiffness of partition walls, except CG, reduced the stiffness of the building. The final stiffness was relatively unaffected by partition walls, and only increased for Fixed detailing.

5.6.3 Nonlinear time history analysis

5.6.3.1 Ground motion selection

The ground motions utilized in this study were a subset of the ATC-62/FEMA P-695 (FEMA 2009) far-field ground motion suite. Twelve components from the set of 22 far-

field records (44 individual components) were chosen. These selected records are listed in Table 5-6 according to their record number in PEER Ground Motion Database (PEER, 2021). The far-field suite was chosen to avoid pulse effects that might add complexity to the interpretation of the results. Three different shaking intensities were considered: service-level earthquake (SLE) with a 72-year return period, design-basis earthquake (DBE) with a 475-year return period, and maximum considered earthquake (MCE) with a 2475 year return period. The motions were amplitude scaled for each intensity level so that the spectral acceleration of each motion corresponded to the target spectral acceleration at the bare structure fundamental period. The target spectra for DBE and MCE corresponded to ASCE 7-16 design spectra for site class D, and the target spectrum for SLE was calculated by the Unified Hazard Tool (USGS 2021). Table 5-6 tabulates the selected earthquake record numbers, earthquake, station, PGAs, and scale factors for the MCE level.

Table 5-6: Ground motions

No.	Record No.	Earthquake	Station Name	PGA (g)	SF-5 (MCE)	SF-12 (MCE)
1	1244	Friuli	Tolmezzo	0.44	3.8	7.8
2	953	Imperial Valley	Delta	0.52	2.3	2.8
3	1602	Superstition Hills	El Centro Imp. Co. Cent	0.82	2.4	2.5
4	1787	Loma Prieta	Capitola	0.34	2.0	3.2
5	169	Landers	Yermo Fire Station	0.35	2.1	2.7
6	1111	Northridge	Beverly Hills - 14145 Mulhol	0.51	0.8	2.0
7	1158	Kobe	Nishi-Akashi	0.36	2.1	2.3
8	900	Kocaeli	Duzce	0.24	2.2	1.4
9	752	Chi-Chi	CHY101	0.53	1.6	1.7
10	1633	Duzce	Bolu	0.51	1.2	1.7
11	721	Manjil	Abbar	0.36	2.3	2.1
12	125	Hector Mine	Hector	0.35	3.4	4.2

The nonlinear time history analysis was performed using the above-ground motion suite scaled to the three different intensities. The following responses were generated and analyzed: inter-story drift, story shear of the rocking wall units, and UFP forces.

5.6.3.2 Influence of partition walls on inter-story drift

Inter-story drift is one of the standard measurements for determining the performance of a structure during a seismic event. Different codes consider different limits for inter-story drifts for immediate occupancy, life safety, and collapse prevention (ASCE 2017; FEMA 2000). Figure 5-10 compares representative roof drift (in %) of 5-story and 12-story buildings for the bare structure and F-Apt. Adding the effect of the fixed partition walls leads to roof drift reductions of 36% for the 5-story building and 17% for the 12-story building. In addition, higher frequency content can be seen in the drift history for the F-Apt due to its decreased fundamental period.

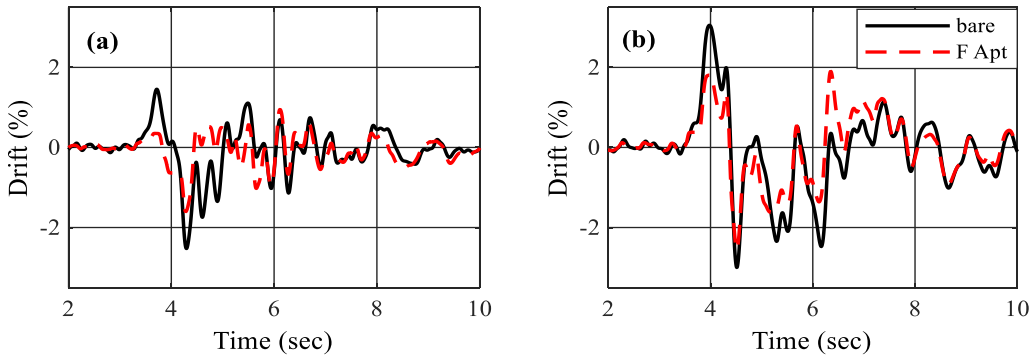

Figure 5-10: Drift histories (a) 5 story (b) 12 story

The peak inter-story drift was calculated in each story as the maximum difference in adjacent floor level displacement over time as a percentage of height. Figure 5-11 shows

the peak inter-story drift, averaged over the suite of motions, for both buildings and all three intensity levels.

For the SLE level, the inclusion of partition walls reduced the maximum inter-story drift significantly. The maximum reduction of peak inter-story drift in any story was observed for F-Apt; peak drift was reduced by 55% and 54% for the 5-story and 12-story buildings, respectively, compared to the bare structure building. Thus, although fixed detailing experiences damage at low drifts, it can significantly benefit the building response and design for the SLE level. The least reduction of peak inter-story drift was observed for CG-Hsp; peak drift in any story was reduced by a maximum of 4.8% and 7.2% for the 5-story and 12-story buildings, respectively. Hence, if this detailing were to make its way into practice, the designer need not consider the effect of partition walls in the design and analysis of the buildings. The peak inter-story drifts of the other building types were between these two extremes, and the only building type that realized inter-story drift reduced by more than 50% was F-Apt. Moreover, another conventional detailing, slip-track detailing, led to significant drift reductions. Peak drift reductions of up to 37% and 42% in the 5-story building and up to 26% and 31% in the 12-story building were observed for ST-Hsp and ST-Apt.

Peak inter-story drift reductions when considering the effects of partition walls were lower for DBE and MCE than for SLE intensity, but still significant. For example, for F-Apt subjected to DBE level, the peak inter-story ratios decreased by a maximum of 46% and 45% for the 5 and 12-story buildings, respectively. For F-Apt subjected to MCE level, the

peak inter-story drift ratios decreased by 36% and 29% for the 5 and 12 story buildings, respectively.

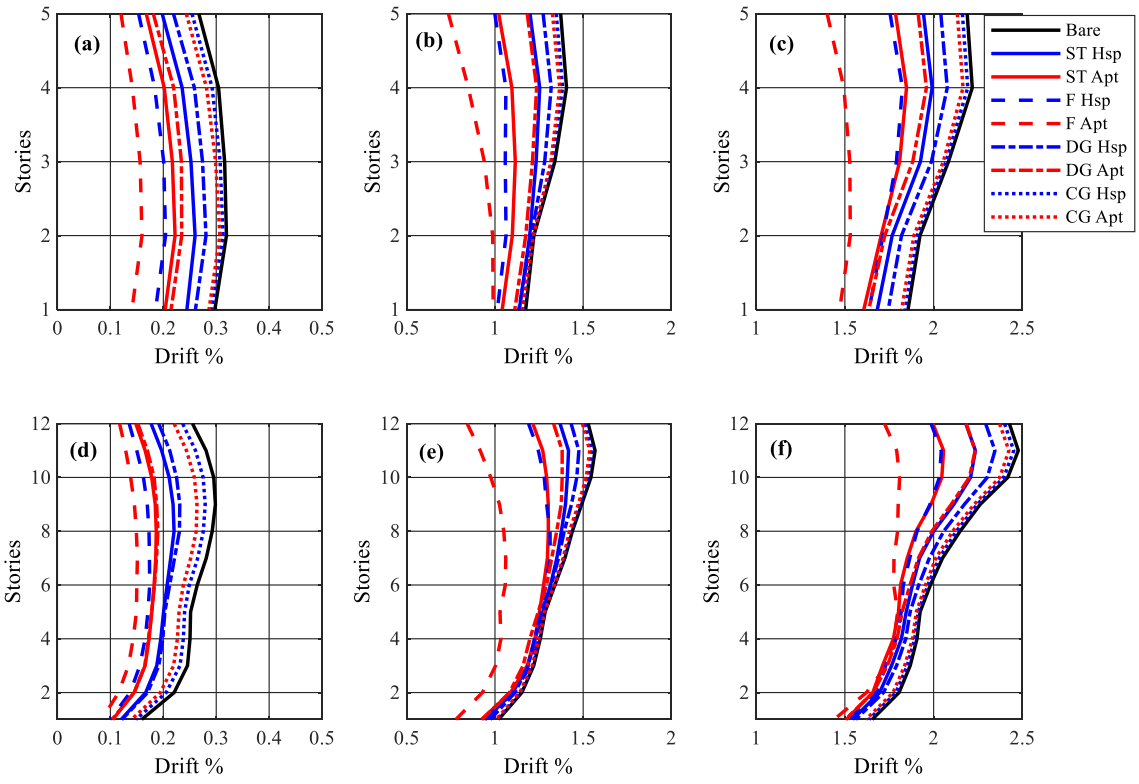

Figure 5-11: Peak drift variation through the height (a) SLE-5 story (b) DBE-5 story (c) MCE-5 story (d) SLE-12 story (e) DBE-12 story (f) MCE-12 story

Moreover, the inclusion of partition walls changed the stiffness distribution, which resulted in a change in the drift profile in buildings. For example, in DBE and MCE levels, the maximum inter-story drift reduction occurred at the top stories where the peak story was observed.

For all building types/details, inter-story drift ratios remained under the FEMA 356 limits (FEMA 2000), which are 0.7% for SLE, 2.5% for DBE, and 5% for MCE. However, these buildings were designed without considering the partition walls. In general, accounting for partition walls, especially those with fixed details with more considerable stiffness and strength, may benefit the design of the relatively flexible mass timber building with post-tensioned rocking walls either by reducing the building drift and helping to keep it under code limits or leading to a more economical design. On the other hand, partition walls with detailing such as the corner gap can be neglected in the building design due to their insignificant reduction in building drift, even though they help eliminate damage to the framing of partition walls (Hasani and Ryan 2021).

5.6.3.3 Effects on story shear

Rocking wall story shear reflects the peak force demands and the governing lateral load on each story for design. The rocking wall story shear was calculated by summing the forces in the three rocking wall panel elements (UFP and PT forces were omitted). Figure 5-12 shows the peak rocking wall story shear averaged over all the motions for each intensity level.

At all intensity levels, reductions in rocking wall story shears were observed for the buildings with partition walls relative to the bare structure due to story drift reductions. Rocking wall story shears decreased more for SLE than for DBE and MCE levels due to the high contribution of partition wall strength at lower drifts. SLE level rocking wall story shear reductions (maximum over all stories) ranged from 1% for CG-Hsp to 53% for F-

Apt in the 5-story building. For the 12-story building, the rocking wall story shear reductions ranged from 4% for CG-Hsp to 52% for F-Apt.

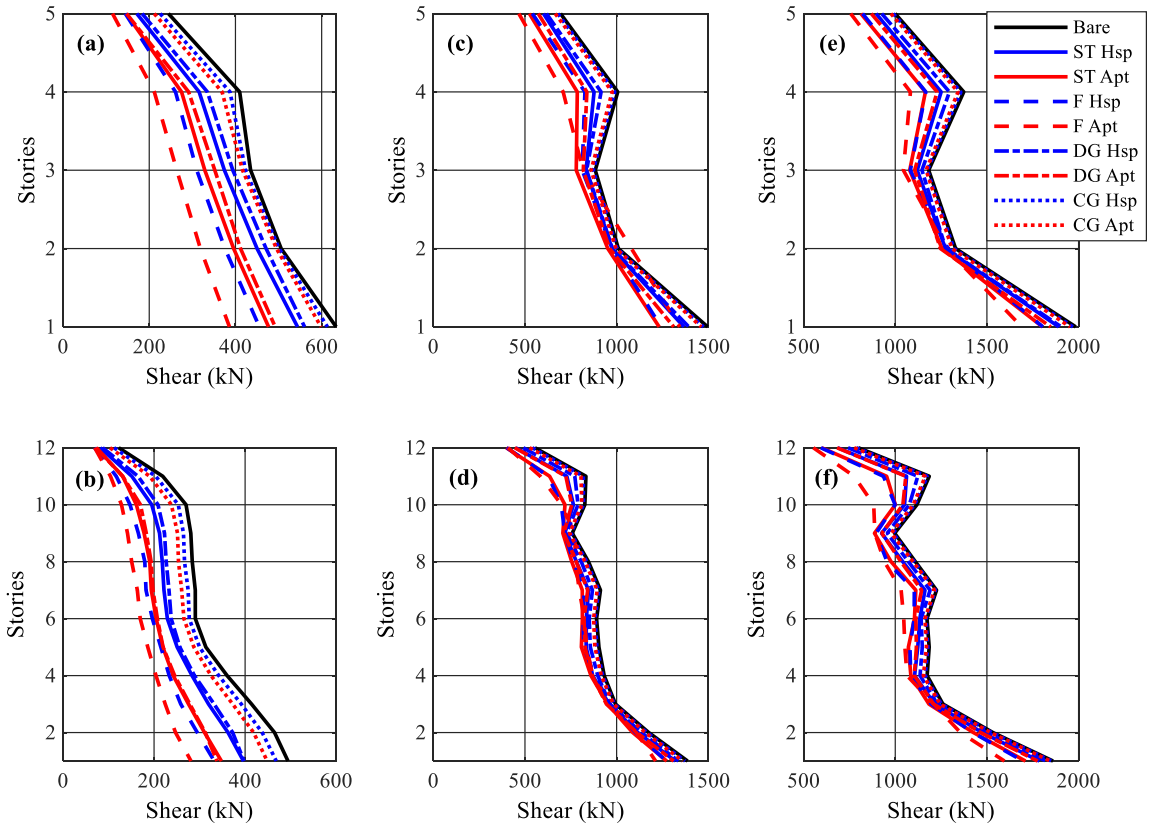

Figure 5-12: Rocking wall shear variation through the height (a) SLE-5 story (b) SLE-12 story (c) DBE-5 story (d) DBE-12 story (e) MCE-5 story (f) MCE-12 story

For the DBE level, rocking wall story shear reductions for CG-Hsp (minimum over all building types) were 7% for the 5-story and 2% for the 12-story buildings. For F-Apt (maximum over all building types), story shear reductions were 32% and 30% for the 5-story and 12-story buildings, respectively. For the MCE level, partition walls reduced the

rocking wall story shears value by 24% and 35% for the 5-story and 12-story F-Apt building type, while story shear reductions for CG-Hsp were negligible.

Moreover, the rocking wall shear profile varied for different building types since partition walls changed the distribution of strength over the height of the rocking wall. For example, partition walls reduced the rocking wall shear more uniformly at the SLE than other intensity levels. For example, the story shear reduction for the 5-story F-Apt building varied over the height from 37% to 53%. This variation over height was 7% to 32% at the DBE level and 4% to 24% at the MCE level. In addition, the story shear tended to be most reduced at the base and the upper stories (Figure 5-12(c) and (e)).

5.7 Summary of results

Figure 5-13 shows the average percent change of inter-story drift, rocking wall story shear, and summation of story UFP force for the structure with partition walls with respect to the bare structure. These values were computed by averaging the percent change of quantities with respect to the bare structure over the ground motions and then again over the stories, and provides a single measure for each building type.

As shown in Figure 5-13, the inclusion of partition walls in the model affected the response of the building at the SLE level more considerably than other intensity levels. For example, assuming DG-Apt in a 5-story building reduced average inter-story drift by 28%, 9%, and 11% for SLE, DBE, and MCE, respectively. This trend was more significant for the UFP force than for other response parameters. For example, for the 12-story building, even CG-

Apt resulted in a 14% reduction in UFP force at the SLE level, while it had a negligible effect at other intensity levels. This observation suggests that the UFP forces are post-yield at higher intensity levels, and thus less sensitive to incremental changes in drift. In addition, the effect of partition wall stiffness on structural element forces was also more considerable at the SLE level than other intensity levels. For example, ST-Hsp reduced the average rocking wall story shear in the 5-story building by 18%, 9%, and 7% for the SLE, DBE, and MCE, respectively (Figure 5-13(b)).

In summary, including strength and stiffness of partition walls in the building models benefit in reducing demands on the structure and corresponding design parameters in these buildings, especially for SLE intensity, which has a frequent return period of 50 years. SLE mainly assesses the serviceability of a structure, wherein little to no structural damage and only minor damage to non-structural elements is allowed. Thus, the inclusion of partition wall stiffness will help the structure satisfy the SLE level targets. In particular, reducing forces in the UFPs to below yield (and preventing the need for UFP replacement at the SLE) is greatly beneficial. However, as the SLE is not the governing intensity for the design of structural elements, including partition walls for structural design is less critical.

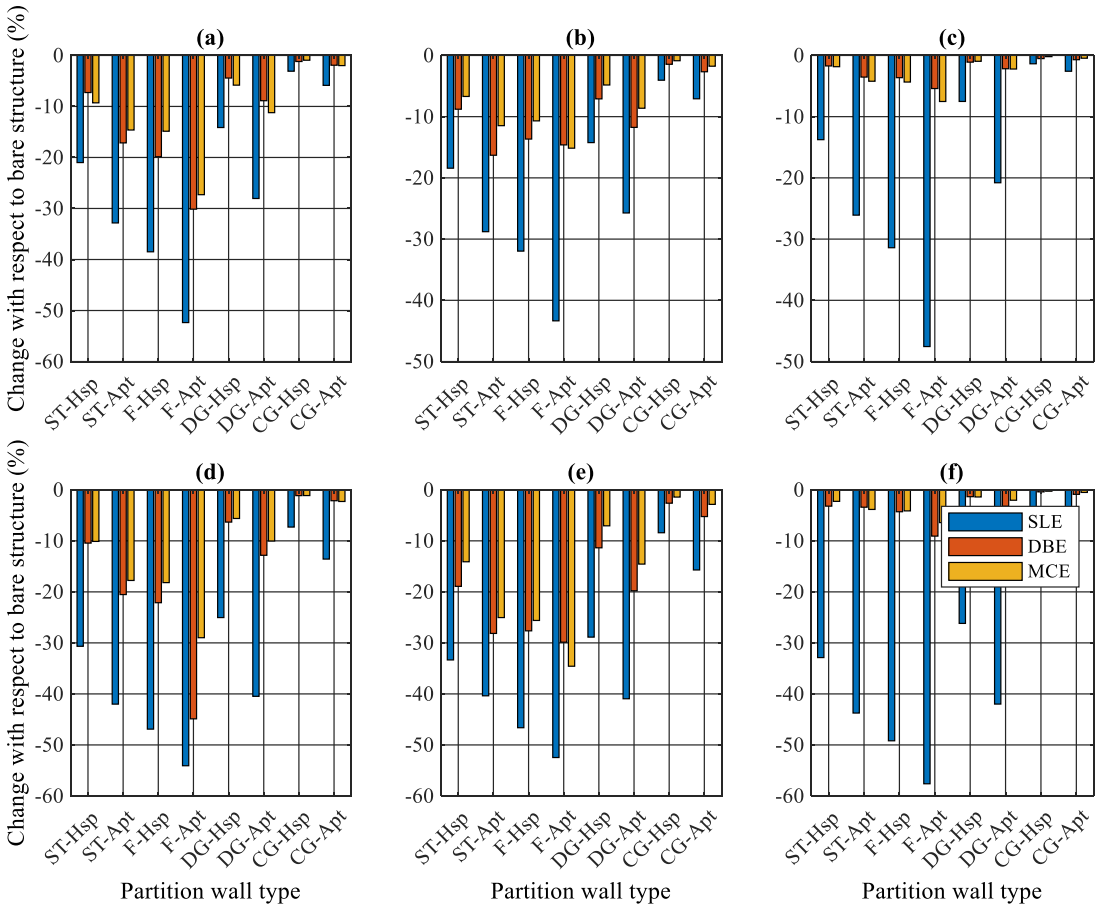

Figure 5-13: Average percent change of various responses for different intensity levels and building types (a) Drift - 5-story (b) Rcking wall story shear - 5-story (c) UFP force - 5-story (d) Drift - 12-story (e) Rocking wall shear - 12-story (f) UFP force - 12-story

5.8 Conclusion

This paper has addressed the effect of partition walls on the dynamic response of mass timber buildings with post-tensioned rocking wall lateral systems. A 2D numerical model of a coupled rocking wall unit was developed for buildings with two different heights (5-story and 12-story), and concentrated springs were added to the models to represent the effects of various densities and types of partition walls. Four different wall configuration

details with two different densities (8 variations in total) were considered. Each model was evaluated using modal, pushover, and time-history analysis techniques. Moreover, time-history analyses were performed for three different earthquake intensities. Finally, different building response parameters were evaluated, and the significant findings are summarized as follows:

- From eigenvalue analysis, the vibration periods in all modes decreased relative to the bare structure due to the stiffening effect of the partition walls. The fundamental period decreased more than other modal periods, ranging from 1% to 29% and 1% to 31% for 5 and 12 story buildings.
- Partition walls affected the total stiffness over the entire drift range of the pushover analysis, with a significant increase in the initial stiffness and a decrease in the stiffness after yielding.
- From dynamic analysis, including the partition walls in the model generally resulted in reductions of inter-story drift, rocking wall story shear, and UFP forces that were significant depending on the partition wall type and density. These reductions were more significant for the SLE level earthquake than for DBE or MCE. Since DBE or MCE generally controls design, the significance may not be apparent. However, the results of loss estimation studies, which generally predict that low-level events contribute significantly to life cycle costs, will be more affected by including partition walls in the models.

- Representing partition walls using simplified spring models was simple and effective in considering their effects in design and analysis. Omitting the effects of partition walls will lead to a conservative but not economical design of the building.
- Among all the partition wall types, fixed connection detailing had the most effect on the structure. The fixed connection detailing stiffens the building, lowers drift demands, and lowers force demands in the rocking walls significantly as forces are carried both by structural elements and partition walls. On the other hand, CG walls have almost no influence on the stiffness and strength of buildings.

5.9 Acknowledgments

This material is based upon work supported by the National Science Foundation under Grant No. CMMI-1635363. Any opinions, findings, conclusions, or recommendations expressed in this publication are those of the authors and do not necessarily reflect the views of the National Science Foundation.

5.10 References

Agliulo, G., Petrone, C., Capozzi, V., Maddaloni, G., Lopez, P., and Manfredi, G. (2014). Seismic performance evaluation of plasterboard partitions via shake table tests. Bulletin of Earthquake Engineering, 12(4), 1657–1677. https://doi.org/10.1007/s10518-013-9567-8

ASCE (2017). ASCE/SEI 7-16: Minimum design loads and associated criteria for buildings and other structures. The American Society of Civil Engineers, Reston, Virginia, USA.

Baird, A., Smith, T., Palermo, A., and Pampanin, S. (2014). Experimental and numerical Study of U-shape Flexural Plate (UFP) dissipators. New Zealand Society for Earthquake Engineering (NZSEE) Annual Technical Conference, Wellington, New Zealand, 9.

Buchanan, A., Deam, B., Fragiacomo, M., Pampanin, S., and Palermo, A. (2008). Multi-story prestressed timber buildings in New Zealand. Structural Engineering International: Journal of the International Association for Bridge and Structural Engineering (IABSE), 18(2), 166–173. https://doi.org/10.2749/101686608784218635

Chancellor, N. B., Eatherton, M. R., Roke, D. A., and Akbas, T. (2014). Self-centering seismic lateral force resisting systems: High performance structures for the city of tomorrow. *Buildings*, MDPI AG.

Davies, R. D., Retamales, R., Mosqueda, G., and Filiatrault, A. (2011). Experimental seismic evaluation, model parameterization, and effect of cold-formed steel-framed gypsum partition walls on the seismic performance of an essential facility.

FEMA (Federal Emergency Management Agency). (2009). Quantification of building seismic performance factors. Washington, DC, USA.

FEMA. (2000). Prestandard and commentary for the seismic rehabilitation of buildings (FEMA 356). Washington, DC: Federal Emergency Management Agency.

FEMA (Federal Emergency Management Agency). (2012). Seismic performance assessment of buildings. Volume 2- Implementation Guide. FEMA P-58-2, 2, 365.

Fiorino, L., Bucciero, B., and Landolfo, R. (2019). Evaluation of seismic dynamic behaviour of drywall partitions, façades, and ceilings through shake table testing. Engineering Structures, 180 (November 2018), 103–123. https://doi.org/10.1016/j.engstruct.2018.11.028

Ganey, R. S. (2015). Seismic design and testing of rocking cross laminated timber walls. The University of Washington (Doctoral dissertation).

Hasani, H., and Ryan, K. L. (2021). Experimental Cyclic Test of Reduced Damage Detailed Drywall Partition Walls Integrated with a Timber Rocking Wall. Journal of Earthquake Engineering. DOI: 10.1080/13632469.2020.1859005

Lee, T.-H., Kato, M., Matsumiya, T., Suita, K., and Nakashima, M. (2007). Seismic performance evaluation of non-structural components: Drywall partitions. Earthquake Engineering and Structural Dynamics, 36, 367–382. https://doi.org/10.1002/eqe.638

Matsuoka, Y., Suita, K., Yamada, S., Shimada, Y., and Akazawa, M. (2008). Non-structural component performance in 4-story frame tested to collapse. The 14th World Conference on Earthquake Engineering, 8. Beijing, China.

Mazzoni, S., Mckenna, F., Scott, M. H., and Fenves, G. L. (2007). Open System for Earthquake Engineering Simulation (OpenSees) OpenSees Command Language Manual.

McCormick, J., Matsuoka, Y., Pan, P., and Nakashima, M. (2008). Evaluation of nonstructural partition walls and suspended ceiling systems through a shake table study. Structures Congress 2008: Crossing the Borders. https://doi.org/10.1061/41016(314)223

Mosqueda, G. (2016). Interior cold-formed steel framed gypsum partition walls - Background document FEMA P-58/BD-3.9.32.

Pali, T., Macillo, V., Terracciano, M. T., Bucciero, B., Fiorino, L., and Landolfo, R. (2018). In-plane quasi-static cyclic tests of nonstructural lightweight steel drywall partitions for seismic performance evaluation. Earthquake Engineering and Structural Dynamics, 47(6), 1566–1588. https://doi.org/10.1002/eqe.3031

PEER (2021). PEER Ground Motion Database. Pacific Earthquake Engineering Research Center. <https://ngawest2.berkeley.edu/> (Jun. 24, 2021).

Shakeel, S., Fiorino, L., and Landolfo, R. (2020). Numerical modelling of lightweight steel drywall partitions for in-plane seismic performance evaluations. Ingegneria Sismica, 37(1), 64–83.

Soroushian, S., Maragakis, E. M., Ryan, K. L., Sato, E., Sasaki, T., Okazaki, T., and Mosqueda, G. (2016). Seismic simulation of an integrated ceiling-partition wall-

piping system at e-defense. II : evaluation of nonstructural damage and fragilities. 142(2), 1–17. https://doi.org/10.1061/(ASCE)ST.1943-541X.0001385.

Taghavi, S., and Miranda, E. (2003). Response assessment of nonstructural building elements. Report PEER 2003/05, Pacific Earthquake Engineering Research Center, University of California, Berkeley, 96.

Tasligedik, A. S., Pampanin, S., and Palermo, A. (2012). In-Plane cyclic testing of non-structural drywalls infilled within RC frames. 15th World Conference on Earthquake Engineering (15WCEE), Lisbon, Portugal.

Tasligedik, A. S., Pampanin, S., and Palermo, A. (2013). Low damage seismic solutions for non-structural drywall partitions. Vienna Congress on Recent Advances in Earthquake Engineering and Structural Dynamics (VEESD 2013), 11. Vienna, Austria. doi:10.1007/s10518-014-9654-5.

Unified Hazard Tool. (2021). <https://earthquake.usgs.gov/hazards/interactive/> (Jun. 27, 2021).

Wang, X., Elide Pantoli T. C., Hutchinson J. I., Restrepo R. L., Wood M. S., Hoehler P. G., Sesma F. H., and Sesma F. H.. (2015). Seismic performance of cold-formed steel wall systems in a full-scale building. Journal of Structural Engineering 141 (10): 1–11. doi: 10.1061/(ASCE)ST.1943-541X.0001245.

Wilson, A. W. (2018). Numerical modeling and seismic performance of post-tensioned cross-laminated timber rocking wall systems. Washington State University (Master

Thesis).

Wood, R. L., and Hutchinson, T. C. (2012). A numerical model for capturing the in-plane seismic response of interior metal stud partition walls. Technical Report MCEES-12-0007.

Zhou, Y., Li, R., and Lu, X. L. (2012). Earthquake-resilient tall buildings using rocking walls. 15th World Conference on Earthquake Engineering, 10.